INORGANIC CHEMISTRY
FRONTIERS

REVIEW

View Article Online
View Journal | View Issue

Cite this: *Inorg. Chem. Front.*, 2020, **7**, 1598

Sensing organic analytes by metal–organic frameworks: a new way of considering the topic

Mao-Lin Hu,*[a] Sayed Ali Akbar Razavi,[b] Maryam Piroozzadeh[b] and Ali Morsali *[b]

Three-dimensional porous coordination polymers, which are known as metal–organic frameworks (MOFs), have drawn considerable attention owing to their properties, such as highly crystalline and ordered structures, inorganic–organic-hybrid nature, tunability of chemical functionality, high porosity and surface area and moderate-to-high stability. Due to these properties, MOFs are applied extensively as probes for the detection of large varieties of organic molecules. In this line, different MOF-based instrumental and material-based methods along with different strategies have been developed to study and extend our information about the capabilities of MOFs as sensing probes for the detection of organic molecules as well as improving and developing their detection limits, selectivity and sensitivity toward specific analytes. Considering these points, we have presented and classified the content of this review based on the chemical structures of organic analytes in three categories, including (I) nitroaromatic explosives and energetic materials, (II) small organic molecules, such as solvents and volatile organic compounds, and (III) organic amines. For each group of these analytes, different material and instrumental methods using MOFs have been explained, with illustrations of remarkable examples. Finally, we compare the methods for the detection of each group of analytes and discuss which instrumentation is more effective for each group of analytes.

Received 10th December 2019,
Accepted 8th January 2020

DOI: 10.1039/c9qi01617a

rsc.li/frontiers-inorganic

1. Introduction

Metal–organic frameworks (MOFs) are a subclass of coordination polymers and porous materials with microporosity/mesoporosity and highly regular crystalline frameworks.[1,2] In recent decades, MOFs have become the center of attention of numerous scientists, particularly chemists and material engineers. MOFs show very practical, interesting and unique characteristics, such as regular structures with high crystallinity, porous frameworks with high surface areas, hybrid structures with organic–inorganic natures, functionalizable structures with tunability of host–guest chemistry and tolerable frameworks with moderately high stability. The advantages of the combination of all these characteristics in one framework lead to wide application of MOFs in different fields, such as gas adsorption and separation,[3–5] removal[6,298] and separation[7] of hazardous materials, catalysis[8] and photocatalysis,[9] electrochemical applications,[10] bio-related applications,[11] and particularly, the detection of dangerous chemicals.[12]

Organic molecules such as organic solvents, volatile organic compounds (VOCs), explosive nitroaromatic compounds (NACs) and energetic heterocyclic molecules have critical negative effects on human safety and environmental protection. As a result, wide efforts are being conducted to detect and discriminate organic molecules in different media. Taking advantage of the chemical and physical properties of MOFs, they are among the groups of materials that are applied extensively for detection of many types of organic molecules using different instrumental methods, such as photoluminescence, electrochemical, photonic, optical and gravimetric instrumental methods.

Because MOFs are porous, the accessible pore volumes inside their frameworks can function as cages to capture and interact with analyte molecules. Due to their functionality, the host–guest chemistry between MOFs and organic molecules with different functional groups can be controlled and optimized. Their hybrid nature causes wide variation in signals, mechanisms and responses (change in the signal in the presence of analyte) to different analytes. Their ordered crystalline frameworks lead to particular responses with appropriate repetition. Finally, due to their stability, they can be used repeatedly to detect particular analytes.

Despite these advantages, the term "signal transduction" is a very critical limitation for the development of MOF-based sensors in different instrumental methods. We will see that

[a]College of Chemistry and Materials Engineering, Wenzhou University, Wenzhou 325035, China. E-mail: maolin_hu@yahoo.com
[b]Department of Chemistry, Faculty of Sciences, Tarbiat Modares University, P.O. Box 14115-4838, Tehran, Iran. E-mail: morsali_a@modares.ac.ir; Tel: (+98) 21-82884416

due to the high consistency between the π-extended aromatic structures of MOFs and the origins of the signal transduction of MOFs in photoluminescence methods, MOFs are widely applied in photoluminescence methods. However, in the case of electrochemical methods, due to limitations of MOFs such as low conductivity and redox activity, their application is not extended as greatly as in photoluminescence methods. However, considering some critical points in the design and modification of MOFs, their limitations in electrochemical methods can be eliminated. These points regarding the advantages and disadvantages of MOFs in different instrumental methods will be discussed precisely in the next sections.

Considering these points, such as structural advantages of MOFs and their limitations or extension in signal transduction in different instrumental methods, we attempted to write this review with a different approach. Most reviews of MOF-based sensors focus only on luminescence[13–19] or electrochemical[20–23] methods or principles of designing MOF-based sensors[24–27] for all kinds of analytes. Although each one of these reviews is useful for its related purpose, the approach of this review is different. First of all, in this review, we focus only on organic molecules; to this end, we classified the organic analytes in three different groups, including (I) nitroaromatic explosives and energetic molecules, (II) organic amines, and (III) small organic molecules, such as organic solvents and volatile organic compounds. Then, we discuss the application of MOFs in different instrumental methods for the detection of each group of these organic analytes. This discussion of MOF-based instrumental methods provides us with the opportunity to evaluate and compare the efficiency of each instrumental method in the detection of specific organic analytes. Finally, we compare the successes achieved by each method. This approach is not presented in other reviews.

2. Explosives and energetic materials

Nitroaromatic compounds (NACs) are organic molecules which contain at least one electron withdrawing nitro group ($-NO_2$) attached to an aromatic or aliphatic molecular skeleton. The high electronegativity of the nitro group is based on the combined action of the two electron-deficient oxygen atoms bonded to the partially positive nitrogen atom. When the nitro group is attached to the aromatic ring, both conjugation and resonance mechanisms are involved in the delocalization of electrons of the aromatic ring, resulting in the π-deficient nature of NACs. Due to this electron deficiency and their molecular structures, NACs are categorized as secondary explosives, especially TNT (2,4,6-trinitrotoluene). The majority of these compounds are synthetic, and they are used in chemical industrials for the synthesis of many products, including dyes, polymers, pesticides, and explosives. Also, some biologically produced NACs have been identified; however, they are relatively rare in nature. NACs are introduced into the environment mainly by human activities. Unfortunately, their extensive use has led to environmental contamination of soil and groundwater. Due to their hazardous nature to human health, they are registered in the U.S. Environmental Protection Agency's list of priority pollutants for environmental remediation. Therefore, real-life and in-field detection of nitroaromatic compounds is essential for environmental safety and human protection due to their explosivity and high toxicity.

With the aim to detect NACs, various instrumental analyses have been applied, such as chromatography coupled with mass spectrometry, surface enhanced Raman spectroscopy, cyclic voltammetry, ion mobility spectrometry, colorimetric immunoassays, nuclear quadrupole resonance, and energy dispersive X-ray diffraction. However, these methods are very expensive, poorly portable and require frequent calibration.[28,29] On the other hand, the vapour phase sensing of nitroaromatics is not always efficient because of the very low vapour pressures of the nitroaromatics. Therefore, rapid and facile detection methods along with probe materials are needed to address these concerns.

Because of the presence of electron-withdrawing nitro groups, NACs have a high degree of electron deficiency, which endows them with oxidative nature and electron-accepting character. Because MOFs are constructed based on conjugated aromatic ligands and organic functional groups containing heteroatoms with non-bonding electrons, they can interact with NACs through multiple host–guest interactions, such as hydrogen bonding and (π-deficient)–(π-rich) interactions. On the other hand, due to the consistency between the photophysical properties of MOFs and the signal transduction in PL methods (based on photo-induced π to π* and n to π* electron transitions), MOFs are extensively applied as probes in the detection of hazardous chemicals by PL methods. As a result of this great matching between the chemical characteristics of MOFs with the electron-deficient nature of NACs and the signal transduction in PL methods, detection of NACs by MOFs has been extensively investigated by PL methods.

The pioneering work in this area was carried out by Li and coworkers.[30,31] They synthesized $[Zn_2(oba)_2(bpy)]\cdot DMA$ (**1**, H_2oba = 4,4′-oxybis(benzoic acid); bpy = 4,4′-bipyridine; DMA = *N*,*N*′-dimethylacetamide) and applied it in the detection of NACs, especially nitrobenzene (Fig. 1).[30] The PL results reveal that **1** acts as a fluorescence quencher in the presence of NACs. The observed quenching efficiency for the selected nitroaromatics is nitrobenzene (NB) > 1,3-dinitrobenzene (1,3-DNB > 2-nitrotoluene (2-NT) ≈ 1,4-dinitrobenzene (1,4-DNB) > 2,4-dinitrotoluene (2,4-DNT). This order is based on the trends of the electron-withdrawing groups and vapor pressure of each analyte. The authors proposed that this PL quenching is based on a donor–acceptor electron-transfer mechanism. Upon excitation, electrons are transferred from the conduction band of **1**′ to the LUMO of the analyte, leading to a quenching effect. Also, cyclic voltammetry measurements showed that NACs have more positive reduction potentials than **1**′, and there is a large overlap between the conduction band of **1**′ and the LUMO of nitrobenzene based on band structure calculations. Thus, **1**′ acts as an electron donor toward NACs.

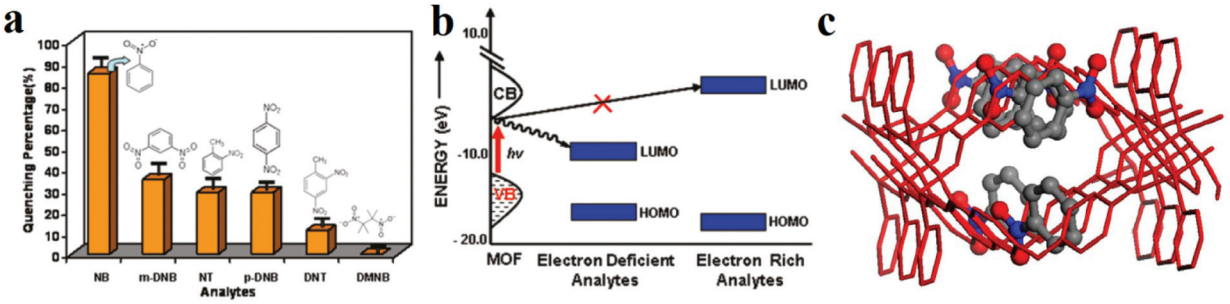

Fig. 1 Application of $[Zn_2(oba)_2(bpy)]\cdot DMA$ (**1**) in the detection of NACs. (a) Percentage of fluorescence quenching after 15 min by five different NAC analytes at room temperature. (b) Schematic of the electronic structure of the fluorescence quenching process by NAC analytes containing electron-withdrawing functional groups. (c) Simulated structure of **1′** with nitrobenzene. Reproduced with permission from ref. 30.

In other work, the same authors reported that $[Zn_2(bpdc)_2(bpee)]$ (bpdc = 4,4′-biphenyldicarboxylate; bpee = 1,2-bipyridylethene) is capable of very fast and fully reversible detection of both 2,4-dinitrotoluene (DNT) and 2,3-dimethyl-2,3-dinitrobutane (DMNB) in the vapor phase.[31]

Since the publication of these two pioneering studies by Li and coworkers in 2009 and 2011, extensive amounts of research have been conducted on the detection of NACs by MOFs. Based on a review of the published papers in this area, most papers focus on the detection of nitrobenzene in the presence of other small organic molecules and solvents[32–84] as well as the detection of 2,4,6-trinitrophenol (TNP).[28,33,34,40,79,85–175] In other examples, efficient quenching responses were achieved toward other NACs, such as 2,4,6-trinitrotoluene (TNT),[176–183] 4-nitrophenol (4-NP),[38,115,136,184–193] 2,4-dinitrophenol (2,4-DNP),[56,194–197] 4-nitrotoluene (4-NT),[198,199] 2-nitrotoluene (2-NT),[54,200–202] 4-nitroaniline (4-NA),[203–216] 1,3-dinitrobenzene (1,3-DNB),[87,217–220] 3,4-dinitrotoluene (3,4-DNT),[221,222] 2,4-dinitrophenylhydrazine,[223] nitromethane,[44,224–226] 2,3-dimethyl-2,3-dinitrobutane,[31,227] 3,4-dinitrotoluene (2,4-DNT),[228,229] 1,3,5-trinitrobenzene (1,3,5-TNB),[230] 4-nitrophenylhydrazine,[207] 2,4-dinitrophenylhydrazine,[231] 4-nitrobenzoic acid,[232] methyl-4-nitroaniline,[215,233] 2-nitrophenol (2-NP)[234] and 2,4-dinitrophenol (2,4-DNP).[235] Also, in some cases, MOFs can detect different NACs.[44–46,49,51,64,87,119,131,173,176,218,236–274] On the other hand, although NACs have low vapor pressure, some papers focus on the detection of NACs in the vapor phase.[115,218,224,237,242–244,275–280] To gain deeper insight into the detection mechanism of NACs, some researchers have conducted computational simulations to compare the energy levels of NACs and MOFs[42,50,52,57,61,67,87,96,111,114,128,131,224,243,262,268,281–293] and recognize possible host–guest interactions[29,282,294–296].

As a result of these studies, some successes have been gained, including selective detection of nitrobenzene in the liquid phase in the presence of other small organic molecules and selective detection of TNP in the liquid phase. Also, because there are many investigations of TNP, we can compare the Stern–Volmer constants of the applied MOFs to evaluate which structure is useful for the detection of TNP. However, there are serious challenges in this area, including selective detection of NACs in the presence of each other and selective detection of NACs in aquatic media and the vapor phase. In this section, we intend to summarize these successes and suggest possible solutions to these challenges.

Nitrobenzene (NB) is the simplest NAC; it is applied extensively in industry for the production of aniline, other NACs and paint solvent. Because NB is highly toxic and can be absorbed through skin, it should be detected rapidly. Therefore, selective detection of NB against other small organic molecules with different functionalities has been extensively studied using MOFs. For this purpose, different MOFs have been applied. Because NB is an electron deficient molecule containing nitro groups, two strategies can be useful for its PL-based detection by MOFs, including: (I) decoration of MOFs with electron rich groups that can interact with NB through π–π interactions[297] and (II) functionalization of MOFs with hydrogen bond donor groups such as urea[219] to interact with nitro groups though hydrogen bonding.

Moon and coworkers synthesized a well-designed MOF with the formula $[Li_3[Li(DMF)_2](CPMA)_2]\cdot 4DMF\cdot H_2O$, where H_2CPMA is bis(4-carboxyphenyl)-*N*-methylamine (Fig. 2).[297] The ligand H_2CPMA is functionalized with electron-donor methyl groups, which are potentially useful for the detection of electron-deficient analytes. Applications show that this MOF presents a distinctive color change from yellow to red and complete quenching in the presence of nitrobenzene, while there is no specific change in the UV-vis or PL spectrum in the presence of benzene or toluene. Based on computational simulations, these sharp changes in the UV-vis and PL spectra after exposure to nitrobenzene are due to charge-transfer transitions between the aromatic rings of the electron-rich $CPMA^{2-}$ molecules and the electron-deficient nitrobenzene due to strong $(CPMA^{2-})\pi\cdots\pi(NB)$ and $(CPMA^{2-})C–H\cdots\pi(NB)$ interactions between trapped nitrobenzene molecules inside the pores, where two benzene rings belonging to neighboring $CPMA^{2-}$ linkers provide situations in which electron-deficient nitrobenzene can act as an electron acceptor for the photo-excited electrons of the MOF, resulting in electron transfer from the MOF to nitrobenzene.

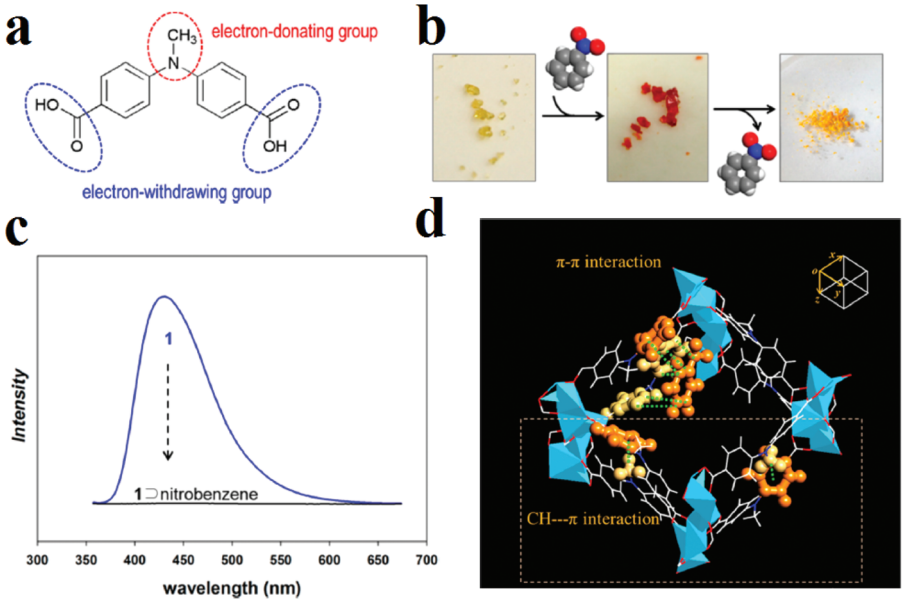

Fig. 2 Application of the $[Li_3[Li(DMF)_2](CPMA)_2]\cdot 4DMF\cdot H_2O$ framework in the detection of nitrobenzene. (a) Schematic structure of the organic ligand H_2CPMA. (b) Color change of the MOF in the presence of nitrobenzene. (c) Fluorescence spectrum of nitrobenzene@MOF. (d) X-ray structure of nitrobenzene@MOF, in which π–π and C–H···π interactions are emphasized by orange ball-and-stick representations (color scheme: C, white; O, red; N, blue; Li, light blue). Reproduced with permission from ref. 297.

In other work, Chang and coworkers synthesized a MOF, $[NH_2(CH_3)_2]_2[Cd_{17}(L)_{12}(m^3\text{-}H_2O)_4(DMF)_2(H_2O)_2]\cdot S$ (S indicates solvent), where the H_3L ligand is 2,4,6-tris[1-(3-carboxylphenoxy)ylmethyl]mesitylene, for detection of NB molecules in the vapor phase.[218] Nitrobenzene quenches the emission by as much as 77.5% in a time of 490 s. Also, the quenching phenomenon in the solid state is consistent with that realized in the liquid sensing process; this indicates that the quenching mechanism is based on the nature of the complex rather than the testing environment.

In other work, we applied a functionalization strategy for selective detection of NACs over other molecules (Fig. 3).[219] In this line, we synthesized urea-decorated TMU-31 ($[Zn(L_1)(L_2)]\cdot DMF$) and TMU-32 ($[Zn(oba)(L_2)]\cdot 2DMF\cdot H_2O$) frameworks ($H_2L_1$, H_2L_2 and H_2OBA are 4,4′-(carbonylbis(azanediyl))dibenzoic acid, 1,3-di(pyridin-4-yl)urea and 4,4′-oxybis (benzoic acid), respectively) and then applied them in the detection of NACs. Selective NACs detection was achieved through enriched host–guest chemistry by urea(NH)···(O–N═O)NAC hydrogen bonding. This is an example of selective detection of NACs in the presence of other organic molecules by a functionalization strategy.

A summary of the results of computational simulations of host–guest interactions between NB and MOFs shows that π-deficient (NB)···π-rich (MOF) and π (NB)···(C–H)MOF interactions play critical roles in the host–guest chemistry of NB and the host MOFs. On the other hand, simulation calculations reveal that the LUMO energy level of NB lies below the energy levels of the conduction bands of the MOFs.[42,50,52,61,162,176,243,281,282] Also, cyclic voltammetry measurements demonstrate that the reduction potential of NB is more positive than that of MOFs, indicating that the MOFs can act as electron donors and NB can act as an electron acceptor.[30,40] These well-matching experimental data and simulation calculations can help us to propose a general mechanism for the detection of NB by MOFs.

Theoretical and experimental results demonstrate that the nitro group is the main cause of the quenching effect in the detection of NACs. Due to the presence of nitro groups, the π* lowest unoccupied molecular orbitals (LUMOs) of nitrobenzene are stabilized through conjugation effects so that the LUMO of nitrobenzene usually lies lower than the LUMO of the π-rich aromatic ligand or the MOF network. Generally speaking, for electron-deficient NACs, their LUMO energy levels lie between the conduction band and valence band of the MOFs. Due to possible π–π and π-(CH) host–guest interactions, the MOFs and NB can interact with each other, and overlap is possible between the conduction band of the MOF and the LUMO of nitrobenzene.[30,294] After irradiation of light photons and migration of electrons from the valence band of the MOF to the conduction band, these excited electrons transfer from the conduction band of the MOF to the LUMO orbitals of NB through a photo-induced electron transfer (PIET) process. As a result, the PL spectrum of the MOF presents quenching signal transduction in the presence of NB.

2,4,6-Trinitrophenol (TNP) is another NAC that is widely applied in metallurgy and in the pharmaceutical industry as an antiseptic. Moreover, TNP is widely used in dyes, fireworks, matches, and the glass and leather industries. TNP is one of the most acidic phenols; it is explosive, like other highly nitrated organic compounds. As a result, TNP is another NAC whose detection has been widely investigated in the literature.

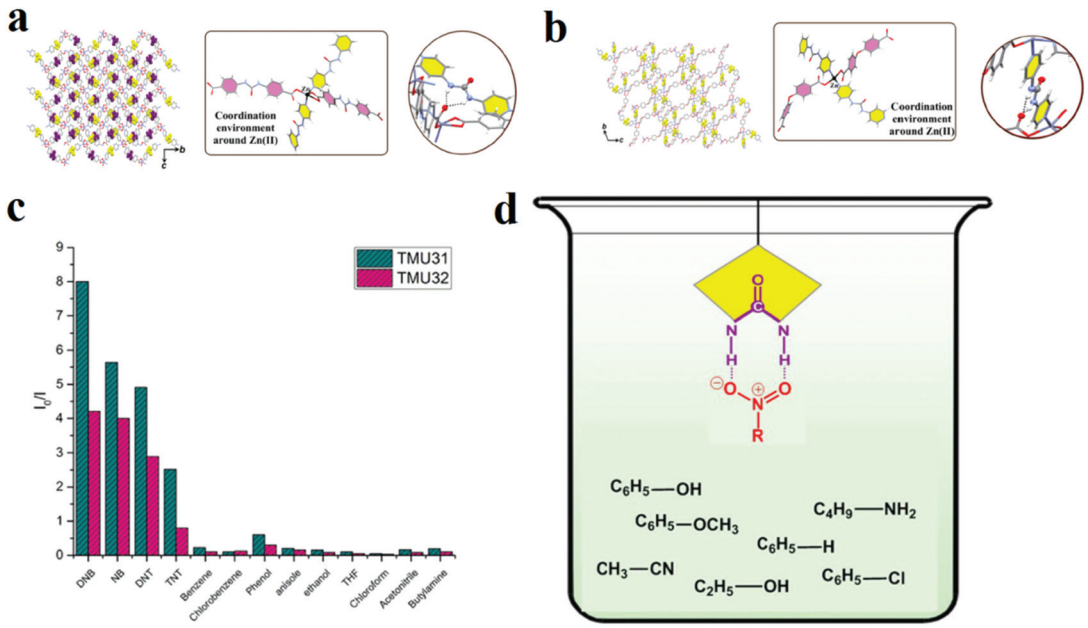

Fig. 3 Application of TMU-31 and TMU-32 in the selective detection of NACs. Representation of the three-dimensional structure, the coordination environment around Zn(II), and the internetwork hydrogen bonding of TMU-31 (a) and TMU-32 (b). (c) Relative fluorescence responses of TMU-31 and TMU-32 to 60 ppm of different organics in toluene. (d) Possible host–guest chemistry between urea-decorated TMU-31 and TMU-31 frameworks and NACs. Reproduced with permission from ref. 219.

Ghosh and coworkers synthesized $[Cd(NDC)_{0.5}(PCA)]\cdot G_x$ (G is the guest molecule, H_2NDC = 2,6-napthalenedicarboxylic acid, and HPCA = 4-pyridinecaboxylic acid) for selective detection of TNP over other NACs in aquatic media (Fig. 4).[95] Computational calculations of the HOMO and LUMO orbital energies of the NACs were in good agreement with the maximum quenching observed for TNP. The order of the observed quenching efficiency is not fully in accordance with the LUMO energies of other nitro compounds. This indicates that photoinduced electron transfer is not the only mechanism of quenching. Non-linear Stern–Volmer plots display that resonance energy transfer (REnT) can occur from MOFs to NACs. The combination of the emission spectrum of the MOF and the absorption band of TNP reveals a noticeable overlap between them, which confirms the possibility of simultaneous PIET and REnT processes.

It is necessary to mention that PL quenching by host–guest interactions between the fluorophores in MOF hosts and the NAC analytes is based on two different mechanisms: resonance energy transfer (REnT) and photoinduced electron transfer (PIET). The extension of REnT depends on the distance between the electronic excited state of the MOF and analyte as well as the spectral overlap between the emission spectrum of the MOF and the absorption band of the analyte, in which the excitation is transferred from a donor (MOF) to an acceptor (analyte) molecule without emission of photons. REnT is observed only when the emission spectrum of the MOF overlaps with the UV-Vis absorption band of the analyte. In these cases, REnT is probable, as well as the PIET mechanism. Also, there is another way to determine whether the REnT mechanism is possible. If the percentage of quenching in the presence of analyte shows the same trend as the energy

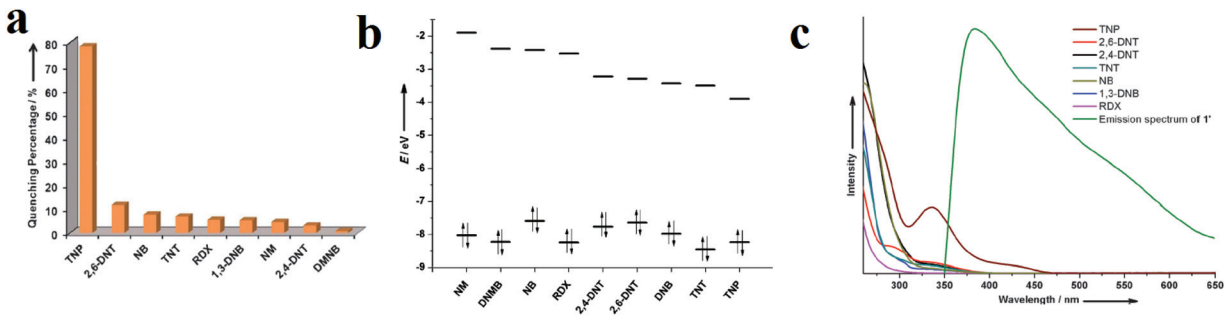

Fig. 4 Application of $[Cd(NDC)_{0.5}(PCA)]\cdot G_x$ in the detection of TNP. (a) Percentage of fluorescence quenching obtained for different analytes at room temperature. (b) HOMO and LUMO energies for explosive analytes arranged in descending order of LUMO energy. (c) Spectral overlap between the absorption spectra of the analytes and the emission spectrum of the MOF in MeCN. Reproduced with permission from ref. 95.

levels of the LUMO orbitals of the analytes, the probability of REnT is low. Otherwise, the possibility of this mechanism should be investigated.

Kwon and coworkers applied $(DMF)_x(H_2O)_y$@[In(OH)(H_2DOBDC)] (**1**; H_4DOBDC is 1,4-benzenedicarboxylic acid) for the detection of NACs in chloroform solutions and aquatic media (Fig. 5).[114] Framework **1** shows quenching responses toward TNP in both aquatic and chloroform solutions, with K_{SV} values (Stern–Volmer constants) of $1.65 \times 10^{+5}$ M^{-1} and $8.33 \times 10^{+4}$ M^{-1} in chloroform and water, respectively. Structural analyses and optimized simulation calculations reveal that a combination of hydrogen-bonding interactions (between the nitro and phenolic groups of TNP and the μ_2-hydroxyl group ligated to indium metal) and π–π stacking interactions (between π-deficient TNP and the π-rich $DOBDC^{2-}$ linker) are responsible for fluorescence quenching in chloroform. Using computational calculations and possible host–guest interactions, it is concluded that a ground-state

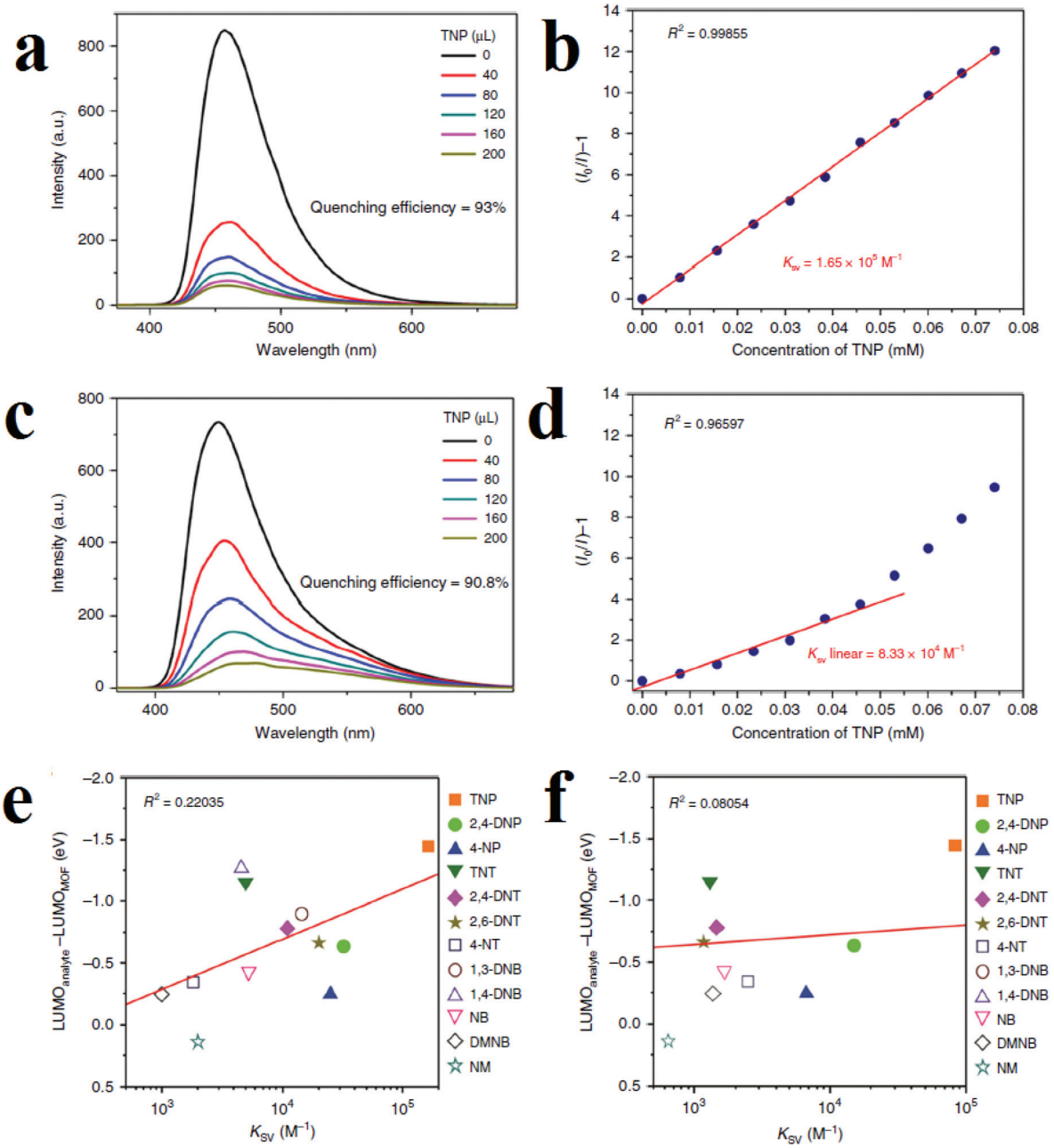

Fig. 5 Application of $(DMF)_x(H_2O)_y$@[In(OH)(H_2DOBDC)] in the detection of TNP. (a) Quenching in chloroform. (b) Stern–Volmer equation in chloroform. (c) Quenching in water. (d) Stern–Volmer equation in water. Correlation graphs for comparison of the trends of the K_{sv} values and the energy differences between the LUMO of the MOF and the LUMOs of the different analytes in chloroform (e) and water (f). Reproduced from open access ref. 114.

TNP@MOF complex is formed in chloroform in which the highest occupied molecular orbital (HOMO) resides only on the MOF fluorophore, whereas the LUMO resides mainly on the TNP. This observation shows that PIET probably operates in chloroform for the quenching of MOFs. Based on these results, the efficiency of the PIET not only depends on the energy difference between the LUMOs of the MOF and analyte, but also depends on the overlap of orbitals between the fluorophore and the analyte. However, spectral overlap between the emission band of the MOF and the UV-Vis absorption band of TNP reveals that REnT is involved in quenching of the MOF as well as the PIET process, which is in accordance with the low linearity of the Stern–Volmer equation in water. The authors illustrated a graph based on the K_{SV} values and the difference in energy levels of the LUMO orbitals of the MOF and analytes ($E_{LUMO}^{analyte} - E_{LUMO}^{MOF}$ (eV)). It is clear that with increasing magnitude of the energy difference, K_{SV} increases.

Using electron-rich MOFs decorated with different Lewis basic functions, such as azine, amine, guanidine, triazole and pyridine, is a good strategy for selective detection of picric acid. This is because in the chemical skeleton of picric acid: (I) the presence of three nitro groups leads to high electron deficiency of the aromatic ring and good electron-accepting ability during the formation of charge transfer donor–acceptor adducts; and (II) the presence of –OH groups enriches the host–guest chemistry and establishes hydrogen bond interactions with the Lewis base-decorated MOFs. Ghosh and coworkers applied adenine-based bio-MOF-1 ($[Zn_8(adenine)_4(BPDC)_6O_2Me_2NH_2]\cdot G$, where H_2BPDC is biphenyl dicarboxylic acid) in the selective detection of picric acid, among other NACs (Fig. 6).[296] The reason for this selective response to picric acid over other NACs is based on hydrogen bond host–guest interactions between the (–OH) group of picric acid and the ($-NH_2$) group of bio-MOF-1. Also, they noted that in addition to hydrogen bonding, the overlap between the absorption band of picric acid and the emission band of bio-MOF-1 is effective in sensitization of the framework toward picric acid through possible resonance energy transfer.

Designing functional MOFs is highly beneficial for detection of NACs, especially those containing functional groups such as (–OH) in phenolic NACs and ($-NH_2$) in aniline NACs as well as the $-NO_2$ groups in the molecular skeletons of all NACs. Investigations reveal that (I) replacement of the benzene moiety of the ligand by a more extended motif, such as a naphthalene,[299] anthracene, or pyrene moiety, for better π–π stacking interactions, (II) decoration of the framework with electron-rich groups such as methyl groups for better donor–acceptor interactions, and (III) introduction of a functional group capable of strong hydrogen-bonding interactions with the analyte, such as urea and amine, are powerful approaches for further enhancing the sensing efficiency of MOFs toward NACs.

One of the most important factors that a sensor is evaluated by is its Stern–Volmer constant (K_{SV}). Investigations of the values of K_{SV} for the detection of TNP by MOFs show that this value is usually in the range of 10^{+4} to 10^{+5} M^{-1}. In some cases, such as triazine-functionalized $[Cd(ATAIA)]\cdot 4H_2O$

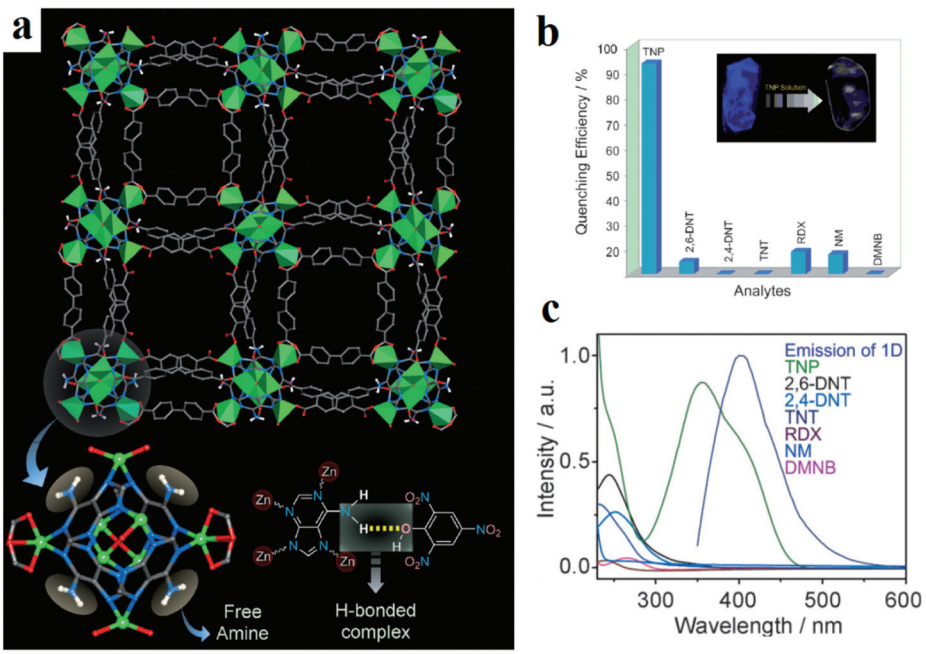

Fig. 6 Application of bio-MOF-1 in the selective detection of picric acid. (a) Crystal structure of bio-MOF-1 showing 1D channels along the *c* crystallographic direction and a plausible H-bonding interaction between adenine and picric acid. (b) Quenching efficiency of bio-MOF-1 for different nitro analytes. (c) Spectral overlaps between the absorption bands of the analytes and the emission band of bio-MOF-1. Reproduced with permission from ref. 296.

(H_2ATAIA = 5-((4,6-diamino-1,3,5-triazin-2-yl)amino)isophthalic acid)[300] and triazole-functionalized $[Me_2NH_2]_4[Zn6(qptc)_3(trz)_4]\cdot 6H_2O$ (H_4qptc = terphenyl-2,5,2′5′-tetracarboxylic acid, trz = 1,2,4-triazole),[103] the K_{SV} values reached levels of 10^{+6} to 10^{+7}. These examples clearly show that construction of MOFs based on d^{10} metal ions and Lewis basic functional ligands is a very practical strategy for selective detection of TNP. Similar results were observed in the case of the TNP detection limit. Usually, the detection limit of MOFs toward TNP is in the range of 10^{-3} to 10^{-8} M. However, in cases with d^{10}-metal ions and Lewis basic functional groups, such as adenine-decorated $[Zn(\mu_2\text{-1H-ade})(\mu_2\text{-}SO_4)]$ (1H-ade is adenine)[168] and $[Zn_8(ad)_4(BPDC)_6O_2Me_2NH_2]\cdot G$ (where G is the guest, ad is adenine and H_2BPDC is biphenyl dicarboxylic acid)[301] and amine-decorated $[Cd(ATAIA)]\cdot 4H_2O$ (5-((4,6-diamino-1,3,5-triazin-2-yl)amino)isophthalic acid),[300] the detection limit reaches 10^{-9} M. These observations of the detection limit and K_{SV} for the detection of TNP show that Lewis basic functionalized MOFs with d^{10} metal centers are promising probes for the luminescent detection of TNP.

In the above, we mentioned and summarized some successes achieved in the detection of NB and TNP using MOFs or functional MOFs by PL methods. However, some challenges still require more investigation. The most important challenge is the detection of NACs in the presence of other NACs. Some strategies applied to overcome this challenge include (I) fabrication of sensitized MOFs or MOF-based composites toward a specific NAC, (II) synthesis of MOFs sensitive to a specific group of NACs and (III) synthesis of multi-responsive MOFs to different NACs.

For highly selective and sensitive detection of TNP in the presence of other NACs and VOCs, we sensitized azine-decorated TMU-5 ($[Zn(OBA)(BPDH)_{0.5}]_n\cdot 1.5DMF$, where H_2OBA and BPDH are 4,4′-oxybis(benzoic acid) and 2,5-bis(4-pyridyl)-3,4-diaza-2,4-hexadiene), with rhodamine dye to obtain a dual emissive Rhb@TMU-5 composite (Fig. 7).[108] Rhb@TMU-5 contains two emissive components, namely Rhb at 583 nm and TMU-5 at 485 nm. Because Rhb@TMU-5 is dual emissive from different centers, it was applied as a ratiometric sensor for detection of TNP by definition of the ratio of ($I_{583(Rhb)}/I_{483(TMU\text{-}5)}$) as the signal. Due to hydrogen bonding between the azine functional groups of TMU-5 and the hydroxyl group of TNP, the PL emission centered at 483 related to TMU-5 experiences quenching, while there is no specific change in the PL emission of Rhb centered at 583 nm. Therefore, as a 2D response toward TNP, the I_{583}/I_{485} ratio increased from 2.3 to 5.1 (2.2 times higher). It is necessary to mention that the TMU-5 framework presents different responses in the presence of NACs. Considering the selective response of Rhb@TMU-5 toward TNP, it can be concluded that the encapsulation of Rhb dyes by TMU-5 is a beneficial strategy for the sensitization of MOFs toward specific NACs. The same strategy was applied by our group for the detection of 4-nitroaniline over other NACs.[203] In other work, the same strategy was applied for selective detection of TNP in the presence of other NACs.[91]

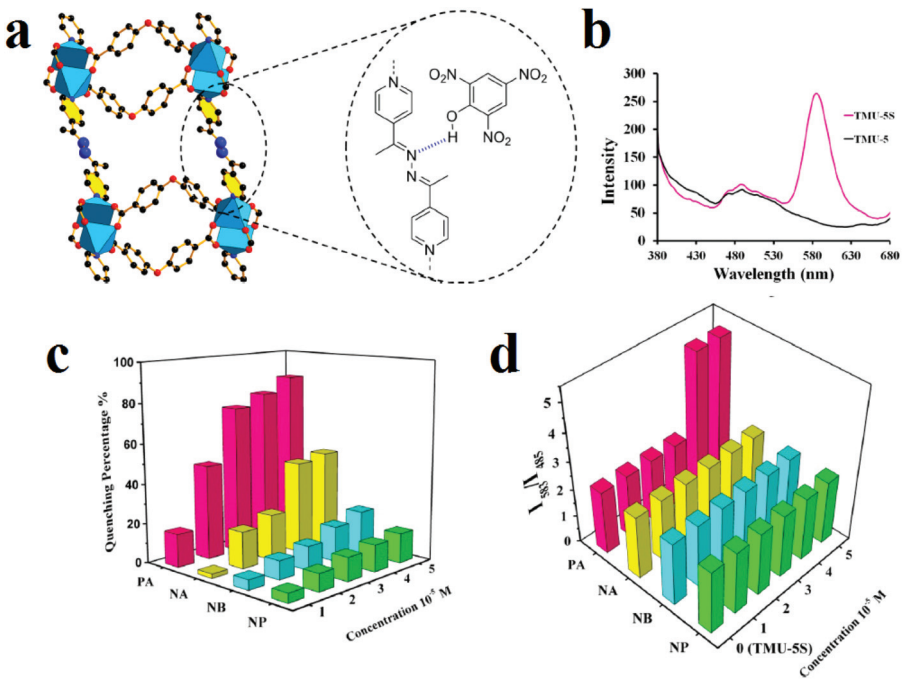

Fig. 7 Application of RhB@TMU-5 composite in the 2D detection of picric acid. (a) Azine-decorated pores of TMU-5 and hydrogen bonding interactions between TNP and TMU-5. (b) Emission spectra of TMU-5 and Rhb@TMU-5 dispersed in acetonitrile upon excitation at 355 nm. Comparisons of the responses of TMU-5 (c) and RhB@TMU-5 (d) in the presence of different nitroaromatic analytes at different concentrations. Reproduced with permission from ref. 108.

Encapsulation of Rhb dyes by TMU-5 is beneficial for discrimination between response and sensitivity as well as selective sensitization toward TNP. In most luminescent MOF sensors, the response is based on quenching or enhancement of the emission intensity upon guest adsorption. The resulting sensor response can be observed by introduction of any analyte to any compound as a sensor; this is usually insufficient for accurate and sensitive detection of a specific analyte. However, only selectivity and not sensitivity can be achieved by this type of signal transduction.[108] In MOF-based sensors, the response (quenching efficiency) is usually defined with eqn (1) as follows:[108]

$$\text{Quenching efficiency} = (I - I_0)/I_0 \quad (1)$$

whereas the sensitivity is defined with eqn (2):[108]

$$\text{Sensitivity} = (R - R_0)/R_0 \quad (2)$$

In these two equations, I and I_0 are the PL intensities before and after addition of analyte; R_0 is the initial response of the sensor and R is the response of the sensor in the presence of the desired analyte.

For RhB@TMU-5, R and R_0 are I_{583}/I_{485} and I^0_{583}/I^0_{485}, which are equal to 5.1 and 2.3, respectively. Therefore, the sensitivity toward TNP is equal to 1.2. Because there is no specific change in the PL intensity of Rhb@TMU-5 in the presence of other NACs, R and R_0 are equal to 2.3 for other NACs. Thus, the sensitivity toward other NACs is equal to 0. However, based on TMU-5, NACs present different quenching efficiencies. Therefore, for TMU-5, the sensor responses with respect to the analyte concentration remain irregular. Thus, it is clear that direct application of I and I_0 will result in low accuracy and precision. I and I_0 can be changed to R and R_0 by self-calibration relative to another emissive component by rendering the singular emissive LMOF as a dual emissive ratiometric sensor. This work is among the extremely rare examples which clearly explain the difference between response and sensitivity.[108]

It is necessary to mention that PL signal transductions and responses in the presence of analytes can be classified in two groups: 1-dimensional (1D) response and 2D response (Scheme 1). 1D responses are based on changes only in the intensity or in the wavelength of the PL emission of the host MOF. A 2D response can be observed based on two different strategies. The first strategy is based on using dual-emissive MOFs with different PL emissive centers as self-calibrating ratiometric sensors. The second strategy is based on a combination of 1D responses (such as changes in intensity and wavelength) in different 2D maps.

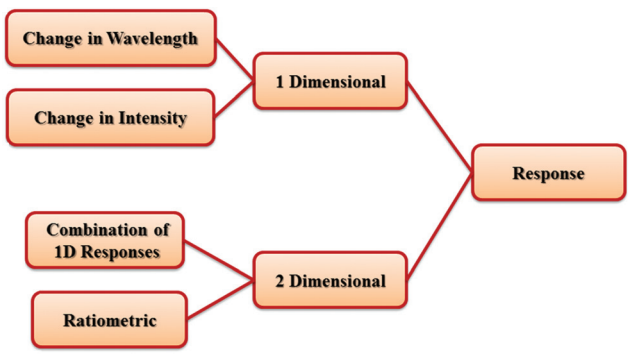

Scheme 1 Different responses of MOFs in the presence of different organic analytes.

Owing to complexities in the skeletons of NACs because of complicated effects of the number and position of nitro groups as well as the effects of other groups, such as –OH, $–NH_2$ and $–CH_3$, on the host–guest chemistry and molecular energy levels of NACs, it is almost impossible to find a generalized trend in the quenching response toward NACs. Li and coworkers applied a novel strategy for the selective detection of NACs among each other based on the construction of two-dimensional (2D) intensity-wavelength curves. This 2D curve illustrates the changes in the intensity and shifts in the wavelength of the of PL emission peak of the host MOF (Fig. 8).[227] The MOF $[Zn_2(ndc)_2P{\cdot}xG]$, where ndc is 2,6-naphthalenedicarboxylate and P is 1,2-bis(4-pyridyl)-ethylene, exhibit a two-dimensional signal response (changes in both intensity and wavelength) toward the analytes of interest in the vapor phase, including aromatic and aliphatic high explosives. Because the LUMO levels of the NAC analytes are lower in energy than the conduction band of the MOF, the interaction between the NAC and MOF will push the conduction band up, leading to a small increase in the band gap and, thereby, a blue shift in the PL emission. MOFs with different structures have different energy levels, and the extent of their interactions with different analytes will vary. Also, the degree of quenching in the presence of NACs is related to their interaction strength and the efficiency of photo-induced MOF-to-NAC electron transfer.

Another strategy for selective detection of a specific NAC is the colorimetric method. For example, $[Li]_4[Cd_3Li_2(BDC)_6]$ (H_2BDC = terphthalic acid) is a selective colorimetric sensor toward trinitrobenzene[230] and $[Zn(bpeb)_{0.5}(tcpb)_{0.5}]{\cdot}G$ (G stands for guest, (bpeb = 1,4-bis [2-(4-pyridyl)ethenyl]benzene and H_4tcpb = 1,2,4,5-tetrakis(4-carboxyphenyl)benzene) is a selective colorimetric sensor toward TNP.[99] Some papers reported MOF-based sensors which can selectively detect specific groups of NACs, such as phenolic[245,302–305] and toluene-based[64] NACs.

Designing multi-responsive MOFs toward NACs is another interesting methodology to overcome the challenge of selective detection of NACs among each other.[87,230,252] Construction of these MOF-based sensors requires the right choice of organic linker and metal ion. Su and coworkers developed a 2D MOF based on flexible 4,4′,4″-((2,2′,2″-(nitrilotris(methylene))tris(1*H*-benzo[*d*]imidazole-2,1-diyl))tris(methylene))tribenzoic acid ligand (H_3L) and Cd(II) metal ions, named NENU-503, with the formula $[Cd_2Cl(H_2O)(L)]{\cdot}4.5DMA$ (Fig. 9).[87] A flexible ligand was chosen because ligand flexibility can facilitate efficient excitation migration between MOFs and electron-deficient NACs. A d^{10} metal ion was selected because the selected metal ion cannot interfere in the PL behavior of the ligand. NENU-503 shows a ligand-based PL emission peak which is

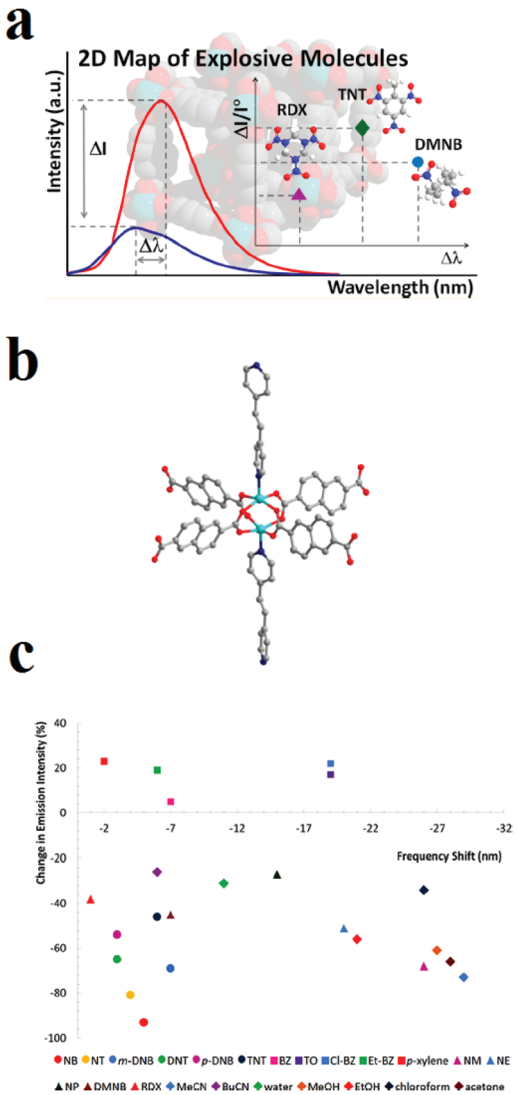

Fig. 8 Application of $[Zn_2(ndc)_2P{\cdot}xG]$ in luminescent 2D sensing of NACs. (a) Illustration of the 2D intensity-wavelength curve. (b) Ball and stick model of the paddle-wheel SBU (Zn: aqua; O: red; N: blue; C: gray). (c) A 2D (color-coded) map of analyte recognition. Reproduced with permission from ref. 227.

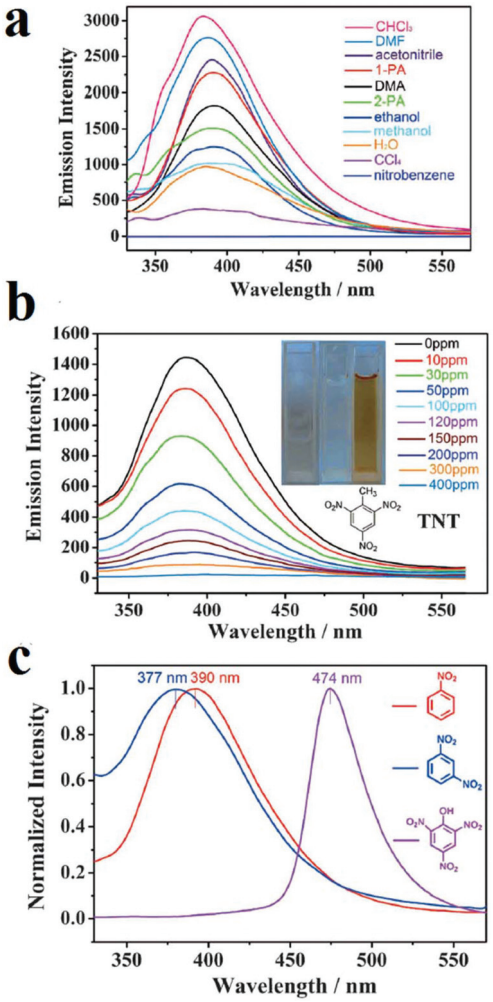

Fig. 9 Application of NENU-503 in the selective detection of NACs. (a) Quenching of NENU-503 in the presence of nitrobenzene. (b) Colorimetric detection of TNT. (c) PL emission shifts in the presence of TNP, DNB and NB. Reproduced with permission from ref. 87.

highly dependent on the solvent. Investigations showed that NENU-503 shows complete quenching behavior in nitrobenzene. This fluorescence quenching arises because of electron transfer from the electron-donating framework to the highly electron-deficient nitrobenzene molecule due to the presence of nitro groups. In next steps, NENU-503 was applied in the detection of other NACs, including 1,3-dinitrobenzene (DNB), 2,4-dinitrophenol (DNP), 2,4,6-trinitrotluene (TNT) and 2,4,6-trinitrophenol (TNP), in DMA solvent. The lowest concentrations of complete quenching were 300 ppm for DNB and DNT and 400 ppm for TNT and TNP. Interestingly, NENU-503 showed a color change upon exposure to TNT, which can be ascribed to the formation of charge-transfer complexes between NENU-503 and TNT. The PL measurements show that the emission peak of NENU-503 experienced a 13 nm blue-shift and an 84 nm red-shift in the presence of DNB and TNP, respectively. The shifts of the PL spectra may be due to the formation of exciplexes (excited complexes) by the interaction of the analytes and MOFs in excited states. Due to these different responses, including color changes and changes in intensity and wavelength, NENU-503 can sense NACs with different methods; this can be considered as an interesting strategy for the selective detection of one NAC in the presence of other nitro-containing analytes.

Here, we have described some strategies for the selective detection of specific NACs against other NACs, such as fabrication of multi-responsive MOFs, colorimetric MOF-based sensors and sensitized MOFs toward specific NACs. However, more investigation in this regard is needed to address the mentioned challenges.

Numerous investigations have been conducted to understand the nature of the quenching response of MOFs toward NACs. However, there are some misunderstandings in this

area. Here, we summarize the findings from these mechanistic studies. As mentioned, for NACs, the LUMO is a low-lying π*-type orbital, and its energy is below the conduction band of the host MOF. This allows charge transfer from the MOF to the analyte upon photoexcitation, leading to fluorescence quenching, which is a very normal response in the detection of NACs. Also, this turn-off behavior can be explained using experimental methods such as cyclic voltammetry. Cyclic voltammetry studies show that NAC analytes have more positive reduction potentials than the host framework. As a result, the host framework acts as an electron donor in the case of NACs.

After diffusion of NACs into the pores of the MOF and interaction with possible guest interactive sites, an NAC@MOF complex can be formed. Based on computational calculations, the HOMO of the complex resides only on the fluorophore MOF, whereas the LUMO resides mainly on the analytes. The higher overlaps between the orbitals of the fluorophore MOF and the NAC result in a more efficient PIET mechanism. The overlap of orbitals that leads to efficient PIET is better when the complexation between the MOF and analyte is stronger. Another effective parameter affecting the efficiency of the PIET mechanism is the difference in the energy levels of the LUMOs of the MOF and analyte. If the order of observed quenching efficiency is fully in accordance with the LUMO energies of other nitro compounds, it can be deduced that PIET is the only mechanism of quenching.

Another mechanism that may be involved in the quenching response of MOFs toward NACs is REnT or competitive adsorption. If the emission spectrum of the MOF overlaps with the UV-Vis absorption band of the NAC, REnT is possible, and if the excitation spectrum of the MOF overlaps with the UV-Vis absorption band of the NAC, competitive absorption is possible. In this situation, the quenching efficiency is not fully in accordance with the LUMO energies of other nitro compounds.

Other mechanisms that must be discussed are based on static (ground state complex-formation) and dynamic (collisional) mechanisms. Quenching occurs when the excited fluorophore contacts an atom or molecules that can facilitate non-radiative transitions to the ground state. Collisional quenching of fluorescence is described by the Stern–Volmer equation ($I/I_0 = 1 + K_{SV}[M]$). In the static mechanism, quenching can also occur as a result of the formation of a nonfluorescent ground-state complex between the fluorophore and quencher. When this complex absorbs light, it immediately returns to the ground state without emission of a photon. Static quenching of fluorescence is described by a formula very similar to the Stern–Volmer (SV) equation ($I/I_0 = 1 + K[M]$). Therefore, it can be concluded that good matching of fluorescence data with the SV equation is not evidence of a dynamic mechanism; however, it indicates that only one mechanism, static or dynamic, is involved. However, if the SV-linearity is not good, it can be concluded that both static and dynamic mechanics are involved. A powerful method for differentiation between static and dynamic mechanisms is PL lifetime spectroscopy. For the static mechanism, the average PL lifetimes are very similar before and after exposure to the analyte; meanwhile, for the dynamic mechanism with turn-off response, the average lifetime will decrease after exposure to the analyte. This is because in the static mechanism, formation of the analyte (quencher)–fluorophore complex leads to a non-fluorescent complex. Therefore, the observed fluorescence arises from the non-fluorescent complex. However, in the dynamic mechanism, the collision between the analyte and fluorophore depopulates the excited state, which results in decreased lifetime decay.

The presence of electron-withdrawing nitro groups in the molecular skeleton and the electron accepting nature of NACs endows the NACs with an oxidizing nature in electrochemical methods, as do electron acceptor guests in photoluminescence methods. Therefore, MOFs or MOF-based composites can be applied in electrochemical detection of NACs. Although some research has been conducted in this regard,[306,307] this field clearly requires more investigation.

Gunasekaran and coworkers applied ZIF-8 ($[Zn(MeIm)_2]$, where MeIM is 2-methylimidazolate) for electrochemical detection of TNT in aquatic media (Fig. 10).[307] Using cyclic voltammetry (CV), they showed that TNT is initially adsorbed at the surface-active sites of a ZIF-8-modified electrode by a diffusion-controlled electrocatalytic process. Also, an amperometric response (i–t) was applied to select the detection potential based on the reduction peak current (i–t method) of TNT by the ZIF-8-modified electrode. The results revealed that applied potentials ranging from −0.40 to −0.85 V accelerated the reduction current, providing the best TNT reduction values. The maximum response current with a good signal/noise ratio was achieved at −0.8 V. Thus, a constant potential of −0.8 V was chosen for further amperometric investigations. Electrochemical pulse amperometry of the ZIF-8 modified electrode at the fixed potential (−0.8 V) exhibited that the peak reduction current density was proportional to the TNT concentration. The differential pulse voltammetry (DPV) voltammograms revealed three well-defined redox processes at −0.40, −0.59, and −0.76 V, reflecting the stepwise reduction of the three nitro groups present in TNT. After the reduction of the first nitro group, the parent symmetry of the TNT molecules will change. This is reflected in the characteristic DPV signals, where each successive peak appears at a more negative potential. The first DPV signal at −0.40 V, displaying the most favorable characteristics, was selected to construct the TNT detection calibration plot. The DPV data were also used to determine the linear range (1 to 460×10^{-9} M), sensitivity (6.94 μA nm^{-1} cm^{-2}) and limit of detection (LOD) (346×10^{-12} M) of the ZIF-8 sensor. The interaction between the electron-deficient aromatic core of TNT and the electron-rich ZIF-8 is considered to favor the occurrence of a donor–acceptor electron-transfer mechanism, and the electron conductivity of ZIF-8 facilitates the effective reduction of TNT.

Comparison of the limits of detection of TNT achieved by photoluminescence and electrochemical methods reveals that although PL methods are easier to operate, electrochemical methods afford lower detection limits.

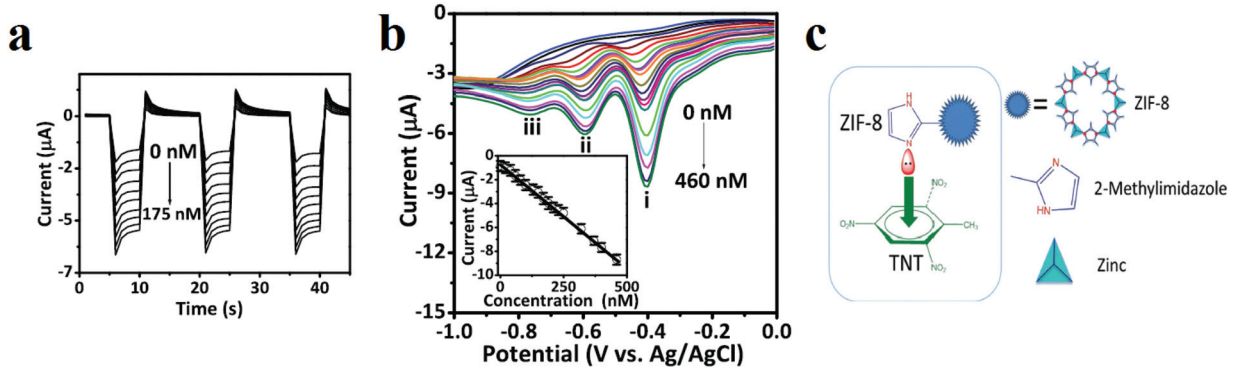

Fig. 10 Application of a ZIF-8-modified electrode in TNT detection. (a) Pulsed amperometric responses (n = 3) of the ZIF-8-modified electrode to different TNT concentrations ($E1$ = 0 V for 5 s, $E2$ = −0.8 V for 5 s, and $E3$ = 0 V for 5 s). (b) DPVs with varying concentrations of TNT at a ZIF-8-modified electrode. The inset displays the calibration curve [I (μA) = −0.0174 to 0.6249 C_{TNT} (×10^{-9} m), R^2 = 0.9981]. DPV parameters: peak width = 0.2 s; pulse period = 0.5 s; increment = 10 mV. (c) Schematic of the charge transfer complex interactions between ZIF-8 and the TNT molecule. Reproduced with permission from ref. 307.

Overall, MOFs are applied for the detection of NACs using photoluminescence and electrochemical methods. NACs are compounds that contain electron withdrawing groups, which results in electron deficiency in the molecular structures of the NACs. As a result of this electron deficiency, NACs can act as electron acceptors in both electrochemical and photoluminescence methods. On the other hand, due to their conjugated π-extended aromatic frameworks, MOFs can be applied in electrochemical and photoluminescence methods. As a result, NACs have been detected using MOFs by both of these methods. However, due to their facile operation, PL methods are applied extensively for the detection of NACs. However, the results of electrochemical methods clearly show that these methods have very great potential to achieve very low detection limits in the selective and sensitive detection of NACs. At any rate, more investigations are necessary to detect NACs by electrochemical methods as well as to remove the barriers of selective detection of NACs in PL methods.

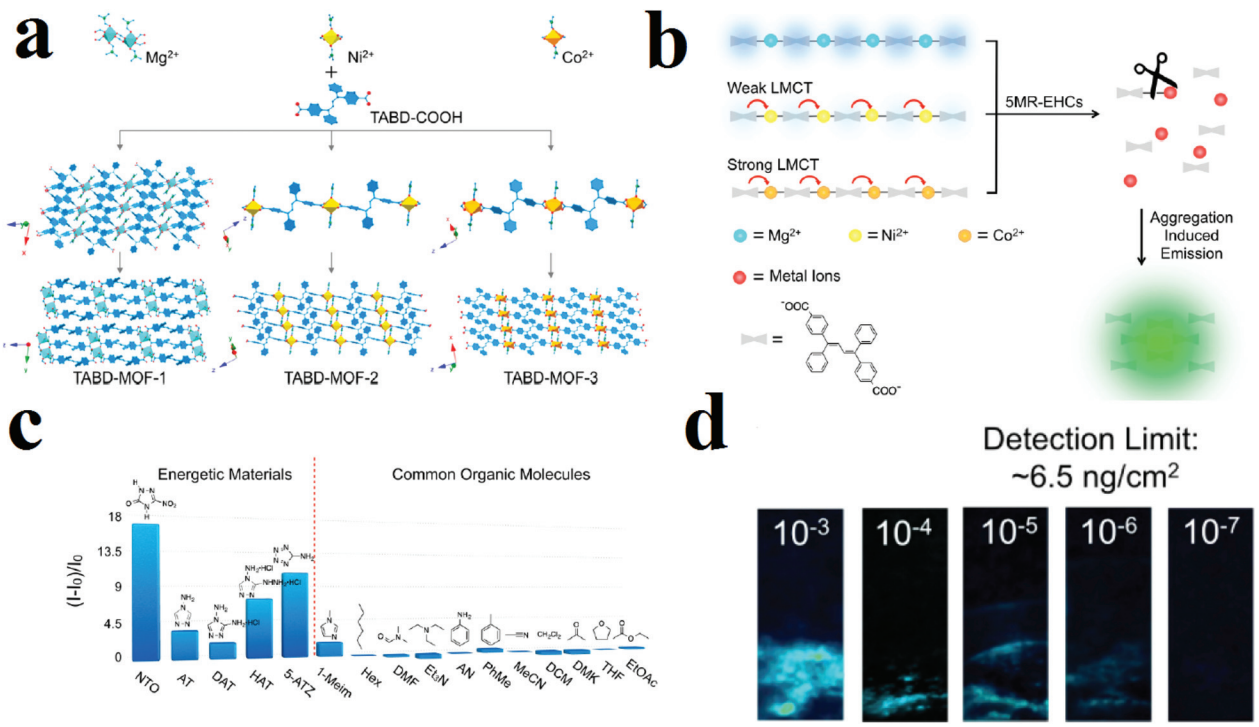

Fig. 11 Application of structures of TABD-MOFs in the detection of 5-MR-EHCs. (a) Structural representation of TABD-MOFs. (b) AIE mechanism of 5-MR-EHCs detection. (c) PL turn-on behavior of TABD-MOF-3 in the presence of 5-MR-EHCs. (d) Photographs of the visual detection limit of TABD-MOF-3. Reproduced with permission from ref. 308.

Another group of energetic materials are based on N-heterocyclic azole molecules, such as RDX (1,3,5-trinitro-1,3,5-triazinane). These molecules are explosive because they have high amounts of C–N, C═N, and N═N energetic bonds. Therefore, MOFs have been applied to detect these energetic molecules using PL methods.[308,309]

Commonly, the luminescence behavior of MOFs is based on signals such as ligand-based emission, metal-based emission, antenna effects and energy transfer. Some other signals are aggregation-induced emission (AIE), excimer and exciplex emission and adsorption-enhanced emission. In the AIE mechanism, a fluorophore shows a weak emission peak (or no emission) in dilute solution; however, upon aggregation the peak becomes bright, with strong emission. This is a very beneficial strategy for turn-on luminescence detection procedures. Using the AIE strategy, Wang and coworkers applied TABD-COOH ligand (4,4′-((*Z*,*Z*)-1,4-diphenylbuta-1,3-diene-1,4-diyl)dibenzoic acid) with different metal ions (Mg(II), Ni(II) and Co(II)) to synthesize luminescent MOFs (Fig. 11).[308] In the case of Mg(II), the synthesized TABD-MOF-1 is strongly emissive (Φ_F = 38.5%), while the incomplete d subshells yield the barely fluorescent and completely non-fluorescent MOFs TABD-MOF-2 and TABD-MOF-3, respectively. These MOFs were applied in selective sensing of five-membered-ring energetic heterocyclic compounds (5-MR-EHCs). 5-MR-EHCs contain C═N and N═N bonds, which can lead to dissociation of the carboxylate–metal bond inside the structure of the MOF; this results in release of the highly emissive TABD-COOH ligand and luminescence turn-on behavior. When TABD-MOF-3 with central Co(II) metal is exposed to 5-MR-EHCs (5-nitro-2,4-dihydro-3*H*-1,2,4-triazole-3-one), it shows turn-on behavior. Selectivity tests show that there is no obvious change in TABD-MOF-3 emission in the presence of common organic compounds. This turn-on behavior, in which a new peak arises from a dark background, is a method with high detection limits and selectivity and improved accuracy because distinguishing a strong new peak from the background noise is easier than distinguishing a quenched emission peak.

3. Small organic molecules

Small organic molecules include a large variety of molecules, such as volatile organic compounds (VOCs), conventional or non-conventional organic solvents and other molecules. Considering their diverse variations in functionality and molecular structure, small organic molecules show different chemical properties. Considering the variations in the chemical structures of small organic molecules and the chemical properties of MOFs, MOFs have been applied for the detection of small organic molecules with different types of instrumental methods, such as photoluminescence, colorimetric, electrochemical, gravimetric, optical and photonic methods. In this section, we explain, illustrate and compare these methods to evaluate their capability.

Gravimetric methods have been applied for the detection of organic molecules, especially in the gas phase. In this method, the analyte gas is absorbed by a chemical layer on the mechanical resonator (such as a resonant cantilever or quartz crystal microbalance). Then, the change in mass of the resonator by the adsorbed gas can be translated into an electrical signal transduction (such as shifts frequency). If the chemical affinity of the layer to the gas molecules is known, the frequency shift can be related to the gas concentration. Therefore, changes in the concentration of adsorbed gas result in changes in the adsorbed mass, and the changes in the adsorbed mass cause a change in the detected frequency ($\Delta C \approx \Delta m$ and $\Delta m \approx \Delta f$). Using eqn (3), the shift in frequency can be converted to the change in the mass:

$$\Delta f = -\mathrm{K}(f_0/m)\Delta m \quad (3)$$

where K is a constant, f_0 and m are the resonant frequency and mass, respectively, of the resonator without adsorbed analyte. Based on eqn (3), decreasing the device dimensions results in Δf enhancement because the ratio of f_0 to m increases with decreasing resonator size. However, this miniaturization suffers from the fact that it is more difficult for smaller resonator scales to detect gas analytes because of the decreased capture area. This increases the time required for a given mass of analyte to accumulate on the sensor surface. Another method is to increase Δm (*i.e.*, the number of analytes at the sensor surface). Clearly, analyte adsorption in the gas phase can be improved by maximizing the accessible pore volume and surface area of the sensor using porous materials. Also, functionalization of the applied porous material is a good strategy for sensitivity and selectivity enhancement of the resonator toward a specific analyte. Due to this limitation of gravimetric sensors and the advantages of MOFs in this regard, MOFs are potentially good candidates as sensing probes for the detection of gas molecules by gravimetric methods. In this line, some papers have been published about the application of MOFs in the detection of organic molecules by gravimetric sensors.[310–315] In addition to shifts in frequency, the changes in the mass of the resonator can be transduced to changes in the work function (the energy difference between the Fermi level and the vacuum level of the semiconductive material) as a detectable signal.[316–318]

Li and coworkers applied HKUST-1 for gravimetric detection of trace-level xylene molecules (Fig. 12).[311] To this end, they loaded as-prepared HKUST-1 ink on a mass-gravimetric resonant cantilever with 1.5 Hz pg^{-1} mass-sensitivity using a commercial available inkjet printer and exposed it to xylene vapors. The resonant-gravimetric sensing experiments revealed that trace-level *p*-xylene of 400 ppb can be detected, which is lower than the human olfactory threshold of 470 ppb. Using other MOFs, such as ZIF-8, MOF-5 and MOF-177, revealed that HKUST-1 presents the highest response toward xylene molecules. Clearly, this is related to the preferred host–guest chemistry between the HKSUT-1 framework and the xylene molecules. Simulations showed that there are two adsorption sites

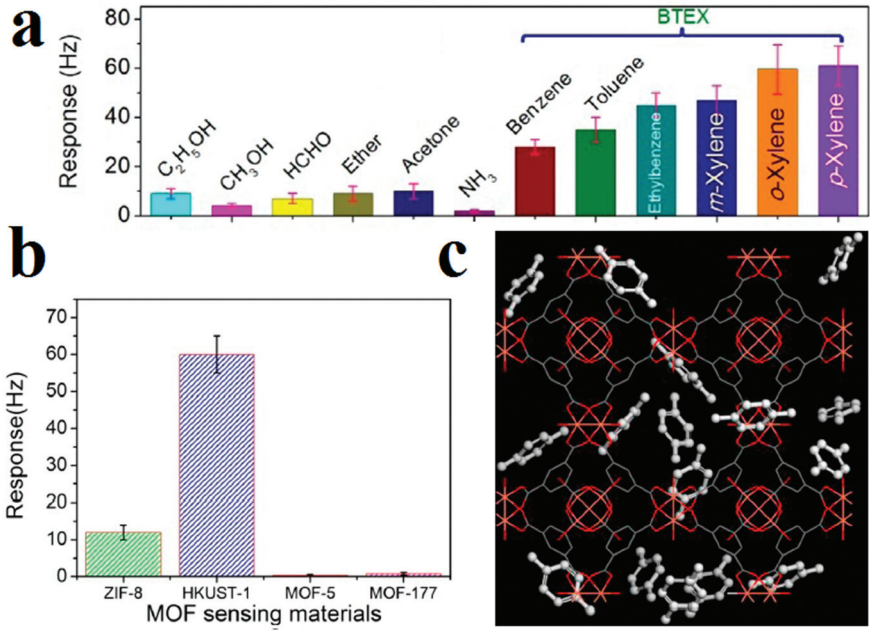

Fig. 12 Application of HKUST-1 in gravimetric detection of BTEX molecules. (a) Responses of the HKUST-1 sensor to 12 different vapors for selectivity evaluation. (b) Resonant-gravimetric sensing results of four different MOFs to xylene vapor with identical concentrations of 50 ppm. (c) Materials Studio simulation results showing two different *para*-xylene adsorbing sites in HKUST-1 crystal. Reproduced with permission from ref. 311.

of HKUST-1 for xylene molecules: Cu(II) and the benzene ring building blocks. Selectivity tests showed negligible sensor responses toward interfering gases (ethanol, acetone, ammonia, ether, or formaldehyde). However, remarkable sensor responses were observed in the cases of benzene, toluene, and ethylbenzene vapors; this may be due to their similar host–guest interactions with the HKUST-1 sensing material. Due to the smaller molecular weights of benzene and toluene than of xylene, the sensor showed lower responses to benzene and toluene than to *p*-xylene at identical concentrations. In general, the HKUST-1 based sensor can be utilized to detect benzene homologues, which are generally categorized as BTEX (*i.e.*, benzene, toluene, ethylbenzene, and xylene).

Gravimetric sensing is a detection method with high sensitivity that is operable at room temperature and has simple packaging requirements and low power consumption. However, it is necessary to use sensor-stabilization methods to achieve higher sensitivity and stability of the response of the sensing material through high control over its uniformity and surface properties. In this line, Bahreyni and coworkers prepared a set of reference sensors by depositing an HKUST-1 layer on the surface of quartz crystal microbalances (QCMs) through drop-casting and vertical electrospraying of an HKUST-1 suspension (Fig. 13).[313] The uniform thin film of HKUST-1 deposited on the QCMs surface using the electrospraying method showed improved response to organic vapours. Through a formula, the change in the mass (Δm) after exposure to the analyte vapors can be transformed directly into a change in frequency (Δf (Hz)). Considering the higher uniformity of deposition of HKUT-1 on QCMs using the electrospraying method, the response of the electrosprayed film is greatly improved compared to that of the drop-casted film. Through this method, thin films of HKUST-1 can detect vapors of tetrahydroforan, acetone and isopropyl alcohol.

Another strategy that is applied for the detection of small organic molecules is electrochemical methods. Electrochemical sensors are recognized to be promising technologies for specific and sensitive detection of targeted VOCs because they can be used for fast, simple, direct, and sensitive analysis even in a complex sample matrix. Fundamentally, potentiometric, amperometric, and conductometric (or chemoresistive) electrochemical sensors are particularly well-suited for environmental and health applications.

MOFs present very unique characteristics in some detection methods, such as photoluminescence and gravimetric-based methods; however, their drawbacks, including their poor electrical conductivity and redox activity, restrict the applications of MOFs in electrochemical detection. Therefore, signal transduction is a major challenge for MOF-based electrochemical sensors. However, their potential physicochemical features have encouraged scientists to achieve highly specific and sensitive MOF-based electrochemical detection.[319–336]

MOFs normally present poor electrical conductivity because their porous nature offers poor concentration and mobility of free charge carriers. High conductivity originates from facile electron-hole separation, high concentration and mobility of free charge carriers and long-range charge movement (through bonds or space). In most cases, "through-bond" charge transportation in MOFs is hindered by the metal cluster nodes. Also, the large distance between building blocks in the MOF skeleton is a deterrent factor for the "through-space" charge transportation mechanism. Therefore, improvements in the

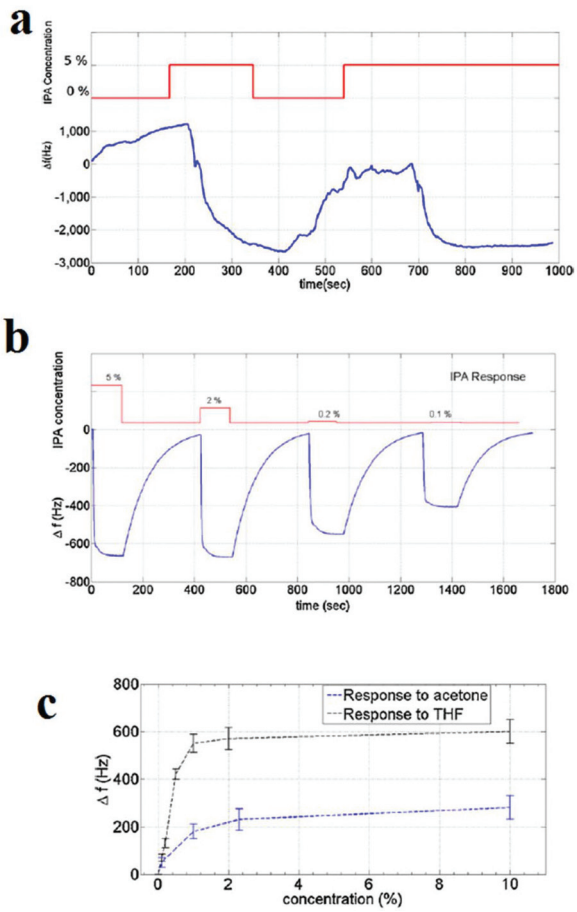

Fig. 13 Application of HKUST-1 thin film in the detection of volatile molecules by gravimetric sensing. (a) The response of the drop-casted film to 5% IPA. (b) Response of the electrosprayed film to IPA. Responses of the sensor with electrosprayed film to different concentrations of (c) acetone and THF. Reproduced with permission from ref. 313.

conductivity and design of redox-active MOFs are still required to enhance their properties to satisfy the requirements for real applications of MOF-modified electrodes.

These limitations and barriers to the application of MOFs in electrochemical sensors can be eliminated by two different strategies, namely synthesis of redox-active conductive MOFs and synthesis of redox-active conductive MOF-based hybrid materials. Through "function-application" and "structure-signal" approaches, it is possible to synthesize a redox-active conductive MOF.[337] For example, it is possible to synthesize a conductive MOF through functionalization of the pore walls of the MOF with electroactive groups, which can participate in the charge transfer process between the donor and acceptor centers.[337] Using organic ligands with extended π-systems is another helpful strategy for improvement of both the "through space" and "through bond" conduction mechanisms. Also, introduction of electroactive metal ions into certain architectures is very helpful for long-range charge delocalization through either bonds or space (*i.e.*, *via* p–p-stacking interactions). In another strategy, it is possible to composite MOFs with other conductive or redox-active materials to overcome the mentioned challenges. These MOF composites/hybrids have the advantages of both MOFs (high porosity with ordered crystalline pores) and other active materials (electrical and catalytic properties), and their electrochemical performance is enhanced.

As mentioned, control over chemical properties through the right choice of metal ions and aromatic ligands is of special importance to achieve conductive MOFs. In this line, Dincă and coworkers applied arrays of 2D structurally analogous conductive MOFs as sensors that could discriminate five different categories of VOCs with different functional groups (Fig. 14).[320] Dincă and coworkers used different metal ions (Cu(II) and Ni(II)) and different aromatic ligands (2,3,6,7,10,11-hexahydroxytriphenylene (HHTP) and 2,3,6,7,10,11-hexaiminotriphenylene (HITP)) to synthesize MOFs with different conductivities, including $Cu_3(HHTP)_2$ (0.002 S cm^{-1}), $Cu_3(HITP)_2$ (0.2 S cm^{-1}) and $Ni_3(HITP)_2$ (2 S cm^{-1}). They applied these three MOFs as array sensors for VOC detection based on changes in conductance as the relative response ($\Delta G/G_0$) upon 30 s exposure to 200 ppm of VOC vapors. The results show that each MOF often displays a difference in the direction and/or the magnitude of response, which varies with the type of analyte. These data were treated with different statistical methods. Principal component analysis (PCA) was used to study the methods applied for the discrimination of VOCs.

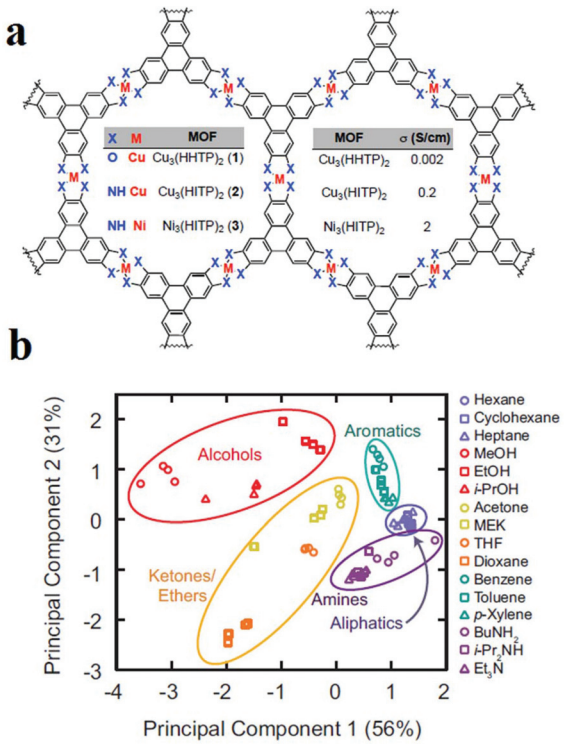

Fig. 14 Application of 2D MOFs as chemoresistive materials in VOC detection. (a) Chemical structures of the conductive 2D MOFs. (b) PCA of the responses of the MOF sensor array to VOCs. Reproduced with permission from ref. 320.

Using PCA analysis, it is possible to group data based on their similarity without any prior knowledge. Based on the PCA method, the VOCs were classified in five groups based on their functionality.

Another electrochemical sensing method is based on capacitive sensors. Capacitive sensors have some benefits, such as less power use, low cost, miniaturization, facile signal treatment and instrumentation, high selectivity and reproducibility, quick response time and good linearity. Changes in the dielectric constant are the basis of signal transduction in capacitive sensors. Because MOFs benefit from insulating effects, they can be applied as dielectric layers in capacitance sensors. Capacitive sensors were fabricated in a sandwich form or parallel plate using copper plate as the back electrode, an MOF layer as the dielectric layer, and interconnected silver spots as the upper electrode of the capacitor. In general, the dielectric layer used in a parallel-plate capacitance sensor should be thick enough to prevent touching or connecting of the two parallel electrodes, which can result in a short-circuit. The response of the capacitance sensor presents the changes in capacitance, measured by an LCR meter. Considering the advantages of capacitance sensors and the potential of MOFs as a dielectric layer, Zeinali and coworkers applied HKUST-1 nanoparticles as a dielectric layer in capacitance sensors for the detection of volatile compounds such as methanol, ethanol, isopropanol and acetone in a moderate environment (10% relative humidity and 25 °C) (Fig. 15).[321] Signal transduction in this method is based on adsorption of gas molecules inside the HKUST-1 pores, which changes the capacitance of the sensor. Because of the rigidity of the nanoporous Cu-BTC layer, changes in the capacitance of the sensor upon exposure to analytes are only related to the changes in dielectric constant of the dielectric material. The results show that adsorption of analytes with higher polarity causes a greater capacitance change. The same results can be achieved for higher concentrations of a special analyte. Overall, the changes in capacitance depend on the polarity, concentration and adsorption tendency of the analyte on the MOF framework. The sensor showed the most sensitivity for methanol because methanol has the highest dielectric constant and, consequently, the greatest adsorption tendency onto the Cu-BTC layer due to its lowest chain length, lowest kinetic diameter, and lowest mass. To study the selectivity of the proposed sensor, the surface was exposed to both polar and non-polar analytes; it showed suitable selectivity for polar analytes.

Similar to explosive organic molecules, photoluminescence methods have been applied extensively for the detection of small organic molecules, such as solvents and VOCs. MOF-based luminescent sensors have been applied for the detection of various organic molecules, such as aldehydes and ketones,[309,338–349] especially acetone[183,338,344,350–379] and formaldehyde;[380–382] chlorinated hydrocarbons,[339,383,384] especially chloroform;[349,358,385] alcohols and ethers,[386–388] especially methanol,[351,369,386,389,390] aliphatic[391] and aromatic hydrocarbons;[280,355,356,388,392–395] and other molecules, such as DMF,[83,387,396,397] acetonitrile,[398] thioethers,[399] and dipicolinic acid.[400]

Investigations reveal that most papers reporting the detection of small organic molecules focus on acetone. This is because this molecule has a strong absorption band in the range of 220 to 330 nm, and many MOFs have excitation or emission bands in this wavelength region. As a result, the overlap mechanism between the absorption band of acetone and the emission or excitation band of the MOF results in resonance energy transfer or competitive adsorption mechanisms. Zhang and coworkers reported a Eu(III)-based MOF with coordinated DMF molecules (**1**, $[Eu_3(bpydb)_3(HCOO)(\mu_3\text{-}OH)_2(DMF)]\cdot(DMF)_3\cdot(H_2O)_2$, where H_2BDC is benzene-1,4-

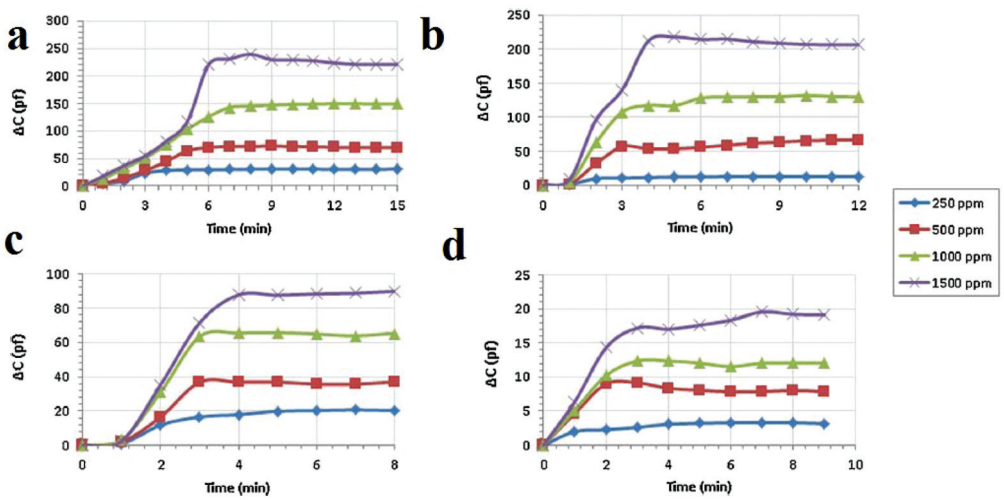

Fig. 15 Application of Cu-BTC MOF nanoparticles in capacitance sensors for the detection of polar VOCs. Real-time capacitive response of the Cu-BTC-based sensor after exposure to vapors of (a) methanol, (b) ethanol, (c) isopropanol and (d) acetone with different concentrations of 250, 500, 1000 and 1500 ppm under ambient conditions with relative humidity below 20% and a frequency of 1 MHz. Reproduced with permission from ref. 321.

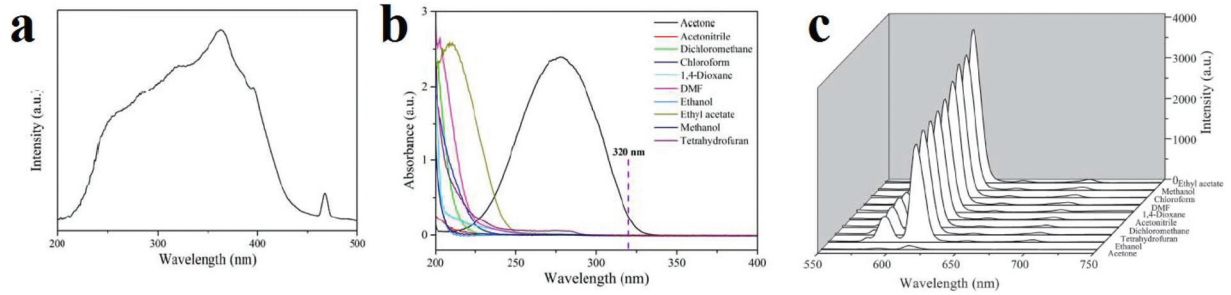

Fig. 16 Application of $[Eu_3(bpydb)_3(HCOO)(\mu_3\text{-}OH)_2(H_2O)]\cdot(x\cdot\text{solvent})$ (**2**) in the detection of small organic molecules. (a) Solid-state PL excitation spectra of activated **2a**. (b) The UV-vis absorption spectra of solvent molecules: acetone, acetonitrile, dichloromethane, chloroform, 1,4-dioxane, DMF, ethanol, ethyl acetate, methanol and tetrahydrofuran. (c) PL spectra of activated **2** samples that were introduced into various pure solvents. Excitation: 320 nm. Reproduced with permission from ref. 370.

dicarboxylic acid and H_2bpydb is (4,4′-(4,4′-bipyridine-2,6-diyl) dibenzoic acid) which transforms into another compound (**2**, $[Eu_3(bpydb)_3(HCOO)(\mu_3\text{-}OH)_2(H_2O)]\cdot(x\cdot\text{solvent})$) by single-crystal-to-single-crystal transformation involving replacement of the coordinated DMF ligands by aqua ligands (Fig. 16).[370] Upon excitation at 362 nm, the emission spectrum of activated **2** reveals well-resolved peaks centered at 593, 615, 650, and 699 nm, corresponding to the f–f electronic transitions ($^5D_0 \rightarrow {}^7F_J$, J = 1 to 4) of Eu(III) ion, with the hypersensitive $^5D_0 \rightarrow {}^7F_J$ transition dominating the spectrum. A broad emission band centered at 450 nm, originating from the organic ligands, is observed; however, it is much weaker than the metal-based red emission. The activated **2** shows solvent dependent-PL behavior upon dispersion in different organic solvents. The most significant quenching is observed in the presence of acetone. Acetone has an observable absorption intensity at 320 nm, while no other solvents absorb at this wavelength. Therefore, there is competition between the absorption of acetone and the excitation of activated **2**, resulting in a decrease (even quenching) of the PL intensity.

In some cases, it is reported that strategies such as using 2D maps[401–403] and synthesis of MOF-based ratiometric sensors[399,404–407] are effective for discriminating and differentiating between organic molecules. In this regard, Wu and co-workers synthesized a ratiometric dye@MOF platform to realize the probing of different volatile organic molecules by tuning the energy transfer efficiency between two different emissions (Fig. 17).[404] They synthesized CZJ-3 ([CdL(H_2O)]·4DMF·2H_2O, where H_2L is (*E*)-4-(2-carboxyvinyl)benzoic acid); then, taking advantage of the porosity of CZJ-3, Rhodamine B molecules were inserted into its pores to form the luminescent material Rho@CZJ-3. The Rho@CZJ-3 composite presents emission peaks of both Rhodamine B (595 nm) and CZJ-3 (420 nm), which originate from the π–π* transitions of the L^{2-} linker (excited at 340 nm). The best composition of Rho@CZJ-3 was achieved when the ratio of Rhodamine B was 12 wt%. After exposing Rho@CZJ-3 to different organic molecules, these solvent molecules were easily distinguished by monitoring the emission peak-height ratios of **L** to those of the dye moieties. The results clearly indicate that Rho@CZJ-3 is an excellent sensor for probing different volatile organic molecules. The unique solvent-dependent emission of Rho@CZJ-3 can be rationalized by the guest-dependent energy transfer from **L** to the dye moieties. Using ratiometric sensors as self-calibrating probes is more reliable because the single-emission intensity is variable depending on many uncontrollable factors, whereas the peak height ratio is almost constant for each molecule. Therefore, this luminescent sensor for

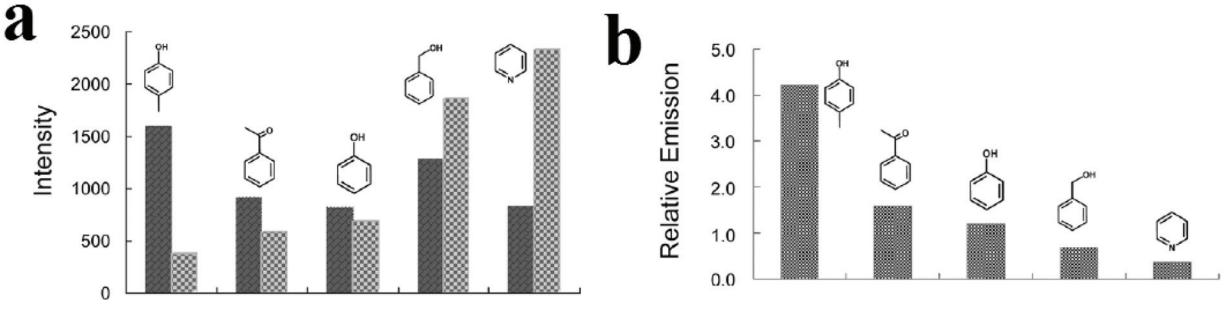

Fig. 17 Application of Rho@CZJ-3 in the detection of volatile organic molecules. (a) Emission peak heights of the L (dark bars) and dye (light bars) moieties. (b) The emission peak-height ratios between L the and dye moieties in Rho@CZJ-3-f after adsorption of 4-methylphenol, acetophenone, phenol, benzyl alcohol, and pyridine molecules excited at 340 nm in the solid state at room temperature. Reproduced with permission from ref. 404.

probing a range of solvent molecules is remarkable because it does not require any additional calibration.

Luminescent sensing of organic solvents using MOFs shows that the non-polar, polar, protic and aprotic natures of these analytes have very important effects on the PL signal transduction. Generally, protic and aprotic solvents show different behaviors.[408–413] Also, solvent polarity plays a very important role in determining the type of signal transduction.

Nanotubular MOF $[(WS_4Cu_4)I_2(dptz)_3]$ 3DMF (**1**), where dptz = 3,6-di-(pyridin-4-yl)-1,2,4,5-tetrazine, was applied as a tetrazine-functionalized probe for colorimetric detection of solvent molecules (Fig. 18).[411] After exposure of framework **1** to different organic solvents, the colors of the solvent@**1** samples differed significantly. Investigations showed that the band-gaps of the solvent@**1** samples show excellent linear correlation with Reichardt's solvent polarity parameter (E_T^N). However, the band-gap (eV)–(E_T^N) differs for protic and aprotic solvents. This solvatochromic behavior of framework **1** is related to the labile electronic states of tetrazine groups, the different MLCT and LLCT transitions, and tetrazine-solvent interactions because of the strong π-acceptor properties of tetrazine and the polarity of the solvent.

In other work, $[Cd_2(TPPBDA)(bpdc)_{3/2}(H_2O)_2]\cdot(CO_3)_{1/2}$, renamed compound **1**, where TPPBDA is *N*,*N*,*N*′,*N*′-tetrakis (4-(4-pyridine)-phenyl) biphenyl-4,4′-diamine and H_2bpdc is bipyridine dicarboxylic acid, were synthesized and showed solvent polarity-based PL behavior (Fig. 19).[409] The solid-state emission spectrum of compound **1** exhibits a broad peak at 573 nm, which is likely due to intraligand transition. Solvents with different polarities and protic natures interact differently with compound **1**. With increasing dielectric constant of the solvent guests, the maximum emission peaks are red-shifted, showing a positive correlation effect for non-protonic solvents and a negative correlation effect for protonic solvents. Control experiments show that the emission position of TPPBDA ligand is not related to the dielectric constant or protonic character of the solvent.

In addition to the polarity and protic/aprotic natures of solvents or small molecules, their electron-rich or electron-deficient natures have remarkable effects on the PL signal transduction of MOFs. A $[Tb_4(\mu^3\text{-}OH)_4(BPDC)_3(BPDCA)_{0.5}(H_2O)_6]ClO_4\cdot 5H_2O$ framework ($BPDC^{2-}$ = 3,3′-dicarboxylate-2,2′-dipyridine anion and $BPDCA^{2-}$ = biphenyl-4,4′-dicarboxylate anion) was synthesized and applied in the detection of small organic molecules (Fig. 20).[355] This Tb(III)-based MOF shows very noticeable quenching and enhancement in the presence of acetone and benzene, respectively, when the Tb-MOF is dispersed in EtOH as the standard suspension. Definitely, these changes in the PL behavior of this Tb-MOF are related to changes in the efficiency of LMEnT (ligand to metal energy transfer) due to interaction of the guest molecules with the framework. Therefore, it can be noted that the different signal-transductions are related to different mechanisms. Investigations show that there is an overlap between the UV-vis spectra of the aromatic ligands and benzene, which increases the efficiency of the ligand ($^1\pi\pi^*$) → ligand ($^3\pi\pi^*$) → Tb* energy transfer. In the case of acetone, due to the intermolecular interactions between the ligands and acetone, a decrease in the LMEnT efficiency can be observed. When comparing the luminescence lifetimes, benzene clearly increases the lifetime of the activated Tb-MOF, whereas acetone shows the opposite effect.

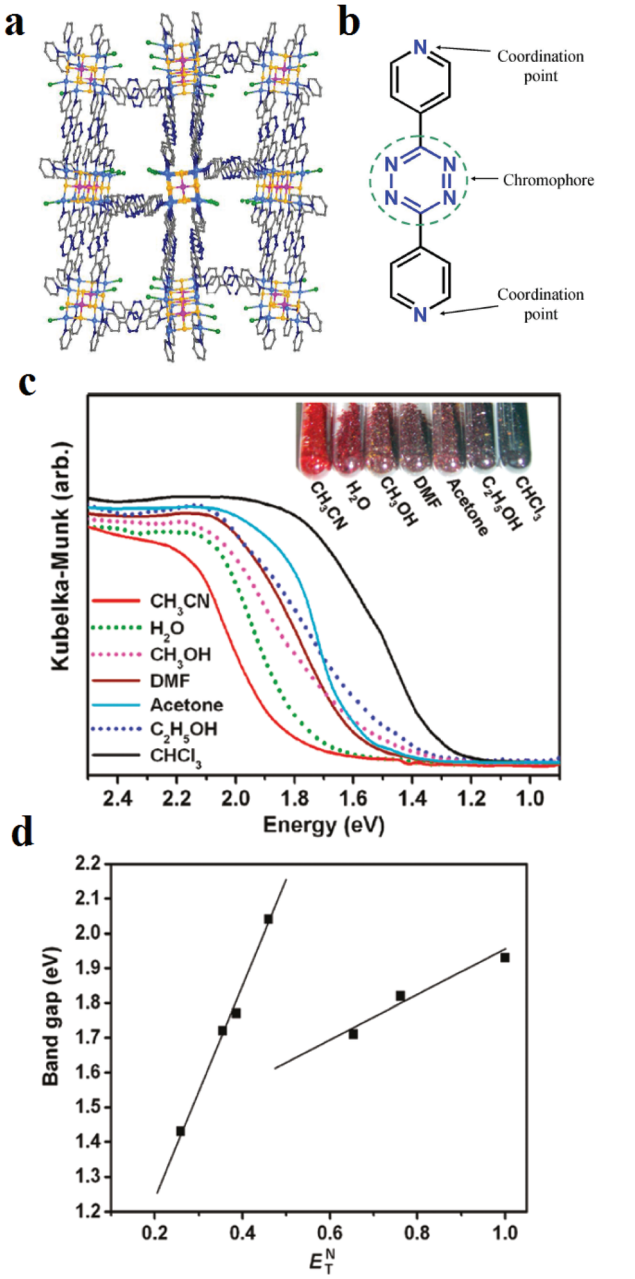

Fig. 18 Application of $[(WS_4Cu_4)I_2(dptz)_3]$ 3DMF (**1**) in the colorimetric detection of solvent molecules. (a) Structural representation. (b) Representation of tetrazine groups responsible for the solvatochromic behavior. (c) Kubelka–Munk functions of the solvent@**1** samples and related colors. (d) Band-gap (eV)–(E_T^N) curves for the solvent@**1** samples. Reproduced with permission from ref. 411.

One strategy in designing MOF-based sensors is the colorimetric approach, in which the color of the MOF changes after

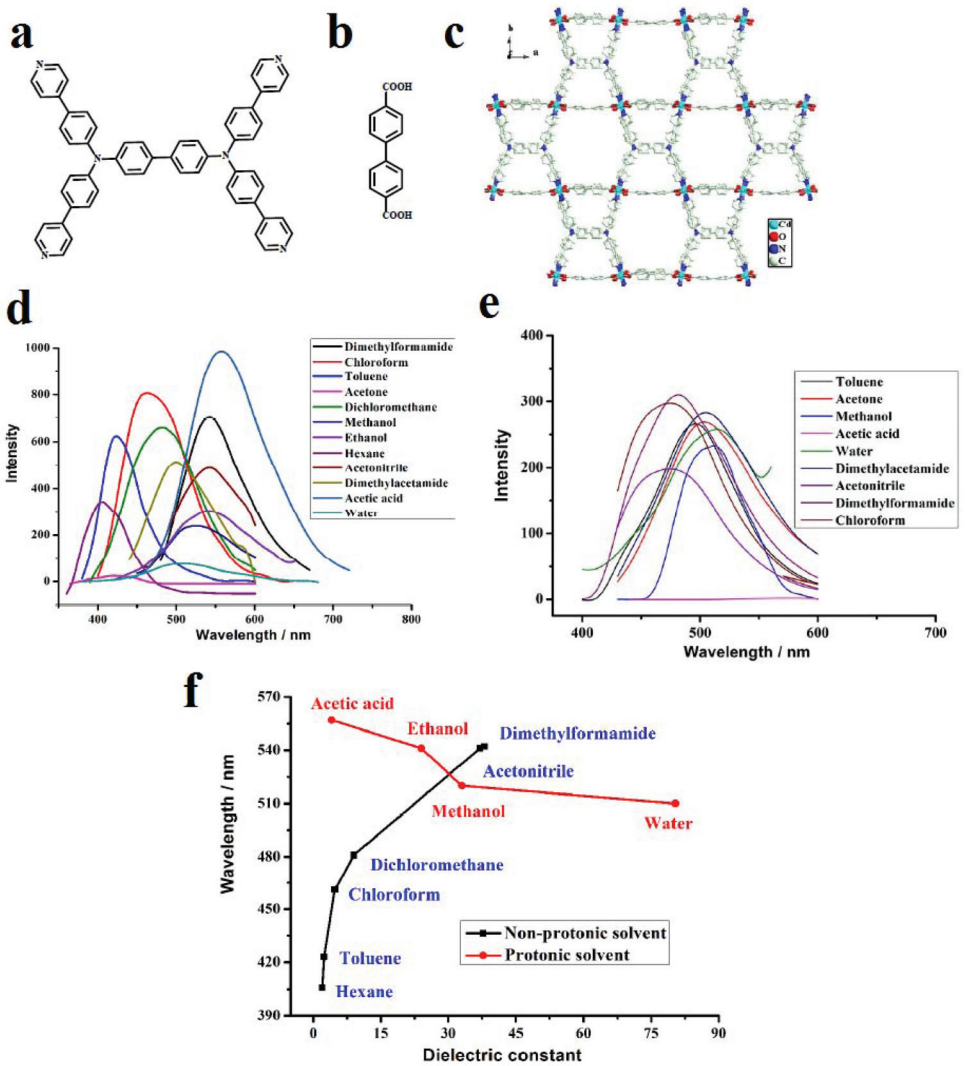

Fig. 19 Application of $[Cd_2(TPPBDA)(bpdc)_{3/2}(H_2O)_2]\cdot(CO_3)_{1/2}$ in the sensing of small organic molecules. (a) Structure of TPPBDA ligand. (b) Structure of H_2bpdc ligand. (c) The emission spectra of compound **1** in suspension in various organic solvents under the same testing conditions. (d) The emission spectra of TPPBDA in suspension in various organic solvents. (e) The maximum emission peaks plotted against the dielectric constant values of the solvents. (f) Compound **1** maximum emission peaks of PL spectra against dielectric constant values of solvents. Reproduced with permission from ref. 409.

exposure to the analyte. This type of signal transduction is very practical because there is no need for instrumentation if the color change can be achieved selectively. Usually, the colorimetric detection procedure is performed in two different ways: (I) a selective color change in the presence of a specific analyte[414,415] and (II) versatile color changes in the presence of different analytes.[416–423]

Considering this strategy, we developed TMU-34, with the formula $[Zn(OBA)(H_2DPT)_{0.5}]$, where H_2DPT and H_2OBA are (3,6-di(pyridin-4-yl)-1,4-dihydro-1,2,4,5-tetrazine) and (4,4′-oxybis(benzoic acid), respectively, as a promising solid-state naked-eye visual chemosensor for the detection of chloroform in the presence of a large variety of analytes (Fig. 21).[415] TMU-34 is decorated with redox-active stimuli-responsive dihydro-tetrazine functional groups, which after exposure to chloroform in both liquid and gas phases can be converted into tetrazine groups. As a result, the color of TMU-34 changes from yellow to pink. TMU-34 can detect chloroform in liquid and gas phases up to 2.5×10^{-5} M. TMU-34 is reversible by exposure to DMF molecules. Selectivity is one of the most important characteristics when designing sensors. TMU-34 shows unique selectivity toward chloroform. In comparison with other MOF-based sensors, which present color changes in the presence of different analytes, the color of TMU-34 only changes in the presence of chloroform.

In other work, Zang and coworkers synthesized a functional silver-cluster-based material $[[(Ag_{12}(S^tBu)_8(CF_3COO)_4(bpy)_4)]_n$ (Ag_{12}bpy), in which bpy is 4,4′-bipyridine) which shows turn-off PL behavior triggered by O_2 and multicolored turn-on PL behavior triggered by volatile organic compounds.[423] The results of exposing Ag_{12}bpy (in vacuum) to the VOCs reveal that the color of Ag_{12}bpy changes instantly in the pres-

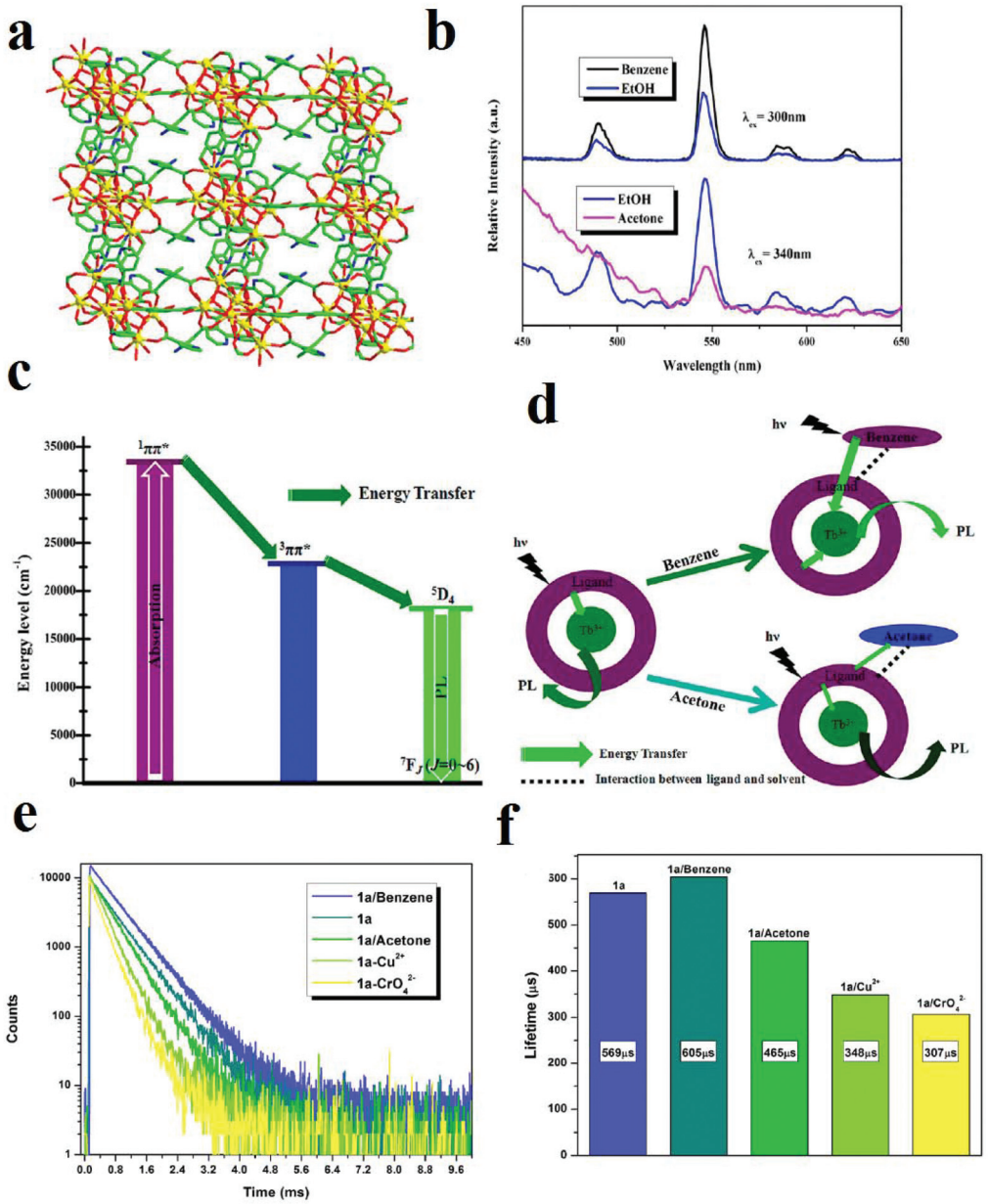

Fig. 20 Application of Tb-MOF in the detection of small organic molecules. (a) The 3D framework of TB-MOF along the *b*-axis. (b) Comparison of the PL spectra of activated Tb-MOF in benzene and acetone with EtOH as a standard. (c) LMEnT process for luminescence emission. (d) The influence of benzene and acetone on LMEnT. (e) and (f) The luminescence lifetime curves of Tb-MOF in the presence of benzene and acetone. Reproduced with permission from ref. 355.

ence of various VOCs with different emission colors, from green to yellow-orange, at room temperature (solvatochromism or vapochromism). Also, in protic or aprotic solvents and VOCs, Ag_{12}bpy uniformly exhibited positive solvatofluorochromism, that is, a bathochromic shift of the emission band with increasing solvent polarity. λ_{em} exhibited an excellent linear correlation with the empirical parameters of the solvent polarity values for protic and aprotic VOCs, demonstrating that Ag_{12}bpy can function as a visual indicator of VOC polarity. The difference in the luminescence behaviour of Ag_{12}bpy in the presence of polar protic and aprotic VOCs can be attributed to their hydrogen-bond donor abilities. In the case of EtOH, the fluorescence intensity increased approximately 26-fold relative to air in less than 1 s. A low ethanol pressure (0 to 0.133 kPa) caused great changes in the emission intensity. The emission intensity saturated and shifted from 507 to 520 nm when the pressure increased to 1.33 kPa, which suggests that the number of incorporated EtOH molecules finely tunes the emission intensity of Ag_{12}bpy in the low pressure range (0 to 1.33 kPa). Other VOCs, including $CHCl_3$, C_6H_{12} and CH_3CN, exhibited similar performance to EtOH.

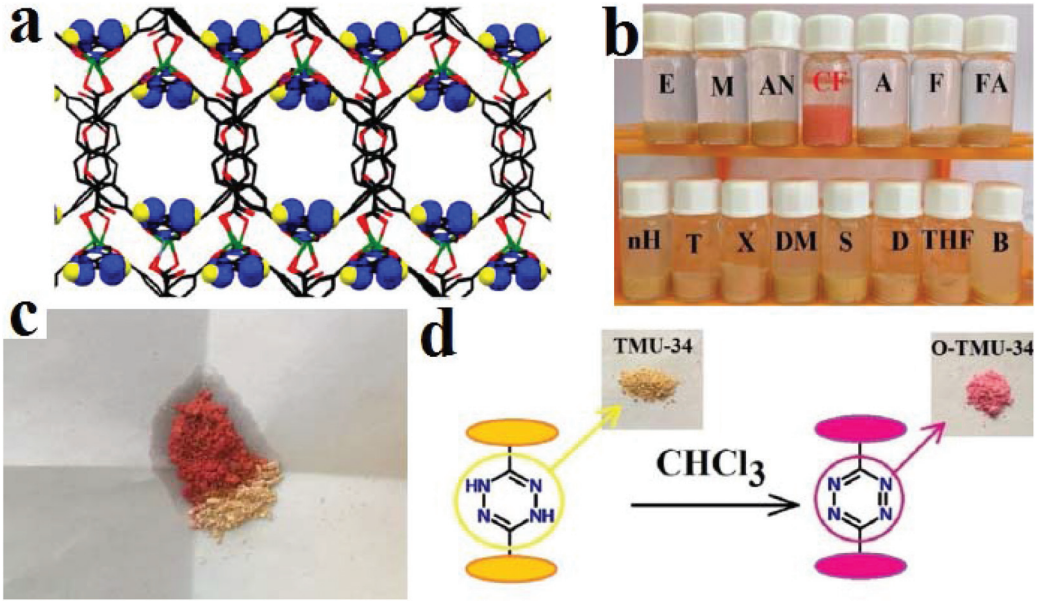

Fig. 21 Application of TMU-34 in colorimetric detection of chloroform. (a) 3D structures of TMU-34 and dihydro-tetrazine decorated pores. (b) Color changes of TMU-34 in the presence of VOCs. (c) Solid state color change of TMU-34 after exposure to chloroform. (d) Mechanism of the color change. Reproduced with permission from ref. 415.

Cheng and coworkers synthesized isostructural Ln-MOF-1 ($[Tb_2(FDA)_3]$) and Ln-MOF-2 ($[Eu_2(FDA)_3]$) frameworks, where H_2FDA is furan-2,5-dicarboxylic acid, with a bi-luminescent center strategy (Fig. 22).[421] Because H_2FDA is an excellent "antenna" ligand for building luminescent Ln-MOFs, Ln-MOF-1 and Ln-MOF-2 present green and red emission, respectively, based on the characteristic peaks of Tb(III) (emission peaks at 488, 546, 588, and 623 nm, which can be assigned to the $^5D_4 \rightarrow {}^7F_J$ (J = 6, 5, 4, and 3) transitions) and Eu(III) ions (emission peaks at 593, 616, 653, and 703 nm from the $^5D_0 \rightarrow {}^7F_J$ (J = 1, 2, 3, and 4) transitions) when excited at 300 nm. The quantum yields are 6.86% and 12.86% for the strongest emissions of Ln-MOF-1 at 546 nm and Ln-MOF-2 at 616 nm, respectively. They attempted to synthesize a dual emissive bimetallic Ln-MOF exhibiting characteristic emission peaks of Tb(III) and Eu(III) ions by adjusting the Eu(III)/Tb(III) ratio ($[Eu_xTb_{(1-x)}(FDA)_3]$). All the bimetallic Ln-MOFs simultaneously showed the characteristic emission peaks of Tb(III) and Eu(III) ions. The authors claim that the emission of Eu(III) ions in the $[Eu_xTb_{(1-x)}(FDA)_3]$ framework can be further sensitized by Tb(III) ions with 488 nm UV light within the same framework by Tb(III)-to-Eu(III) REnT between the excited states $^5D_4$ (for Tb(III) at 546 nm) and $^5D_0$ (for Eu(III) at 616 nm) with maximum emissions. They stated that almost all bimetallic Ln-MOFs can be seen to have shorter $^5D_4$ lifetimes than Ln-MOF-1 and longer $^5D_0$ lifetimes than Ln-MOF-2, which implies the presence of Tb(III)-to-Eu(III) REnT in the $[Eu_xTb_{(1-x)}(FDA)_3]$ frameworks. Due to the solvent-dependent PL behavior of $[Eu_{0.5}Tb_{1.5}(FDA)_3]$, it presents both a more linear relative intensity-to-volume ratio of 1,4-dioxane in glycol and a higher slope of the working curve (indicative of higher accuracy) compared to the other frameworks, including $Eu_xTb_{(1-x)}(FDA)_3$, where x is the opposite of 0.5, Ln-MOF-1 and Ln-MOF-2.

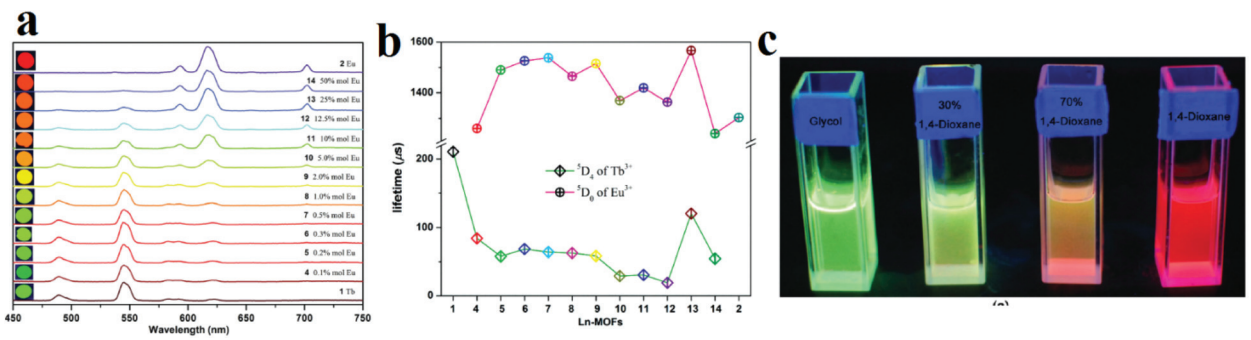

Fig. 22 Structure-signal relationships in $[Eu_xTb_{(2-x)}(FDA)_3]$. (a) Luminescence emission spectra of $[Eu_xTb_{(2-x)}(FDA)_3]$, Ln-MOF-1 and Ln-MOF-2 when excited at 300 nm and corresponding images of their luminescence colors under a 254 nm UV lamp. (b) The $^5D_4$ and $^5D_0$ lifetimes of $[Eu_xTb_{(2-x)}(FDA)_3]$ with various amounts of x. (c) Luminescence images of $[Eu_{0.5}Tb_{1.5}(FDA)_3]$ under 254 nm UV light. Reproduced with permission from ref. 420.

Some other methods, such as optical and photonic instrumentation, have been applied for the detection of small organic molecules in addition to gravimetric, electrochemical, colorimetric and photoluminescence methods.[424–431] These methods involve the refractive index (RI or *n*). The key to chemical sensing is the tunability of n. In optics, the refractive index or index of refraction of a material is a dimensionless number that is calculated from the ratio of the speed of light in a vacuum to that in a second medium of greater density. This approach is based on the distinctive readout of the changes observed in the refractive index (RI), which depend on the RI and amount of the guest. Studies have revealed that light–matter interactions are highly sensitive to structural and RI changes and can be individually exploited for signal transduction; this provides unique opportunities for optical sensors using ultrathin MOFs. ZIF-8 and HKUST-1 are the most applied MOFs in this area.

4. Organic amines

Organic amines are well-known because of their harmful negative effects on the human respiration system and corneal subepithelial cells as well as many other problems. Despite these dangers, organic amines are applied in industry. Therefore, detection of organic amines at low concentrations is of critical importance to the control of food standard levels, human safety and environmental protection. MOFs are among the materials applied for the detection of organic amines. MOFs have been applied for discrimination between aromatic and aliphatic amines[432] and selective detection of aliphatic amines[433–441] and aromatic amines,[442–446] especially aniline.[35,354,447–449] As material-based sensors, MOFs have been applied for colorimetric detection of organic amines.[449–451] Some other approaches, such as gravimetric[452] and chemoresistive[453] methods, have been applied for the detection of aniline.

Differentiation between aliphatic and aromatic amines depends on the structural and chemical properties of the organic amines and the MOF structure. Eddaoudi and coworkers designed a thiadazole-functionalized Uio-68 framework (Zr-BTDB-**fcu**-MOF) by incorporating a π-conjugated, electron-deficient, thiadiazole-functionalized ligand, H_2BTDB (H_2BTDB = 4,4′-(benzoic[*i*-1,2,5]-thiadiazole-4,7-diyl)dibenzoic acid) (Fig. 23).[432] The PL behavior of Zr-BTDB-**fcu**-MOF is based on ligand-based π–π* transitions. This MOF can discriminate aliphatic and aromatic amines through PL quenching and enhancement behaviors. Quenching in the presence of aromatic amines can be observed, suggesting an electron transfer process that can also quench fluorescence. To understand the nature of the increase in the fluorescence intensity in the presence of aliphatic amines, they measured the PL behavior of the MOF at different pH values; first they suggest that the enhancement in the presence of methyl amine is based on the amine basicity and changes in the pH or chemical properties of methyl amine. Based on the PL results, only a negligible enhancement in fluorescence intensity was observed, corroborating that the change in sensitivity was not related to pH. Application of an anthracene core instead of a thiadazole core showed no specific changes in the PL spectra of the anthracene-decorated framework, confirming that aliphatic amines strongly interact with

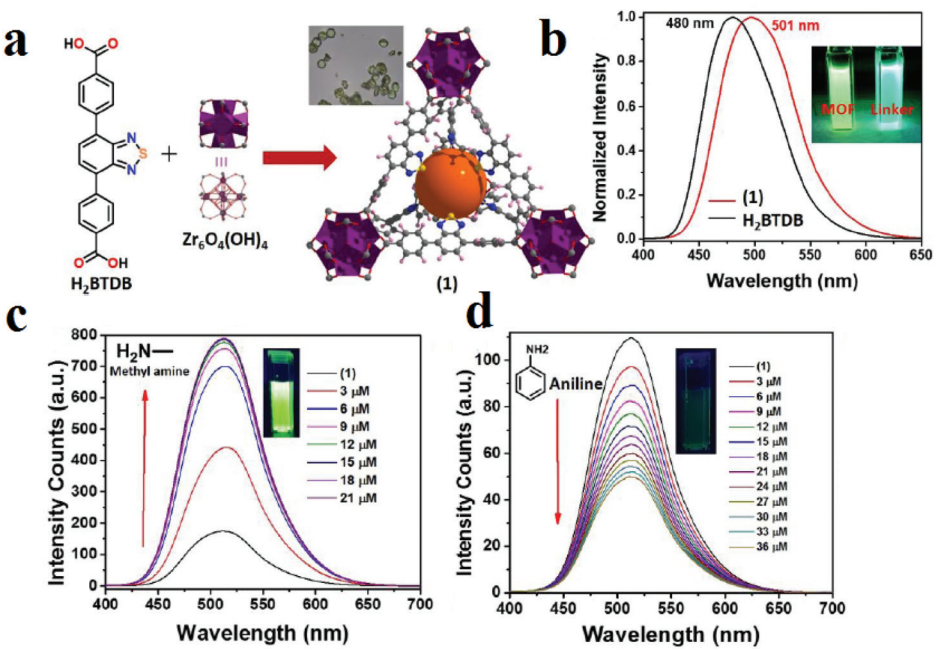

Fig. 23 Application of Zr-BTDB-**fcu**-MOF in amine detection. (a) Schematic of the synthesis of Zr-BTDB-**fcu**-MOF. (b) PL spectra of the MOF (red) and linker (black). Fluorescence intensities of MOF aqueous suspension upon addition of 3 μM increments of methylamine (c) and aniline (d) (λ_{max} = 515 nm). Reproduced with permission from ref. 432.

the thiadiazole core. Their investigation showed that hydrogen bonding between the thiadazole N-atom and protonated methylamine (alkylamines can be protonated in water) induces structural changes of the $BTDB^{2-}$ linker, resulting in reduction of the non-radiative recombination pathways.

Among the important different characteristics of aliphatic and aromatic compounds are their basicities and aromatic structures. Due to the basicity of aliphatic amines, the change in pH in aquatic media is considerable. In this line, using H-donor functional groups such as hydroxy groups can be effective for selective detection of aliphatic amines. Based on this strategy, Wang and coworkers constructed a dual emissive MOF as a ratiometric sensor for detection of organic amines (Fig. 24).[433] They applied the fluorescent organic linker H_2-

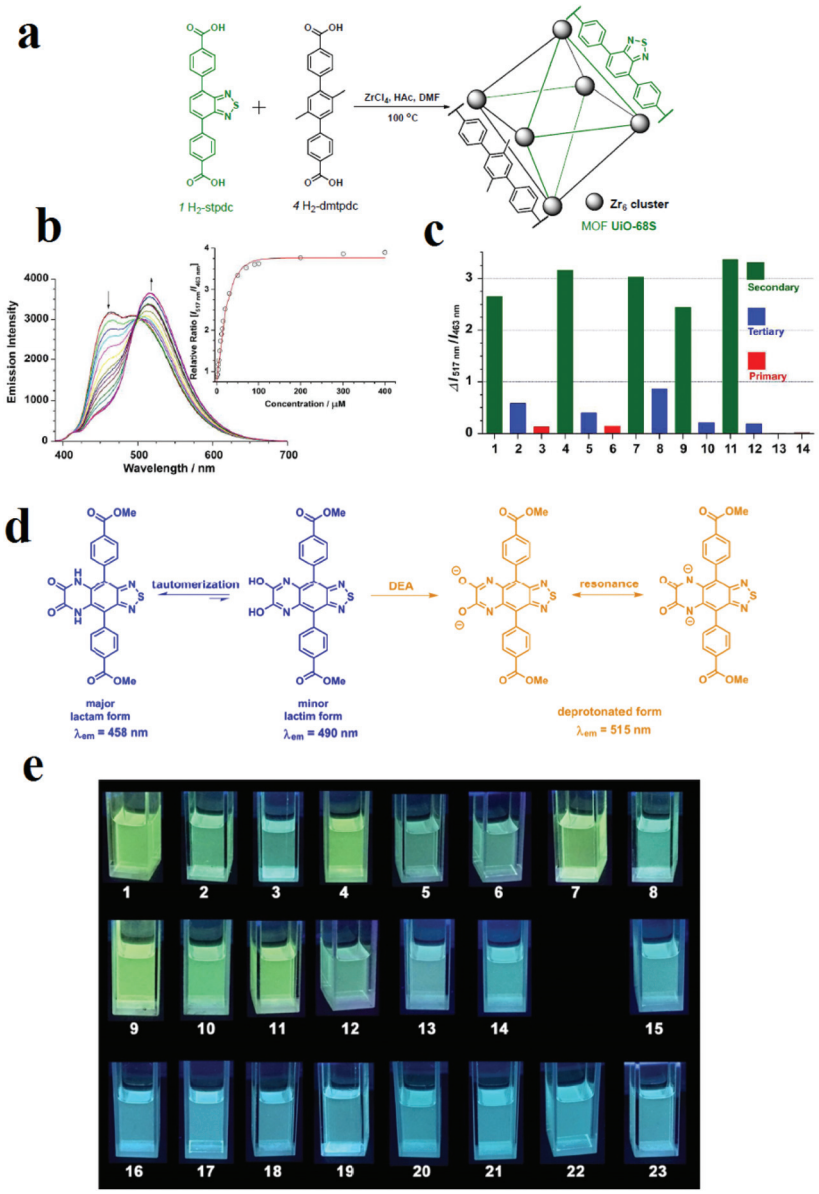

Fig. 24 Application of UiO-68-osdm in amine detection. (a) Synthesis and structure of UiO-68-osdm. (b) Emission spectra of the MOF UiO-68-osdm dispersed in chloroform (0.02 mg mL^{-1}) upon titration with diethylamine (0 to 0.1 mM, λ_{ex} = 370 nm). Inset: The relative emission ratio ($I_{517\ nm}/I_{463\ nm}$) varies as a function of diethylamine concentration. (c) The changes in the emission ratio of UiO-68-osdm ($\Delta I_{517\ nm}/I_{463\ nm}$) in the presence of different amines (0.1 mM): 1, diethylamine; 2, triethylamine; 3, propylamine; 4, piperidine; 5, *N*-methyl piperidine; 6, cyclohexylamine; 7, piperazine; 8, *N*,*N*-dimethylpiperazine; 9, diisopropylamine; 10, *N*,*N*-diisopropylethylamine; 11, pyrrolidine; 12, *N*-methyl pyrrolidine; 13, aniline; 14, pyridine. (d) Tautomeric forms of H_2-ostpdc linker and its typical resonance process and 0d deprotonated form in the presence of diethylamine. (e) Fluorescence photographs of UiO-68-osdm (0.2 mg ml^{-1}) in chloroform after addition of various amines (#1–14, 0.1 mM) and other VOCs (#15–23, 1 mM) under a UV lamp (365 nm). 1: diethylamine; 2: triethylamine; 3: propylamine; 4: piperidine; 5: *N*-methyl piperidine; 6: cyclohexylamine; 7: piperazine; 8: *N*,*N*-dimethylpiperazine; 9: diisopropylamine; 10: *N*,*N*-diisopropylethylamine; 11: pyrrolidine; 12: 1-methylpyrrolidine; 13: aniline; 14: pyridine; 15: nitrobenzene; 16: butyraldehyde; 17: methanol; 18: acetone; 19: tetrahydrofuran; 20: acetonitrile; *N*,*N*-dimethylformamide; dimethylsulfoxide; 23: benzene. Reproduced with permission from ref. 433.

ostpdc, 4,4′-(6,7-dioxo-5,6,7,8-tetrahydro-[1,2,5]thiadiazolo[3,4-*g*]quinoxaline-4,9-diyl)dibenzoicacid for the construction of a luminescent MOF in the UiO-MOF topology, which was named UiO-68-osdm. This MOF shows dual PL emissive bands in chloroform which are centered at 458 and 490 nm. This dual emissive signal is based on lactam–lactim tautomerization of the H_2-ostpdc organic ligand, in which the second signal can be attributed to the emission from a small amount of tautomeric lactim form. It was found that the emission at 458 nm from the lactam form of UiO-68-osdm rapidly decreased upon addition of diethylamine; meanwhile, a new red-shift peak at 515 nm arising from the deprotonated species gradually appeared, with an isoemission point at 493 nm. Also, the detection of diethylamine by UiO-68-osdm can be clearly and easily observed by the naked eye under a portable 365 nm UV lamp. Moreover, application of UiO-68-osdm toward a range of amines shows that this MOF can differentiate secondary alkylamines from other amines (including tertiary, primary and aromatic amines) *via* significant fluorescence changes.

Because aromatic amines are electron-rich spices, decoration of MOFs with electron-deficient groups is a practical strategy for selective detection of this type of organic analyte. In this situation, electron-rich organic amines as donors can form donor–acceptor complexes with electron-deficient functional groups inside the skeletons of MOFs. Consequently, the photophysical properties of MOFs can be changed, which results in changes in the PL emission spectrum and UV-Vis adsorption band of the host MOF. Banerjee and coworkers synthesized a naphthalene diimide-decorated Mg-NDI framework for colorimetric detection of aniline in the presence of other aromatic compounds.[450] Electron-rich organic amines can form charge transfer complexes with the NDI moieties within the framework, resulting a change in color. Treatment of Mg-NDI with various organic amines, such as aniline, hydrazine, ethylene diamine, triethylamine, dimethylamine, 1,3-propanediamine, ethylamine, and methylamine, showed a distinct color change (to black) compared to other functionalized analytes, such as chlorobenzene, toluene, benzene, phenol, 4-nitrophenol, nitrobenzene, and 4-bromotoluene. This color change is extremely rapid and very prominent and can be easily detected by naked eye inspection. Mg-NDI is able to detect the presence of amines from a very low concentration (10^{-5} M) in the solid state. Due to the presence of the chromophoric NDI moiety, Mg-NDI is capable of sensing organic amines in the solid state.

In addition to PL methods, gravimetric methods have been applied for the detection of aniline. Li and coworkers synthesized MOF-5 and applied it in the gravimetric detection of aniline using a typical micro-gravimetric transducer of a resonant microcantilever (Fig. 25).[452] Inkjet printing technology was used to deposit MOF-5 material onto the lab-made resonant microcantilever for mass-type sensor fabrication. Then, the fabricated sensor was placed inside the testing chamber at room temperature to evaluate its vapour sensing performance. Upon exposure of MOF-5 to aniline vapors, adsorption of the

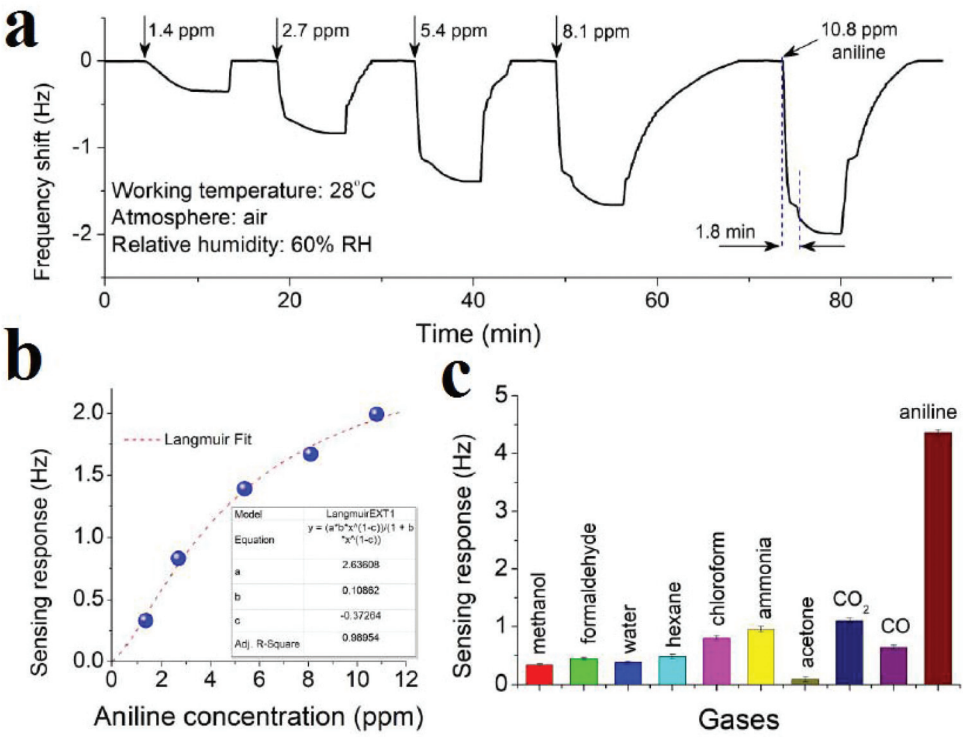

Fig. 25 Application of MOF-5 in gravimetric detection of aniline. (a) Micro-gravimetric sensing curve of the MOF-5 based microcantilever sensor for aniline vapor with concentrations in the range of 1.4 to 10.8 ppm; (b) relationship between aniline concentration and sensing response, which can be well fitted with the function of the Langmuir equation; (c) cross-sensitivity of the sensor to nine different interfering gases (each with a concentration of 50 ppm). Reproduced with permission from ref. 452.

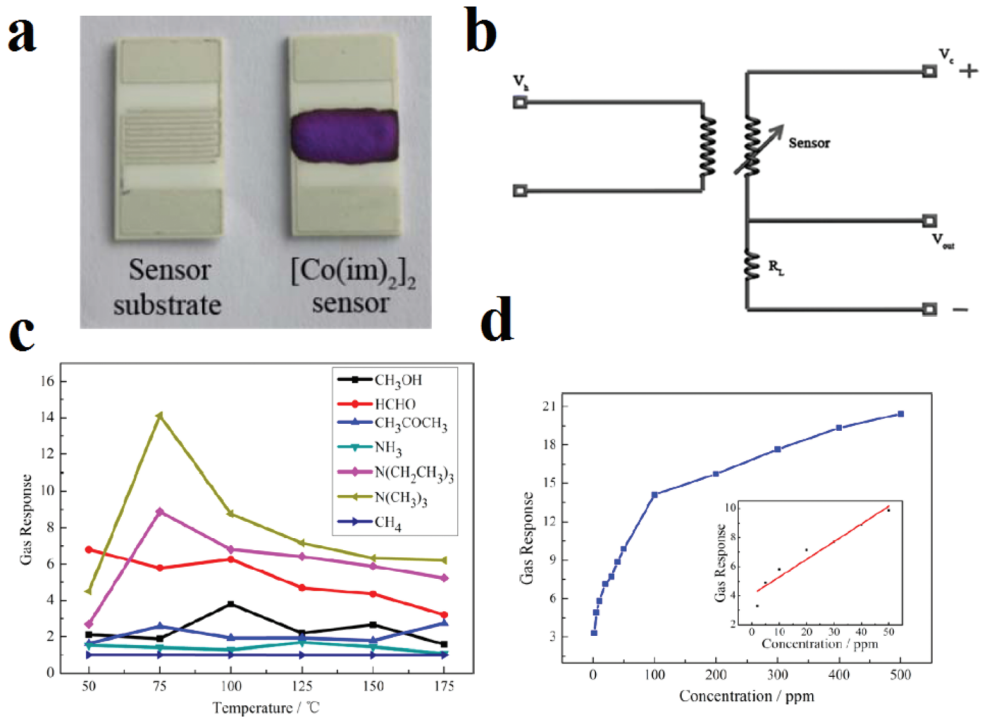

Fig. 26 Application of $[Co(im)_2]_n$ as a chemoresistive sensor for detection of TMA. (a) A view of the sensor substrate and the $[Co(im)_2]_n$ sensor. (b) Image of the operating principle. (c) Sensitivity of the $[Co(im)_2]_n$ sensor to 100 ppm of various gases in the temperature range of 50 °C to 175 °C. Response of the $[Co(im)_2]_n$ sensor to different concentrations of TMA at 75 °C. (d) The inset presents the linear dependence of the response on the TMA concentration between 2 and 50 ppm. Reproduced with permission from ref. 453.

aniline caused a mass increase of the MOF-5 sensing material; this led to a frequency decrease in the sensor, as indicated by the sensing curve (frequency change *versus* aniline concentration). Although humidity has negative effects on aniline detection, when the sensor is operated in air atmosphere with stable humidity, the sensor is suitable for detection of low concentrations of aniline, equal to 1.4 ppm. Simulations showed that aniline molecules prefer to be adsorbed onto the building block of 1,4-benzenedicarboxylic (BDC) ligand rather than on the Zn(II) center inside the pores of MOF-5; the isosteric heat of aniline adsorption is equal to 35.9 kJ mol^{-1}, which is indicative of physisorption of aniline molecules.

Trimethylamine (TMA) is a small organic amine that is hazardous to the human respiratory system; its detection is very important in the food industry to evaluate the freshness of seafood. Therefore, selective and sensitive detection of TMA is very beneficial for human safety. Zhang and coworkers applied a $[Co(im)_2]_n$ (im = imidazole) sensor to the detection of TMA in the vapor phase (Fig. 26).[453] To fabricate the sensor on the electrode, a paste was prepared from ground $[Co(im)_2]_n$ with an appropriate amount of ethanol; then, the paste was coated on the interdigital electrodes (five pairs of Ag–Pd interdigitated electrodes) of the sensor substrates with a tiny brush. The coated sensors were heated at 80 °C in a furnace to eliminate ethanol and then were calcined at 200 °C for 1.5 h. The response value of the $[Co(im)_2]_n$ sensor is depicted as R_g/R_a, where R_g and R_a are the resistance in the target gas and air, respectively. The response time was defined as the time needed for the sensor to obtain 90% of the total resistance change in the response. The responses to 100 ppm of diverse gases were measured as a function of the sensor temperature, and the results show that the optimum operating temperature of the $[Co(im)_2]_n$ sensor for TMA was defined as about 75 °C. By increasing the concentration of TMA, the response increased to 20.4 at 500 ppm TMA. The high sensitivity of $[Co(im)_2]_n$ to TMA is due to the optimized host–guest interaction and size-selective diffusion. Compared to the electron-rich O-atoms of other gases, such as methanol, the N atom of TMA possesses higher electron density because of the presence of three electron-donating methyl groups. In combination with trimethylamine, there may be slightly more steric hindrance in $(CH_3CH_2)_3N$ than in $(CH_3)_3N$. Therefore, the response to $(CH_3CH_2)_3N$ is slightly lower than that to $(CH_3)_3N$. Thus, the $[Co(im)_2]_n$ sensor could measure TMA at concentrations as low as 2 ppm, and the response was 2.5 at 75 °C.

5. Conclusions and outlook

The aim of this review is to investigate the detection of organic molecules by MOFs using different instrumental methods, such as photoluminescence, electrochemical, gravimetric, optical and photonic methods. To this aim, we classified organic compounds in three categories, including nitroaro-

matic and heterocyclic energetic molecules, small organic molecules, such as solvents and VOCs, and organic amines. Investigations reveal that each instrumental method has some benefits and limits for the detection of organic molecules, which we will discuss here to provide a different and distinctive conclusion of our review.

Due to the presence of nitro groups in the molecular structures of NACs, they are highly electron deficient, which endows them with π-deficient natures and reducibility (oxidizer agent) in redox reactions. Due to possible π–π interactions and hydrogen bonding between the MOF frameworks and NACs, photoluminescence is applied extensively for the detection of NACs. However, this method has achieved some important successes and demonstrated some limitations to date. In the case of the detection of nitrobenzene in the presence of other organic molecules (without nitro groups) and selective detection of 2,4,6-trinitrophenol, photoluminescence methods show effective rules. Especially in the case of detection of 2,4,6-trinitrophenol by PL methods, a summary of the published results in the literature reveals that MOFs based on d^{10}-metal centers (Zn(II) and Cd(II)) and functional ligands with Lewis basic groups (especially amines and adenine) are very promising. However, the photoluminescence method is not very successful for the detection of specific NAC molecules in the presence of other NACs. This may be because the presence of nitro groups in the structure of NACs results in competitive interactions between the MOF and NACs; thus, there are multiple signal-transductions in the presence of different NACs. However, some successful strategies have been investigated in this line.

Another strategy applied for the detection of NACs is based on the development of MOF-based electrochemical sensors. Although MOFs suffer from low conductivity and redox activity, their porous and functionalizable natures help remove these barriers when designing MOF-based electrochemical sensors by the synthesis of MOFs with redox-active organic ligands and metal centers and the synthesis of MOF-based composites using additional conductive components. NACs can participate in redox reactions through reduction of nitro groups. Because each nitro group in the molecular skeleton of an NAC has a particular reduction potential, and the reduction of nitro groups to nitrous or amine groups requires at least 6 electrons, it appears that current-based electrochemical methods such as amperometric methods are very sensitive for the detection of nitro NACs. Potentially, because each NAC molecule has a specific reduction potential, construction of MOFs with desirable potentials is beneficial for the selective detection of desired NACs and discrimination between NACs.

Small organic molecules include molecules with large varieties of functional groups and molecular skeletons; thus, they can interact with MOF skeletons through different host–guest chemistry. This is very helpful for the detection of this group of organic molecules, in the sense that we can develop specific MOFs with specific functionalities for the detection of desired small organic molecules through specific host–guest chemistry. This rule is practical for almost all possible detection methods. For example, in photoluminescence-based methods, different host–guest chemistry results in different signal-transductions of the luminescence of the host MOF, which can be specialized for specific analytes. In gravimetric methods, higher affinity between the MOF and organic molecules results in much higher diffusion and adsorption of organic molecules into the pores of the MOF; this results in a greater change in the mass of the resonator and higher sensitivity and shifts in the frequency as detectable responses. In electrochemical methods, different structures of organic analytes result in different interactions between the MOF and analytes, which can lead to different resistances or conductivities for the analyte@MOF complex compared to the pristine MOF. Therefore, different host–guest chemistry between the MOF and organic analytes results in different conductivity or resistance in chemoresistive and conductometric methods. Also, organic molecules with different structures and functions have different physical properties, such as different refractive indices. Because the refractive index is highly sensitive to changes in the chemical structure of the host in optical detection methods, the pristine MOF and analyte@MOF complex present different refractive indices, which results in different signal transductions in optical sensors. Therefore, optical sensors are another successful strategy for the detection of small organic molecules.

Organic amines are electron-rich and Lewis basic. These two characteristics effectively rule the host–guest chemistry of organic amines. When designing MOF-based sensors for detection of organic amines, these two points should be considered. Therefore, a suitable MOF for detection of organic amines must be electron deficient and acidic. In this regard, construction of (–OH) and naphthalene diimide or pyridinium-functionalized MOFs has been very successful for colorimetric or luminescence-based detection of organic amine molecules as well as discrimination between aromatic and aliphatic amines.

In this review, we attempted to clarify and discuss the effectiveness of instrumental methods for the detection of organic molecules using MOFs. We hope that this review will be helpful for anyone who takes the time to read it.

Conflicts of interest

There are no conflicts to declare.

Acknowledgements

Support of this investigation by the National Natural Science Foundation of China (no. 21571143) and Tarbiat Modares University is gratefully acknowledged.

References

1 O. Yaghi and H. Li, *J. Am. Chem. Soc.*, 1995, **117**, 10401–10402.

2 O. M. Yaghi, G. Li and H. Li, *Nature*, 1995, **378**, 703.
3 K. Sumida, D. L. Rogow, J. A. Mason, T. M. McDonald, E. D. Bloch, Z. R. Herm, T.-H. Bae and J. R. Long, *Chem. Rev.*, 2011, **112**, 724–781.
4 Y. He, W. Zhou, G. Qian and B. Chen, *Chem. Soc. Rev.*, 2014, **43**, 5657–5678.
5 M. P. Suh, H. J. Park, T. K. Prasad and D.-W. Lim, *Chem. Rev.*, 2011, **112**, 782–835.
6 N. A. Khan, Z. Hasan and S. H. Jhung, *J. Hazard. Mater.*, 2013, **244**, 444–456.
7 S. Qiu, M. Xue and G. Zhu, *Chem. Soc. Rev.*, 2014, **43**, 6116–6140.
8 A. Corma, H. García and F. X. Llabrés i Xamena, *Chem. Rev.*, 2010, **110**, 4606–4655.
9 Y. Li, H. Xu, S. Ouyang and J. Ye, *Phys. Chem. Chem. Phys.*, 2016, **18**, 7563–7572.
10 A. Morozan and F. Jaouen, *Energy Environ. Sci.*, 2012, **5**, 9269–9290.
11 A. C. McKinlay, R. E. Morris, P. Horcajada, G. Férey, R. Gref, P. Couvreur and C. Serre, *Angew. Chem., Int. Ed.*, 2010, **49**, 6260–6266.
12 L. E. Kreno, K. Leong, O. K. Farha, M. Allendorf, R. P. Van Duyne and J. T. Hupp, *Chem. Rev.*, 2011, **112**, 1105–1125.
13 E. A. Dolgopolova, A. M. Rice, C. R. Martin and N. B. Shustova, *Chem. Soc. Rev.*, 2018, **47**, 4710–4728.
14 S. Wu, H. Min, W. Shi and P. Cheng, *Adv. Mater.*, 2019, 1805871.
15 Y. Zhang, S. Yuan, G. Day, X. Wang, X. Yang and H.-C. Zhou, *Coord. Chem. Rev.*, 2018, **354**, 28–45.
16 W. P. Lustig, S. Mukherjee, N. D. Rudd, A. V. Desai, J. Li and S. K. Ghosh, *Chem. Soc. Rev.*, 2017, **46**, 3242–3285.
17 Y. Cui, B. Chen and G. Qian, *Coord. Chem. Rev.*, 2014, **273–274**, 76–86.
18 B. Yan, *Acc. Chem. Res.*, 2017, **50**, 2789–2798.
19 J. He, J. Xu, J. Yin, N. Li and X.-H. Bu, *Sci. China Mater.*, 2019, 1–24.
20 W. Liu and X.-B. Yin, *TrAC, Trends Anal. Chem.*, 2016, **75**, 86–96.
21 P. Kumar, K.-H. Kim, P. K. Mehta, L. Ge and G. Lisak, *Crit. Rev. Environ. Sci. Technol.*, 2019, 1–33.
22 W.-T. Koo, J.-S. Jang and I.-D. Kim, *Chem*, 2019, **5**, 1938–1963.
23 L. Liu, Y. Zhou, S. Liu and M. Xu, *ChemElectroChem*, 2018, **5**, 6–19.
24 Y. Cui, Y. Yue, G. Qian and B. Chen, *Chem. Rev.*, 2011, **112**, 1126–1162.
25 I. Stassen, N. Burtch, A. Talin, P. Falcaro, M. Allendorf and R. Ameloot, *Chem. Soc. Rev.*, 2017, **46**, 3185–3241.
26 J. Heine and K. Müller-Buschbaum, *Chem. Soc. Rev.*, 2013, **42**, 9232–9242.
27 B. Chen, S. Xiang and G. Qian, *Acc. Chem. Res.*, 2010, **43**, 1115–1124.
28 X. Xin, M. Zhang, S. Ji, H. Dong and L. Zhang, *J. Solid State Chem.*, 2018, **262**, 186–190.
29 Z. Zhao, X. Song, L. Liu, G. Li, S. Shah and C. Hao, *J. Mol. Graphics Modell.*, 2018, **80**, 132–137.
30 S. Pramanik, C. Zheng, X. Zhang, T. J. Emge and J. Li, *J. Am. Chem. Soc.*, 2011, **133**, 4153–4155.
31 A. Lan, K. Li, H. Wu, D. H. Olson, T. J. Emge, W. Ki, M. Hong and J. Li, *Angew. Chem., Int. Ed.*, 2009, **48**, 2334–2338.
32 M. Guo and Z.-M. Sun, *J. Mater. Chem.*, 2012, **22**, 15939–15946.
33 X.-J. Hong, Q. Wei, Y.-P. Cai, S.-R. Zheng, Y. Yu, Y.-Z. Fan, X.-Y. Xu and L.-P. Si, *ACS Appl. Mater. Interfaces*, 2017, **9**, 4701–4708.
34 X.-L. Hu, F.-H. Liu, C. Qin, K.-Z. Shao and Z.-M. Su, *Dalton Trans.*, 2015, **44**, 7822–7827.
35 X.-L. Huang, L. Liu, M.-L. Gao and Z.-B. Han, *RSC Adv.*, 2016, **6**, 87945–87949.
36 Z. Zhang, S. Xiang, X. Rao, Q. Zheng, F. R. Fronczek, G. Qian and B. Chen, *Chem. Commun.*, 2010, **46**, 7205–7207.
37 S. Zhao, X.-X. Lv, L.-L. Shi, B.-L. Li and B. Wu, *RSC Adv.*, 2016, **6**, 56035–56041.
38 J.-C. Jin, X.-R. Wu, Z.-D. Luo, F.-Y. Deng, J.-Q. Liu, A. Singh and A. Kumar, *CrystEngComm*, 2017, **19**, 4368–4377.
39 D. Singh and C. Nagaraja, *Dalton Trans.*, 2014, **43**, 17912–17915.
40 X. Li, L. Yang, L. Zhao, X.-L. Wang, K.-Z. Shao and Z.-M. Su, *Cryst. Growth Des.*, 2016, **16**, 4374–4382.
41 Y. Wu, G.-P. Yang, Y. Zhao, W.-P. Wu, B. Liu and Y.-Y. Wang, *Dalton Trans.*, 2015, **44**, 3271–3277.
42 Y.-C. He, H.-M. Zhang, Y.-Y. Liu, Q.-Y. Zhai, Q.-T. Shen, S.-Y. Song and J.-F. Ma, *Cryst. Growth Des.*, 2014, **14**, 3174–3178.
43 P. Karthik, A. Pandikumar, M. Preeyanghaa, M. Kowsalya and B. Neppolian, *Microchim. Acta*, 2017, **184**, 2265–2273.
44 X.-Q. Yao, G.-B. Xiao, H. Xie, D.-D. Qin, H.-C. Ma, J.-C. Liu and P.-J. Yan, *CrystEngComm*, 2019, **21**, 2559–2570.
45 L.-L. Ren, Y.-Y. Cui, A.-L. Cheng and E.-Q. Gao, *J. Solid State Chem.*, 2019, **270**, 463–469.
46 C. Xu, C. Bi, Z. Zhu, R. Luo, X. Zhang, D. Zhang, C. Fan, L. Cui and Y. Fan, *CrystEngComm*, 2019, **21**, 2333–2344.
47 Y. Wu, Y. Li, L. Zou, J. Feng, J. Liu, M. Luo, J. Xu, R. Yadav and A. Kumar, *Z. Anorg. Allg. Chem.*, 2017, **643**, 214–219.
48 L. Zhou, K. Zhao, Y.-J. Hu, X.-C. Feng, P.-D. Shi and H.-G. Zheng, *Inorg. Chem. Commun.*, 2018, **89**, 68–72.
49 J.-L. Du, J.-P. Gao, C.-P. Li, X.-Y. Zhang, J.-X. Hou, X. Jing, Y.-J. Mu and L.-J. Li, *RSC Adv.*, 2017, **7**, 49618–49625.
50 L. Yang, C. Lian, X. Li, Y. Han, L. Yang, T. Cai and C. Shao, *ACS Appl. Mater. Interfaces*, 2017, **9**, 17208–17217.
51 S. Srivastava, B. K. Gupta and R. Gupta, *Cryst. Growth Des.*, 2017, **17**, 3907–3916.
52 Y. Pan, J. Wang, X. Guo, X. Liu, X. Tang and H. Zhang, *J. Colloid Interface Sci.*, 2018, **513**, 418–426.
53 Q.-Q. Wang, X. Li, G.-z. Li, K.-Z. Shao and Z.-M. Su, *Inorg. Chem. Commun.*, 2017, **86**, 271–275.
54 X.-J. Lei, X.-Y. Hou, S.-N. Li, Y.-C. Jiang, G.-X. Sun, M.-C. Hu and Q.-G. Zhai, *Inorg. Chem.*, 2018, **57**, 14280–14289.

55 B. Ma, Y. Fan, L. Wang, J. Xu and J. Zhao, *Inorg. Chim. Acta*, 2018, **480**, 166–172.
56 W.-P. Wu, J. Wu, J.-Q. Liu, M. Trivedi and A. Kumar, *RSC Adv.*, 2017, **7**, 54522–54531.
57 S. Xian, H.-L. Chen, W.-L. Feng, X.-Z. Yang, Y.-Q. Wang and B.-X. Li, *J. Solid State Chem.*, 2019, **280**, 120984.
58 Y. Zhang, P. Zhang, J. Cheng, W. Huang, P. Li and Y. Ma, *Inorg. Chim. Acta*, 2018, **471**, 336–344.
59 A. Yousaf, N. Xu, A. M. Arif, J. Zhou, C.-Y. Sun, X.-L. Wang and Z.-M. Su, *Dyes Pigm.*, 2019, **163**, 159–167.
60 S.-R. Zhang, W. Wang, G.-J. Xu, C. Yao, Y.-H. Xu and Z.-M. Su, *Inorg. Chem. Commun.*, 2017, **84**, 36–39.
61 W.-Q. Kan and S.-Z. Wen, *Dyes Pigm.*, 2017, **139**, 372–380.
62 Y.-N. Zhao, S.-R. Zhang, W. Wang, Y.-H. Xu and G.-B. Che, *New J. Chem.*, 2018, **42**, 14648–14654.
63 L. Chen, L. Zhang, Y.-H. Zhao, K.-Z. Shao, X.-L. Wang, M.-X. Huo and Z.-M. Su, *Inorg. Chem. Commun.*, 2017, **86**, 267–270.
64 L. Lu, J. Wang, W.-P. Wu, A. Ma, J.-Q. Liu, R. Yadav and A. Kumar, *J. Lumin.*, 2017, **186**, 40–47.
65 Y.-Q. Zhang, V. A. Blatov, T.-R. Zheng, C.-H. Yang, L.-L. Qian, K. Li, B.-L. Li and B. Wu, *Dalton Trans.*, 2018, **47**, 6189–6198.
66 Q.-Q. Liu, X.-J. Weng and K.-F. Yue, *J. Solid State Chem.*, 2019, **279**, 120933.
67 Z. Sun, Y. Bao, C. Wang, Z. Lin, A. Shi and H. Li, *Inorg. Chim. Acta*, 2019, **494**, 266–270.
68 H. Li, Y. Han, Z. Shao, N. Li, C. Huang and H. Hou, *Dalton Trans.*, 2017, **46**, 12201–12208.
69 J. Wang, F. Yuan, H.-M. Hu, B. Xu and G.-L. Xue, *Inorg. Chem. Commun.*, 2016, **71**, 19–22.
70 R. Ma, Z. Chen, S. Wang, Q. Yao, Y. Li, J. Lu, D. Li and J. Dou, *J. Solid State Chem.*, 2017, **252**, 142–151.
71 J. Zhang, L. Gong, J. Feng, J. Wu and C. Zhang, *New J. Chem.*, 2017, **41**, 8107–8117.
72 L. Liu, X. Chen, J. Qiu and C. Hao, *Dalton Trans.*, 2015, **44**, 2897–2906.
73 D.-M. Chen, J.-Y. Tian and C.-S. Liu, *Inorg. Chem. Commun.*, 2016, **68**, 29–32.
74 J.-Q. Liu, J. Wu, F.-M. Li, W.-C. Liu, B.-H. Li, J. Wang, Q.-L. Li, R. Yadav and A. Kumar, *RSC Adv.*, 2016, **6**, 31161–31166.
75 Z.-J. Li, X.-Y. Li, Y.-T. Yan, L. Hou, W.-Y. Zhang and Y.-Y. Wang, *Cryst. Growth Des.*, 2018, **18**, 2031–2039.
76 X.-M. Cao, N. Wei, L. Liu, L. Li and Z.-B. Han, *RSC Adv.*, 2016, **6**, 19459–19462.
77 R.-X. Yao, X. Cui, X.-X. Jia, F.-Q. Zhang and X.-M. Zhang, *Inorg. Chem.*, 2016, **55**, 9270–9275.
78 Y.-S. Xue, Y. He, L. Zhou, F.-J. Chen, Y. Xu, H.-B. Du, X.-Z. You and B. Chen, *J. Mater. Chem. A*, 2013, **1**, 4525–4530.
79 X.-L. Hu, C. Qin, X.-L. Wang, K.-Z. Shao and Z.-M. Su, *New J. Chem.*, 2015, **39**, 7858–7862.
80 X.-L. Hu, C. Qin, L. Zhao, F.-H. Liu, K.-Z. Shao and Z.-M. Su, *RSC Adv.*, 2015, **5**, 49606–49613.
81 R.-M. Wen, S.-D. Han, G.-J. Ren, Z. Chang, Y.-W. Li and X.-H. Bu, *Dalton Trans.*, 2015, **44**, 10914–10917.
82 C. Zhan, S. Ou, C. Zou, M. Zhao and C.-D. Wu, *Anal. Chem.*, 2014, **86**, 6648–6653.
83 J. Zhao, Y.-N. Wang, W.-W. Dong, Y.-P. Wu, D.-S. Li and Q.-C. Zhang, *Inorg. Chem.*, 2016, **55**, 3265–3271.
84 D. Wang, B. Liu, S. Yao, T. Wang, G. Li, Q. Huo and Y. Liu, *Chem. Commun.*, 2015, **51**, 15287–15289.
85 C. Zhang, L. Sun, Y. Yan, J. Li, X. Song, Y. Liu and Z. Liang, *Dalton Trans.*, 2015, **44**, 230–236.
86 Y.-N. Gong, Y.-L. Huang, L. Jiang and T.-B. Lu, *Inorg. Chem.*, 2014, **53**, 9457–9459.
87 S.-R. Zhang, D.-Y. Du, J.-S. Qin, S.-J. Bao, S.-L. Li, W.-W. He, Y.-Q. Lan, P. Shen and Z.-M. Su, *Chem. – Eur. J.*, 2014, **20**, 3589–3594.
88 X.-H. Zhou, L. Li, H.-H. Li, A. Li, T. Yang and W. Huang, *Dalton Trans.*, 2013, **42**, 12403–12409.
89 J.-D. Xiao, L.-G. Qiu, F. Ke, Y.-P. Yuan, G.-S. Xu, Y.-M. Wang and X. Jiang, *J. Mater. Chem. A*, 2013, **1**, 8745–8752.
90 L. H. Cao, F. Shi, W. M. Zhang, S. Q. Zang and T. C. Mak, *Chem. – Eur. J.*, 2015, **21**, 15705–15712.
91 D.-M. Chen, N.-N. Zhang, C.-S. Liu and M. Du, *ACS Appl. Mater. Interfaces*, 2017, **9**, 24671–24677.
92 R. Dalapati and S. Biswas, *Sens. Actuators, B*, 2017, **239**, 759–767.
93 R. Lv, J. Wang, Y. Zhang, H. Li, L. Yang, S. Liao, W. Gu and X. Liu, *J. Mater. Chem. A*, 2016, **4**, 15494–15500.
94 B. Joarder, A. V. Desai, P. Samanta, S. Mukherjee and S. K. Ghosh, *Chem. – Eur. J.*, 2015, **21**, 965–969.
95 S. S. Nagarkar, B. Joarder, A. K. Chaudhari, S. Mukherjee and S. K. Ghosh, *Angew. Chem., Int. Ed.*, 2013, **52**, 2881–2885.
96 J. Li and J. Li, *Inorg. Chem. Commun.*, 2018, **89**, 51–54.
97 S. Pal and P. K. Bharadwaj, *Cryst. Growth Des.*, 2016, **16**, 5852–5858.
98 Y. Rachuri, B. Parmar, K. K. Bisht and E. Suresh, *Dalton Trans.*, 2016, **45**, 7881–7892.
99 S. Sanda, S. Parshamoni, S. Biswas and S. Konar, *Chem. Commun.*, 2015, **51**, 6576–6579.
100 Y. Gao, Y. Qi, K. Zhao, Q. Wen, J. Shen, L. Qiu and W. Mou, *Sens. Actuators, B*, 2018, **257**, 553–560.
101 X.-L. Hu, C. Qin, X.-L. Wang, K.-Z. Shao and Z.-M. Su, *Chem. Commun.*, 2015, **51**, 17521–17524.
102 J. Hu, K. Wu, S. Dong and M. Zheng, *Polyhedron*, 2018, **153**, 261–267.
103 X.-X. Jia, R.-X. Yao, F.-Q. Zhang and X.-M. Zhang, *Inorg. Chem.*, 2017, **56**, 2690–2696.
104 X. Jiang, Y. Liu, P. Wu, L. Wang, Q. Wang, G. Zhu, X.-l. Li and J. Wang, *RSC Adv.*, 2014, **4**, 47357–47360.
105 Z.-Q. Shi, Z.-J. Guo and H.-G. Zheng, *Chem. Commun.*, 2015, **51**, 8300–8303.
106 L. Sun, H. Xing, J. Xu, Z. Liang, J. Yu and R. Xu, *Dalton Trans.*, 2013, **42**, 5508–5513.
107 K.-M. Wang, L. Du, Y.-L. Ma and Q.-H. Zhao, *Inorg. Chem. Commun.*, 2016, **68**, 45–49.

108 M. Bagheri, M. Y. Masoomi, A. Morsali and A. Schoedel, *ACS Appl. Mater. Interfaces*, 2016, **8**, 21472–21479.
109 J. Li, X. Luo, Y. Zhou, L. Zhang, Q. Huo and Y. Liu, *Cryst. Growth Des.*, 2018, **18**, 1857–1863.
110 Z.-W. Zhai, S.-H. Yang, M. Cao, L.-K. Li, C.-X. Du and S.-Q. Zang, *Cryst. Growth Des.*, 2018, **18**, 7173–7182.
111 X.-S. Zeng, H.-L. Xu, Y.-C. Xu, X.-Q. Li, Z.-Y. Nie, S.-Z. Gao and D.-R. Xiao, *Inorg. Chem. Front.*, 2018, **5**, 1622–1632.
112 L. Hu, X.-J. Hong, X.-M. Lin, J. Lin, Q.-X. Cheng, B. Lokesh and Y.-P. Cai, *Cryst. Growth Des.*, 2018, **18**, 7088–7093.
113 A. Hakimifar and A. Morsali, *Ultrason. Sonochem.*, 2019, **52**, 62–68.
114 A. Sharma, D. Kim, J.-H. Park, S. Rakshit, J. Seong, G. H. Jeong, O.-H. Kwon and M. S. Lah, *Commun. Chem.*, 2019, **2**, 39.
115 F. Zhong, C. Li, Y. Xie, H. Xu and J. Gao, *J. Solid State Chem.*, 2019, **278**, 120892.
116 M.-L. Han, S.-T. Wang, Z.-Q. Li, Z. Zhou, D.-S. Li, L.-F. Ma and Y.-Y. Wang, *Inorg. Chem. Commun.*, 2017, **79**, 12–16.
117 S. Eom, H. G. Lee, D. W. Kang, M. Kang, H. Kim, Y. Kim, S. Park, D. Moon and C. S. Hong, *ACS Appl. Mater. Interfaces*, 2018, **10**, 40372–40377.
118 S. Senthilkumar, R. Goswami, N. L. Obasi and S. Neogi, *ACS Sustainable Chem. Eng.*, 2017, **5**, 11307–11315.
119 N. He, M. Gao, D. Shen, H. Li, Z. Han and P. Zhao, *Forensic Sci. Int.*, 2019, **297**, 1–7.
120 H.-G. Hao, Y.-C. Wang, S.-X. Yuan, D.-M. Chen, D.-C. Li and J.-M. Dou, *Inorg. Chem. Commun.*, 2018, **98**, 120–126.
121 K. Xing, R. Fan, J. Wang, S. Zhang, K. Feng, X. Du, Y. Song, P. Wang and Y. Yang, *ACS Appl. Mater. Interfaces*, 2017, **9**, 19881–19893.
122 J. Wang, X.-R. Wu, J.-Q. Liu, B.-H. Li, A. Singh, A. Kumar and S. R. Batten, *CrystEngComm*, 2017, **19**, 3519–3525.
123 H. He, S.-H. Chen, D.-Y. Zhang, E.-C. Yang and X.-J. Zhao, *RSC Adv.*, 2017, **7**, 38871–38876.
124 Y. Rachuri, B. Parmar and E. Suresh, *Cryst. Growth Des.*, 2018, **18**, 3062–3072.
125 S. Halder, P. Ghosh, C. Rizzoli, P. Banerjee and P. Roy, *Polyhedron*, 2017, **123**, 217–225.
126 L. Wang, *J. Inorg. Organomet. Polym.*, 2019, 1–8.
127 B. Parmar, Y. Rachuri, K. K. Bisht, R. Laiya and E. Suresh, *Inorg. Chem.*, 2017, **56**, 2627–2638.
128 S. Ning, H. Chen, S. Zhang and P. Cheng, *Polyhedron*, 2018, **155**, 457–463.
129 Y. Jiang, L. Sun, J. Du, Y. Liu, H. Shi, Z. Liang and J. Li, *Cryst. Growth Des.*, 2017, **17**, 2090–2096.
130 J. Zhang, Y. Liu, J. Feng, L. Gong, M. G. Humphrey and C. Zhang, *Inorg. Chem.*, 2019, **58**, 9749–9755.
131 X.-L. Hu, X.-L. Wang and Z.-M. Su, *J. Solid State Chem.*, 2018, **258**, 781–785.
132 M. X. Guo, L. Yang, Z. W. Jiang, Z. W. Peng and Y. F. Li, *Spectrochim. Acta, Part A*, 2017, **187**, 43–48.
133 J. Hu, T. Cheng, S. Dong, C. Zhou, X. Huang and L. Zhang, *Microporous Mesoporous Mater.*, 2018, **272**, 177–183.
134 P. Das and S. K. Mandal, *ACS Appl. Mater. Interfaces*, 2018, **10**, 25360–25371.
135 X. Wang, P. Yan, Y. Li, G. An, X. Yao and G. Li, *Cryst. Growth Des.*, 2017, **17**, 2178–2185.
136 Z. Sun, P. Hu, Y. Ma and L. Li, *Dyes Pigm.*, 2017, **143**, 10–17.
137 H.-B. Zhu, Y. Shen, Z.-Z. Fu, Y.-Y. Yu, Y.-F. Jiang and Y. Zhao, *Inorg. Chem. Commun.*, 2019, **103**, 21–24.
138 F. Zhang, G. Zhang, H. Yao, Y. Wang, T. Chu and Y. Yang, *Microchim. Acta*, 2017, **184**, 1207–1213.
139 M. Peng, K. Huang, X. Li, D. Han, Q. Qiu, L. Jing and D. Qin, *J. Solid State Chem.*, 2019, **280**, 120993.
140 F. Guo, *Inorg. Chem. Commun.*, 2019, **102**, 108–112.
141 Z.-R. Pan, Z.-Z. Shi, X.-J. Gao and H.-G. Zheng, *Inorg. Chem. Commun.*, 2017, **86**, 290–294.
142 L. Jiang, J. Wang, C. Gong, C. Li, L. Lu, H. Li, A. Singh, A. Kumar and A. Ma, *Inorg. Chem. Commun.*, 2019, **106**, 18–21.
143 J.-H. Qin, H.-R. Wang, M.-L. Han, X.-H. Chang and L.-F. Ma, *Dalton Trans.*, 2017, **46**, 15434–15442.
144 S. Singh Dhankhar, N. Sharma, S. Kumar, T. J. Dhilip Kumar and C. M. Nagaraja, *Chem. – Eur. J.*, 2017, **23**, 16204–16212.
145 J. Zhang, J. Wu, G. Tang, J. Feng, F. Luo, B. Xu and C. Zhang, *Sens. Actuators, B*, 2018, **272**, 166–174.
146 D. Fu, N. Wang, H. Fan, T. Shu and S. Yue, *Inorg. Chem. Commun.*, 2017, **86**, 262–266.
147 S. Dong, J. Hu, K. Wu and M. Zheng, *Inorg. Chem. Commun.*, 2018, **95**, 111–116.
148 Y. Deng, N. Chen, Q. Li, X. Wu, X. Huang, Z. Lin and Y. Zhao, *Cryst. Growth Des.*, 2017, **17**, 3170–3177.
149 T. Wang, K. Huang, M. Peng, X. Li, D. Han, L. Jing and D. Qin, *CrystEngComm*, 2019, **21**, 494–501.
150 N. Goel and N. Kumar, *RSC Adv.*, 2018, **8**, 10746–10755.
151 L. Zhao, J. Gan, T. Xia, L. Jiang, J. Zhang, Y. Cui, G. Qian and Z. Yang, *J. Mater. Chem. C*, 2019, **7**, 897–904.
152 Y. Tang, H. Huang, Y. Peng, Q. Ruan, K. Wang, P. Yi, D. Liu and C. Zhong, *Chin. J. Chem.*, 2017, **35**, 1091–1097.
153 N. Singh, U. P. Singh and R. J. Butcher, *CrystEngComm*, 2017, **19**, 7009–7020.
154 Z.-F. Wu and X.-Y. Huang, *Dalton Trans.*, 2017, **46**, 12597–12604.
155 K. Wang, X. Tian, Y. Jin, J. Sun and Q. Zhang, *Cryst. Growth Des.*, 2017, **17**, 1836–1842.
156 Y.-Q. Zhang, V. A. Blatov, T.-R. Zheng, C.-H. Yang, L.-L. Qian, K. Li, B.-L. Li and B. Wu, *Dalton Trans.*, 2018, **47**, 6189–6198.
157 K. Wu, J. Hu, S. Shi, J. Li and X. Cheng, *Dyes Pigm.*, 2019, 107993.
158 D.-M. Chen, J.-Y. Tian, Z.-W. Wang, C.-S. Liu, M. Chen and M. Du, *Chem. Commun.*, 2017, **53**, 10668–10671.
159 C. Yu, X. Sun, L. Zou, G. Li, L. Zhang and Y. Liu, *Inorg. Chem.*, 2019, **58**, 4026–4032.
160 K. Wang, H. Tang, D. Zhang, Y. Ma and Y. Wang, *Crystals*, 2018, **8**, 456.

161 Y. Mu, Y. Ran, J. Du, X. Wu, W. Nie, J. Zhang, Y. Zhao and H. Liu, *Polyhedron*, 2017, **124**, 125–130.
162 Z. Sun, Y. Bao, C. Wang, Z. Lin, A. Shi and H. Li, *Inorg. Chim. Acta*, 2019, **494**, 266–270.
163 S. Mukherjee, A. V. Desai, B. Manna, A. I. Inamdar and S. K. Ghosh, *Cryst. Growth Des.*, 2015, **15**, 4627–4634.
164 Z.-J. Wang, L. Qin, J.-X. Chen and H.-G. Zheng, *Inorg. Chem.*, 2016, **55**, 10999–11005.
165 S. Senthilkumar, R. Goswami, V. J. Smith, H. C. Bajaj and S. Neogi, *ACS Sustainable Chem. Eng.*, 2018, **6**, 10295–10306.
166 K. Shen, Z. Ju, L. Qin, T. Wang and H. Zheng, *Dyes Pigm.*, 2017, **136**, 515–521.
167 J. Ye, L. Zhao, R. F. Bogale, Y. Gao, X. Wang, X. Qian, S. Guo, J. Zhao and G. Ning, *Chem. – Eur. J.*, 2015, **21**, 2029–2037.
168 Y. Rachuri, B. Parmar, K. K. Bisht and E. Suresh, *Cryst. Growth Des.*, 2017, **17**, 1363–1372.
169 W. Liu, X. Huang, C. Xu, C. Chen, L. Yang, W. Dou, W. Chen, H. Yang and W. Liu, *Chem. – Eur. J.*, 2016, **22**, 18769–18776.
170 C. Zhang, Y. Yan, Q. Pan, L. Sun, H. He, Y. Liu, Z. Liang and J. Li, *Dalton Trans.*, 2015, **44**, 13340–13346.
171 H. He, Y. Song, F. Sun, Z. Bian, L. Gao and G. Zhu, *J. Mater. Chem. A*, 2015, **3**, 16598–16603.
172 A. Li, L. Li, Z. Lin, L. Song, Z.-H. Wang, Q. Chen, T. Yang, X.-H. Zhou, H.-P. Xiao and X.-J. Yin, *New J. Chem.*, 2015, **39**, 2289–2295.
173 X. Liu, B. Liu, G. Li and Y. Liu, *J. Mater. Chem. A*, 2018, **6**, 17177–17185.
174 J. Wang, L. Zhang, L. Bao, L. Zhou, Y. Liu and P. Wu, *Dyes Pigm.*, 2018, **150**, 301–305.
175 B. Wang, X.-L. Lv, D. Feng, L.-H. Xie, J. Zhang, M. Li, Y. Xie, J.-R. Li and H.-C. Zhou, *J. Am. Chem. Soc.*, 2016, **138**, 6204–6216.
176 B. Gole, A. K. Bar and P. S. Mukherjee, *Chem. Commun.*, 2011, **47**, 12137–12139.
177 H. Xu, F. Liu, Y. Cui, B. Chen and G. Qian, *Chem. Commun.*, 2011, **47**, 3153–3155.
178 J. A. Greathouse, N. W. Ockwig, L. J. Criscenti, T. Guilinger, P. Pohl and M. D. Allendorf, *Phys. Chem. Chem. Phys.*, 2010, **12**, 12621–12629.
179 S. Tarasi, A. A. Tehrani, A. Morsali and P. Retailleau, *New J. Chem.*, 2018, **42**, 14772–14778.
180 J.-S. Hu, S.-J. Dong, K. Wu, X.-L. Zhang, J. Jiang, J. Yuan and M.-D. Zheng, *Sens. Actuators, B*, 2019, **283**, 255–261.
181 V. K. Maka, A. Mukhopadhyay, G. Savitha and J. N. Moorthy, *Nanoscale*, 2018, **10**, 22389–22399.
182 Y. Wu, J. Wu, B. Xie, L. Zou, Y. Li, Y. Han and X. Wu, *J. Lumin.*, 2017, **192**, 775–782.
183 F.-H. Liu, C. Qin, Y. Ding, H. Wu, K.-Z. Shao and Z.-M. Su, *Dalton Trans.*, 2015, **44**, 1754–1760.
184 A. Das and S. Biswas, *Sens. Actuators, B*, 2017, **250**, 121–131.
185 P. Karthik, A. Pandikumar, M. Preeyanghaa, M. Kowsalya and B. Neppolian, *Microchim. Acta*, 2017, **184**, 2265–2273.
186 S. Sun, F. Wang, Y. Sun, X. Guo, R. Ma, M. Zhang, H. Guo, Y. Xie and T. Hu, *Ind. Eng. Chem. Res.*, 2019, **58**, 17784–17791.
187 Y. Tang, H. Wu, J. Chen, J. Jia, J. Yu, W. Xu, Y. Fu, Q. He, H. Cao and J. Cheng, *Dyes Pigm.*, 2019, **167**, 10–15.
188 J.-J. Ma and W.-s. Liu, *Dalton Trans.*, 2019, **48**, 12287–12295.
189 R. F. Bogale, Y. Chen, J. Ye, Y. Yang, A. Rauf, L. Duan, P. Tian and G. Ning, *Sens. Actuators, B*, 2017, **245**, 171–178.
190 C. Gogoi and S. Biswas, *Dalton Trans.*, 2018, **47**, 14696–14705.
191 Z.-J. Wang, L. Qin, J.-X. Chen and H.-G. Zheng, *Inorg. Chem.*, 2016, **55**, 10999–11005.
192 D. Wang, L. Sun, C. Hao, Y. Yan and Z. Liang, *RSC Adv.*, 2016, **6**, 57828–57834.
193 R. Wang, X. Liu, A. Huang, W. Wang, Z. Xiao, L. Zhang, F. Dai and D. Sun, *Inorg. Chem.*, 2016, **55**, 1782–1787.
194 J. A. Smith, M. A. Singh-Wilmot, K. P. Carter, C. L. Cahill and J. A. Ridenour, *Cryst. Growth Des.*, 2019, **19**, 305–319.
195 X.-S. Wang, L. Li, D.-Q. Yuan, Y.-B. Huang and R. Cao, *J. Hazard. Mater.*, 2018, **344**, 283–290.
196 Z. Sun, Y. Li, Y. Ma and L. Li, *Dyes Pigm.*, 2017, **146**, 263–271.
197 L. Lu, J. Wu, J. Wang, J.-Q. Liu, B.-H. Li, A. Singh, A. Kumar and S. R. Batten, *CrystEngComm*, 2017, **19**, 7057–7067.
198 K. S. Asha, K. Bhattacharyya and S. Mandal, *J. Mater. Chem. C*, 2014, **2**, 10073–10081.
199 H. Jin, J. Xu, L. Zhang, B. Ma, X. Shi, Y. Fan and L. Wang, *J. Solid State Chem.*, 2018, **268**, 168–174.
200 X.-X. Wu, H.-R. Fu, M.-L. Han, Z. Zhou and L.-F. Ma, *Cryst. Growth Des.*, 2017, **17**, 6041–6048.
201 Q. Fu, Y. Zhang, B. Liu and F. Guo, *J. Mol. Struct.*, 2018, **1171**, 69–75.
202 S. Mistri, E. Zangrando, P. Vojtíšek and S. C. Manna, *ChemistrySelect*, 2017, **2**, 2634–2642.
203 M. Bagheri, M. Y. Masoomi and A. Morsali, *Sens. Actuators, B*, 2017, **243**, 353–360.
204 F. Wang, C. Wang, Z. Yu, Q. He, X. Li, C. Shang and Y. Zhao, *RSC Adv.*, 2015, **5**, 70086–70093.
205 X.-Q. Wang, D.-D. Feng, Y.-D. Zhao, D.-D. Fang, J. Tang, L.-M. Fan and J. Yang, *J. Solid State Chem.*, 2019, **274**, 40–46.
206 F. Wang, Z. Yu, C. Wang, K. Xu, J. Yu, J. Zhang, Y. Fu, X. Li and Y. Zhao, *Sens. Actuators, B*, 2017, **239**, 688–695.
207 X. Wang, W. Fan, M. Zhang, Y. Shang, Y. Wang, D. Liu, H. Guo, F. Dai and D. Sun, *Chin. Chem. Lett.*, 2019, **30**, 801–805.
208 T. Shu, N. Wang, Y. Li, D. Fu, H. Fan, M. Luo and S. Yue, *ChemistrySelect*, 2017, **2**, 12046–12050.
209 N. Xu, Q. Zhang and G. Zhang, *Dalton Trans.*, 2019, **48**, 2683–2691.
210 Z. Tang, H. Chen, Y. Zhang, B. Zheng, S. Zhang and P. Cheng, *Cryst. Growth Des.*, 2019, **19**, 1172–1182.
211 F. Wang, K. Xu, Z. Jiang, T. Yan, C. Wang, Y. Pu and Y. Zhao, *J. Lumin.*, 2018, **194**, 22–28.
212 G. Chakraborty, P. Das and S. K. Mandal, *ACS Appl. Mater. Interfaces*, 2018, **10**, 42406–42416.

213 J.-H. Wang, G.-Y. Li, X.-J. Liu, R. Feng, H.-J. Zhang, S.-Y. Zhang and Y.-H. Zhang, *Inorg. Chim. Acta*, 2018, **473**, 70–74.
214 Z. Yu, F. Wang, X. Lin, C. Wang, Y. Fu, X. Wang, Y. Zhao and G. Li, *J. Solid State Chem.*, 2015, **232**, 96–101.
215 Y.-J. Yang, M.-J. Wang and K.-L. Zhang, *J. Mater. Chem. C*, 2016, **4**, 11404–11418.
216 M. Chen, W.-M. Xu, J.-Y. Tian, H. Cui, J.-X. Zhang, C.-S. Liu and M. Du, *J. Mater. Chem. C*, 2017, **5**, 2015–2021.
217 D. Singh and C. M. Nagaraja, *Dalton Trans.*, 2014, **43**, 17912–17915.
218 D. Tian, Y. Li, R.-Y. Chen, Z. Chang, G.-Y. Wang and X.-H. Bu, *J. Mater. Chem. A*, 2014, **2**, 1465–1470.
219 A. Azhdari Tehrani, L. Esrafili, S. Abedi, A. Morsali, L. Carlucci, D. M. Proserpio, J. Wang, P. C. Junk and T. Liu, *Inorg. Chem.*, 2017, **56**, 1446–1454.
220 H.-P. Li, Z. Dou, S.-Q. Chen, M. Hu, S. Li, H.-M. Sun, Y. Jiang and Q.-G. Zhai, *Inorg. Chem.*, 2019, **58**, 11220–11230.
221 X. Zhou, H. Li, H. Xiao, L. Li, Q. Zhao, T. Yang, J. Zuo and W. Huang, *Dalton Trans.*, 2013, **42**, 5718–5723.
222 X.-G. Liu, H. Wang, B. Chen, Y. Zou, Z.-G. Gu, Z. Zhao and L. Shen, *Chem. Commun.*, 2015, **51**, 1677–1680.
223 I.-H. Park, R. Medishetty, J.-Y. Kim, S. S. Lee and J. J. Vittal, *Angew. Chem., Int. Ed.*, 2014, **53**, 5591–5595.
224 Z.-Q. Shi, Z.-J. Guo and H.-G. Zheng, *Chem. Commun.*, 2015, **51**, 8300–8303.
225 W. Yan, C. Zhang, S. Chen, L. Han and H. Zheng, *ACS Appl. Mater. Interfaces*, 2017, **9**, 1629–1634.
226 D. Liu, X. Liu, Y. Liu, Y. Yu, F. Chen and C. Wang, *Dalton Trans.*, 2014, **43**, 15237–15244.
227 Z. Hu, S. Pramanik, K. Tan, C. Zheng, W. Liu, X. Zhang, Y. J. Chabal and J. Li, *Cryst. Growth Des.*, 2013, **13**, 4204–4207.
228 K.-H. Wang, *J. Coord. Chem.*, 2017, **70**, 3982–3995.
229 J. Roales, F. Moscoso, F. Gámez, T. Lopes-Costa, A. Sousaraei, S. Casado, J. Castro-Smirnov, J. Cabanillas-Gonzalez, J. Almeida and C. Queirós, *Materials*, 2017, **10**, 992.
230 X. Qi, Y. Jin, N. Li, Z. Wang, K. Wang and Q. Zhang, *Chem. Commun.*, 2017, **53**, 10318–10321.
231 Y. Li, X. Wang, C. Xing, X. Zhang, Z. Liang, X. Wang, K. Zhang, Y. Wang, D. Liu, W. Fan and F. Dai, *Chin. Chem. Lett.*, 2019, **30**, 1440–1444.
232 X.-H. Xin, W. Lu, J. Lu, J.-G. Xu, S.-H. Wang, F.-K. Zheng and G.-C. Guo, *Inorg. Chem. Commun.*, 2018, **97**, 129–133.
233 E. Gao, D. Liu, J. Xing, Y. Feng, J. Su, J. Liu, H. Zhao, N. Wang, Z. Jia, X. Zhang, V. P. Fedin and M. Zhu, *Appl. Organomet. Chem.*, 2019, **33**, e5109.
234 Y. Li, Z. Wei, Y. Zhang, Z. Guo, D. Chen, P. Jia, P. Chen and H. Xing, *ACS Sustainable Chem. Eng.*, 2019, **7**, 6196–6203.
235 X. Zhang, G. Ren, M. Li, W. Yang and Q. Pan, *Cryst. Growth Des.*, 2019, **19**, 6308–6314.
236 M. Gharib, V. Safarifard and A. Morsali, *Ultrason. Sonochem.*, 2018, **42**, 112–118.
237 A. K. Chaudhari, S. S. Nagarkar, B. Joarder and S. K. Ghosh, *Cryst. Growth Des.*, 2013, **13**, 3716–3721.
238 L. Huo, J. Zhang, L. Gao, X. Wang, L. Fan, K. Fang and T. Hu, *CrystEngComm*, 2017, **19**, 5285–5292.
239 J.-C. Jin, X.-R. Wu, Z.-D. Luo, F.-Y. Deng, J.-Q. Liu, A. Singh and A. Kumar, *CrystEngComm*, 2017, **19**, 4368–4377.
240 S. Pramanik, C. Zheng, X. Zhang, T. J. Emge and J. Li, *J. Am. Chem. Soc.*, 2011, **133**, 4153–4155.
241 R. Fu, S. Hu and X. Wu, *J. Mater. Chem. A*, 2017, **5**, 1952–1956.
242 S. Pramanik, Z. Hu, X. Zhang, C. Zheng, S. Kelly and J. Li, *Chem. – Eur. J.*, 2013, **19**, 15964–15971.
243 J. Qin, B. Ma, X.-F. Liu, H.-L. Lu, X.-Y. Dong, S.-Q. Zang and H. Hou, *J. Mater. Chem. A*, 2015, **3**, 12690–12697.
244 C.-L. Tao, Y.-M. Ying, H. Wang, B. Chen, G.-P. Zhu, Y.-J. Song, X.-G. Liu, Z. Zhao, L. Shen and B. Z. Tang, *J. Mater. Chem. C*, 2018, **6**, 12371–12376.
245 H. Xue, D. Song, C. Liu, G. Lyu, D. Yuan, F. Jiang, Q. Chen and M. Hong, *Chem. – Eur. J.*, 2018, **24**, 11033–11041.
246 Y. Sun, B.-X. Dong and W.-L. Liu, *Spectrochim. Acta, Part A*, 2019, **223**, 117283.
247 J. D. Einkauf, R. E. Ortega, L. Mathivathanan and D. T. de Lill, *New J. Chem.*, 2017, **41**, 10929–10934.
248 H.-G. Hao, Y.-C. Wang, S.-X. Yuan, D.-M. Chen, D.-C. Li and J.-M. Dou, *Inorg. Chem. Commun.*, 2018, **98**, 120–126.
249 W.-L. Duan, H.-C. Wang, J. Martí-Rujas and F. Guo, *CrystEngComm*, 2018, **20**, 323–327.
250 H.-R. Fu, X.-X. Wu, L.-F. Ma, F. Wang and J. Zhang, *ACS Appl. Mater. Interfaces*, 2018, **10**, 18012–18020.
251 F. G. M. Mauricio, J. Y. R. Silva, M. Talhavini, S. A. Júnior and I. T. Weber, *Microchem. J.*, 2019, **150**, 104037.
252 Z. Zhang, S. Chen, R. Shi, J. Ji, D. Wang, S. Jin, T. Han, C. Zhou and Q. Shu, *Talanta*, 2017, **166**, 228–233.
253 M. N. Ahamad, M. Shahid, M. Ahmad and F. Sama, *ACS Omega*, 2019, **4**, 7738–7749.
254 M.-L. Han, G.-X. Wen, W.-W. Dong, Z.-H. Zhou, Y.-P. Wu, J. Zhao, D.-S. Li, L.-F. Ma and X. Bu, *J. Mater. Chem. C*, 2017, **5**, 8469–8474.
255 Y. Wang, K. Gao, J. Li, L. Wang and J. Wu, *Inorg. Chem. Commun.*, 2018, **96**, 189–193.
256 Y. Yang, F. Qiu, C. Xu, Y. Feng, G. Zhang and W. Liu, *Dalton Trans.*, 2018, **47**, 7480–7486.
257 W.-H. Huang, J. Ren, Y.-H. Yang, X.-M. Li, Q. Wang, N. Jiang, J.-Q. Yu, F. Wang and J. Zhang, *Inorg. Chem.*, 2019, **58**, 1481–1491.
258 J.-Q. Liu, J. Wu, F.-M. Li, W.-C. Liu, B.-H. Li, J. Wang, Q.-L. Li, R. Yadav and A. Kumar, *RSC Adv.*, 2016, **6**, 31161–31166.
259 G. Chakraborty and S. K. Mandal, *Inorg. Chem.*, 2017, **56**, 14556–14566.
260 L. Lu, J. He, J. Wang, W.-P. Wu, B. Li, A. Singh, A. Kumar and X. Qin, *J. Mol. Struct.*, 2019, **1179**, 612–617.
261 J. Liu, J. Wu, Z. Luo, B. Li, A. Singh and K. Abhinav, *J. Coord. Chem.*, 2017, **70**, 3946–3958.

262 H. He, D.-Y. Zhang, F. Guo and F. Sun, *Inorg. Chem.*, 2018, **57**, 7314–7320.
263 R. Goswami, S. C. Mandal, B. Pathak and S. Neogi, *ACS Appl. Mater. Interfaces*, 2019, **11**, 9042–9053.
264 T. Xia, F. Zhu, Y. Cui, Y. Yang, Z. Wang and G. Qian, *J. Solid State Chem.*, 2017, **245**, 127–131.
265 A. Gogia and S. K. Mandal, *Dalton Trans.*, 2019, **48**, 2388–2398.
266 D. Das and K. Biradha, *Cryst. Growth Des.*, 2018, **18**, 3683–3692.
267 B. Ma, J. Xu, H. Qi, J. Sun, J. Chai, J. Jia, S. Jing, Y. Fan and L. Wang, *J. Solid State Chem.*, 2018, **258**, 42–48.
268 Y. Yang, K. Shen, J.-z. Lin, Y. Zhou, Q.-y. Liu, C. Hang, H. N. Abdelhamid, Z.-q. Zhang and H. Chen, *RSC Adv.*, 2016, **6**, 45475–45481.
269 X. Luo, X. Zhang, Y. Duan, X. Wang and J. Zhao, *Dalton Trans.*, 2017, **46**, 6303–6311.
270 Y. Wu, J. Wu, Z. Luo, J. Wang, Y. Li, Y. Han and J. Liu, *RSC Adv.*, 2017, **7**, 10415–10423.
271 Y.-N. Gong, L. Jiang and T.-B. Lu, *Chem. Commun.*, 2013, **49**, 11113–11115.
272 S. Zhang, L. Han, L. Li, J. Cheng, D. Yuan and J. Luo, *Cryst. Growth Des.*, 2013, **13**, 5466–5472.
273 X.-Y. Wan, F.-L. Jiang, C.-P. Liu, K. Zhou, L. Chen, Y.-L. Gai, Y. Yang and M.-C. Hong, *J. Mater. Chem. A*, 2015, **3**, 22369–22376.
274 J. Wang, W. Sun, S. Chang, H. Liu, G. Zhang, Y. Wang and Z. Liu, *RSC Adv.*, 2015, **5**, 48574–48579.
275 Z.-F. Wu, B. Tan, M.-L. Feng, A.-J. Lan and X.-Y. Huang, *J. Mater. Chem. A*, 2014, **2**, 6426–6431.
276 D. Banerjee, Z. Hu, S. Pramanik, X. Zhang, H. Wang and J. Li, *CrystEngComm*, 2013, **15**, 9745–9750.
277 L. Sun, H. Xing, J. Xu, Z. Liang, J. Yu and R. Xu, *Dalton Trans.*, 2013, **42**, 5508–5513.
278 D.-M. Chen, J.-Y. Tian, M. Chen, C.-S. Liu and M. Du, *ACS Appl. Mater. Interfaces*, 2016, **8**, 18043–18050.
279 M. Jurcic, W. J. Peveler, C. N. Savory, D. O. Scanlon, A. J. Kenyon and I. P. Parkin, *J. Mater. Chem. A*, 2015, **3**, 6351–6359.
280 D.-M. Chen, N.-N. Zhang, C.-S. Liu and M. Du, *J. Mater. Chem. C*, 2017, **5**, 2311–2317.
281 S. Abedi, A. A. Tehrani and A. Morsali, *New J. Chem.*, 2015, **39**, 5108–5111.
282 H. Ghasempour, A. Azhdari Tehrani, A. Morsali, J. Wang and P. C. Junk, *CrystEngComm*, 2016, **18**, 2463–2468.
283 Z.-W. Zhai, S.-H. Yang, M. Cao, L.-K. Li, C.-X. Du and S.-Q. Zang, *Cryst. Growth Des.*, 2018, **18**, 7173–7182.
284 K. Xing, R. Fan, J. Wang, S. Zhang, K. Feng, X. Du, Y. Song, P. Wang and Y. Yang, *ACS Appl. Mater. Interfaces*, 2017, **9**, 19881–19893.
285 S. Halder, P. Ghosh, C. Rizzoli, P. Banerjee and P. Roy, *Polyhedron*, 2017, **123**, 217–225.
286 X.-J. Hong, Q. Wei, Y.-P. Cai, S.-R. Zheng, Y. Yu, Y.-Z. Fan, X.-Y. Xu and L.-P. Si, *ACS Appl. Mater. Interfaces*, 2017, **9**, 4701–4708.
287 L.-H. Cao, F. Shi, W.-M. Zhang, S.-Q. Zang and T. C. W. Mak, *Chem. – Eur. J.*, 2015, **21**, 15705–15712.
288 R. Lv, J. Wang, Y. Zhang, H. Li, L. Yang, S. Liao, W. Gu and X. Liu, *J. Mater. Chem. A*, 2016, **4**, 15494–15500.
289 J. Hu, T. Cheng, S. Dong, C. Zhou, X. Huang and L. Zhang, *Microporous Mesoporous Mater.*, 2018, **272**, 177–183.
290 M. Peng, K. Huang, X. Li, D. Han, Q. Qiu, L. Jing and D. Qin, *J. Solid State Chem.*, 2019, **280**, 120993.
291 L. Jiang, J. Wang, C. Gong, C. Li, L. Lu, H. Li, A. Singh, A. Kumar and A. Ma, *Inorg. Chem. Commun.*, 2019, **106**, 18–21.
292 N. Goel and N. Kumar, *RSC Adv.*, 2018, **8**, 10746–10755.
293 K. Wu, J. Hu, S. Shi, J. Li and X. Cheng, *Dyes Pigm.*, 2020, **173**, 107993.
294 T. K. Kim, J. H. Lee, D. Moon and H. R. Moon, *Inorg. Chem.*, 2013, **52**, 589–595.
295 J. A. Greathouse, N. W. Ockwig, L. J. Criscenti, T. R. Guilinger, P. Pohl and M. D. Allendorf, *Phys. Chem. Chem. Phys.*, 2010, **12**, 12621–12629.
296 B. Joarder, A. V. Desai, P. Samanta, S. Mukherjee and S. K. Ghosh, *Chem. – Eur. J.*, 2015, **21**, 965–969.
297 T. K. Kim, J. H. Lee, D. Moon and H. R. Moon, *Inorg. Chem.*, 2012, **52**, 589–595.
298 M.-Q. Li, Y.-L. Wong, T.-S. Lum, K. Sze-Yin Leung, P. K. S. Lam and Z. Xu, *J. Mater. Chem. A*, 2018, **6**, 14566–14570.
299 A. Azhdari Tehrani, H. Ghasempour, A. Morsali, G. Makhloufi and C. Janiak, *Cryst. Growth Des.*, 2015, **15**, 5543–5547.
300 P. Das and S. K. Mandal, *ACS Appl. Mater. Interfaces*, 2018, **10**, 25360–25371.
301 B. Joarder, A. V. Desai, P. Samanta, S. Mukherjee and S. K. Ghosh, *Chem. – Eur. J.*, 2014, **21**, 965–969.
302 C. Zhang, Y. Yan, L. Sun, Z. Liang and J. Li, *CrystEngComm*, 2016, **18**, 4102–4108.
303 H.-R. Fu, Y. Zhao, T. Xie, M.-L. Han, L.-F. Ma and S.-Q. Zang, *J. Mater. Chem. C*, 2018, **6**, 6440–6448.
304 F. Zhang, Y. Wang, T. Chu, Z. Wang, W. Li and Y. Yang, *Analyst*, 2016, **141**, 4502–4510.
305 Y.-Q. Wang, Q.-H. Tan, H.-T. Liu, W. Sun and Z.-L. Liu, *RSC Adv.*, 2015, **5**, 86614–86619.
306 C. Liu, X. Bo and L. Guo, *Sens. Actuators, B*, 2019, **297**, 126741.
307 M. U. A. Prathap and S. Gunasekaran, *Adv. Sustainable Syst.*, 2018, **2**, 1800053.
308 Y. Guo, X. Feng, T. Han, S. Wang, Z. Lin, Y. Dong and B. Wang, *J. Am. Chem. Soc.*, 2014, **136**, 15485–15488.
309 Z. Hu, K. Tan, W. P. Lustig, H. Wang, Y. Zhao, C. Zheng, D. Banerjee, T. J. Emge, Y. J. Chabal and J. Li, *Chem. Sci.*, 2014, **5**, 4873–4877.
310 Y. Hwang, H. Sohn, A. Phan, O. M. Yaghi and R. N. Candler, *Nano Lett.*, 2013, **13**, 5271–5276.
311 T. Xu, P. Xu, D. Zheng, H. Yu and X. Li, *Anal. Chem.*, 2016, **88**, 12234–12240.

312 P. Davydovskaya, A. Ranft, B. V. Lotsch and R. Pohle, *Anal. Chem.*, 2014, **86**, 6948–6958.
313 A. H. Khoshaman and B. Bahreyni, *Sens. Actuators, B*, 2012, **162**, 114–119.
314 M. Tu, S. Wannapaiboon, K. Khaletskaya and R. A. Fischer, *Adv. Funct. Mater.*, 2015, **25**, 4470–4479.
315 H. Yamagiwa, S. Sato, T. Fukawa, T. Ikehara, R. Maeda, T. Mihara and M. Kimura, *Sci. Rep.*, 2014, **4**, 6247.
316 P. Davydovskaya, A. Ranft, B. V. Lotsch and R. Pohle, *Procedia Eng.*, 2014, **87**, 1433–1436.
317 P. Davydovskaya, R. Pohle, A. Tawil and M. Fleischer, *Sens. Actuators, B*, 2013, **187**, 142–146.
318 P. Davydovskaya, V. Pentyala, O. Yurchenko, L. Hussein, R. Pohle and G. A. Urban, *Sens. Actuators, B*, 2014, **193**, 911–917.
319 M. Ghanbarian, S. Zeinali and A. Mostafavi, *Sens. Actuators, B*, 2018, **267**, 381–391.
320 M. G. Campbell, S. F. Liu, T. M. Swager and M. Dincă, *J. Am. Chem. Soc.*, 2015, **137**, 13780–13783.
321 S. Homayoonnia and S. Zeinali, *Sens. Actuators, B*, 2016, **237**, 776–786.
322 M. Leidinger, M. Rieger, D. Weishaupt, T. Sauerwald, M. Nägele, J. Hürttlen and A. Schütze, *Procedia Eng.*, 2015, **120**, 1042–1045.
323 C. Sapsanis, H. Omran, V. Chernikova, O. Shekhah, Y. Belmabkhout, U. Buttner, M. Eddaoudi and K. Salama, *Sensors*, 2015, **15**, 18153–18166.
324 E.-X. Chen, H. Yang and J. Zhang, *Inorg. Chem.*, 2014, **53**, 5411–5413.
325 M. G. Campbell, D. Sheberla, S. F. Liu, T. M. Swager and M. Dincă, *Angew. Chem., Int. Ed.*, 2015, **54**, 4349–4352.
326 J. Gu, X. Yin, X. Bo and L. Guo, *ChemElectroChem*, 2018, **5**, 2893–2901.
327 F. Gándara, F. J. Uribe-Romo, D. K. Britt, H. Furukawa, L. Lei, R. Cheng, X. Duan, M. O'Keeffe and O. M. Yaghi, *Chem. – Eur. J.*, 2012, **18**, 10595–10601.
328 S. G. Surya, S. S. Nagarkar, S. K. Ghosh, P. Sonar and V. Ramgopal Rao, *Sens. Actuators, B*, 2016, **223**, 114–122.
329 W.-w. Zhan, Q. Kuang, J.-z. Zhou, X.-j. Kong, Z.-x. Xie and L.-s. Zheng, *J. Am. Chem. Soc.*, 2013, **135**, 1926–1933.
330 A. Doménech, H. García, M. T. Doménech-Carbó and F. Llabrés-i-Xamena, *J. Phys. Chem. C*, 2007, **111**, 13701–13711.
331 Y. Li, C. Huangfu, H. Du, W. Liu, Y. Li and J. Ye, *J. Electroanal. Chem.*, 2013, **709**, 65–69.
332 S. Dong, G. Suo, N. Li, Z. Chen, L. Peng, Y. Fu, Q. Yang and T. Huang, *Sens. Actuators, B*, 2016, **222**, 972–979.
333 T. Q. N. Tran, G. Das and H. H. Yoon, *Sens. Actuators, B*, 2017, **243**, 78–83.
334 X. Fu, Y. Yang, N. Wang and S. Chen, *Sens. Actuators, B*, 2017, **250**, 584–590.
335 M. Deng, S. Lin, X. Bo and L. Guo, *Talanta*, 2017, **174**, 527–538.
336 Y. Zhang, A. Nsabimana, L. Zhu, X. Bo, C. Han, M. Li and L. Guo, *Talanta*, 2014, **129**, 55–62.
337 S. A. A. Razavi and A. Morsali, *Coord. Chem. Rev.*, 2019, **399**, 213023.
338 H. Yang, F. Wang, Y. X. Tan, Y. Kang, T. H. Li and J. Zhang, *Chem. – Asian J.*, 2012, **7**, 1069–1073.
339 Z. Hao, X. Song, M. Zhu, X. Meng, S. Zhao, S. Su, W. Yang, S. Song and H. Zhang, *J. Mater. Chem. A*, 2013, **1**, 11043–11050.
340 Y. Zhao, X. Xu, L. Qiu, X. Kang, L. Wen and B. Zhang, *ACS Appl. Mater. Interfaces*, 2017, **9**, 15164–15175.
341 X.-Y. Xu and B. Yan, *J. Mater. Chem. A*, 2017, **5**, 2215–2223.
342 X. Wan, H. Song, D. Zhao, L. Zhang and Y. Lv, *Sens. Actuators, B*, 2014, **201**, 413–419.
343 P. Wu, J. Wang, Y. Li, C. He, Z. Xie and C. Duan, *Adv. Funct. Mater.*, 2011, **21**, 2788–2794.
344 S. Li, L. Lu, M. Zhu, C. Yuan and S. Feng, *Sens. Actuators, B*, 2018, **258**, 970–980.
345 Z.-Q. Liu, Y. Zhao, X.-D. Zhang, Y.-S. Kang, Q.-Y. Lu, M. Azam, S. I. Al-Resayes and W.-Y. Sun, *Dalton Trans.*, 2017, **46**, 13943–13951.
346 Z. Sun, M. Yang, Y. Ma and L. Li, *Cryst. Growth Des.*, 2017, **17**, 4326–4335.
347 P.-Y. Du, S.-Y. Liao, W. Gu and X. Liu, *J. Solid State Chem.*, 2016, **244**, 31–34.
348 Y. Kang, X.-J. Zheng and L.-P. Jin, *J. Colloid Interface Sci.*, 2016, **471**, 1–6.
349 C. E. Kivi and D. Song, *Dalton Trans.*, 2016, **45**, 17087–17090.
350 X. Wang, L. Zhang, J. Yang, F. Liu, F. Dai, R. Wang and D. Sun, *J. Mater. Chem. A*, 2015, **3**, 12777–12785.
351 F.-Y. Yi, W. Yang and Z.-M. Sun, *J. Mater. Chem.*, 2012, **22**, 23201–23209.
352 Z. Guo, H. Xu, S. Su, J. Cai, S. Dang, S. Xiang, G. Qian, H. Zhang, M. O'Keeffe and B. Chen, *Chem. Commun.*, 2011, **47**, 5551–5553.
353 B. Chen, Y. Yang, F. Zapata, G. Lin, G. Qian and E. B. Lobkovsky, *Adv. Mater.*, 2007, **19**, 1693–1696.
354 X. Shen and B. Yan, *RSC Adv.*, 2016, **6**, 28165–28170.
355 J.-M. Zhou, W. Shi, H.-M. Li, H. Li and P. Cheng, *J. Phys. Chem. C*, 2014, **118**, 416–426.
356 H. Li, W. Shi, K. Zhao, Z. Niu, H. Li and P. Cheng, *Chem. – Eur. J.*, 2013, **19**, 3358–3365.
357 C. Liu and B. Yan, *Photochem. Photobiol. Sci.*, 2015, **14**, 1644–1650.
358 J.-N. Hao and B. Yan, *New J. Chem.*, 2016, **40**, 4654–4661.
359 S. Liu, Z. Xiang, Z. Hu, X. Zheng and D. Cao, *J. Mater. Chem.*, 2011, **21**, 6649–6653.
360 D. Ma, W. Wang, Y. Li, J. Li, C. Daiguebonne, G. Calvez and O. Guillou, *CrystEngComm*, 2010, **12**, 4372–4377.
361 L.-H. Cao, Y.-L. Wei, C. Ji, M.-L. Ma, S.-Q. Zang and T. C. W. Mak, *Chem. – Asian J.*, 2014, **9**, 3094–3098.
362 Z. Hao, G. Yang, X. Song, M. Zhu, X. Meng, S. Zhao, S. Song and H. Zhang, *J. Mater. Chem. A*, 2014, **2**, 237–244.
363 C.-Y. Sun, X.-L. Wang, C. Qin, J.-L. Jin, Z.-M. Su, P. Huang and K.-Z. Shao, *Chem. – Eur. J.*, 2013, **19**, 3639–3645.
364 Y. Xiao, L. Wang, Y. Cui, B. Chen, F. Zapata and G. Qian, *J. Alloys Compd.*, 2009, **484**, 601–604.

365 X.-Y. Xu and B. Yan, *ACS Appl. Mater. Interfaces*, 2015, **7**, 721–729.
366 W. Yang, J. Feng, S. Song and H. Zhang, *ChemPhysChem*, 2012, **13**, 2734–2738.
367 J.-M. Zhou, W. Shi, N. Xu and P. Cheng, *Inorg. Chem.*, 2013, **52**, 8082–8090.
368 D. Wang, L. Zhang, G. Li, Q. Huo and Y. Liu, *RSC Adv.*, 2015, **5**, 18087–18091.
369 J. Wang, M. Jiang, L. Yan, R. Peng, M. Huangfu, X. Guo, Y. Li and P. Wu, *Inorg. Chem.*, 2016, **55**, 12660–12668.
370 X. Z. Song, S. Y. Song, S. N. Zhao, Z. M. Hao, M. Zhu, X. Meng, L. L. Wu and H. J. Zhang, *Adv. Funct. Mater.*, 2014, **24**, 4034–4041.
371 F. Liu, W. Gao, P. Li, X.-M. Zhang and J.-P. Liu, *J. Solid State Chem.*, 2017, **253**, 202–210.
372 H. Wang, J. Qin, C. Huang, Y. Han, W. Xu and H. Hou, *Dalton Trans.*, 2016, **45**, 12710–12716.
373 S.-S. Zhao, J. Yang, Y.-Y. Liu and J.-F. Ma, *Inorg. Chem.*, 2016, **55**, 2261–2273.
374 J. Wang, J. Wang, Y. Li, M. Jiang, L. Zhang and P. Wu, *New J. Chem.*, 2016, **40**, 8600–8606.
375 X.-Y. Xu and B. Yan, *ACS Appl. Mater. Interfaces*, 2014, **7**, 721–729.
376 T. Wang, Q.-H. Liu, Y. Gao, X.-Y. Yang, W. Yang, S. Dang and Z.-M. Sun, *Chin. Chem. Lett.*, 2016, **27**, 497–501.
377 B.-L. Li, H.-N. Wang, L. Zhao, G.-Z. Li and Z.-M. Su, *Inorg. Chem. Commun.*, 2016, **66**, 87–89.
378 X. Zheng, L. Zhou, Y. Huang, C. Wang, J. Duan, L. Wen, Z. Tian and D. Li, *J. Mater. Chem. A*, 2014, **2**, 12413–12422.
379 H.-N. Wang, S.-Q. Jiang, Q.-Y. Lu, Z.-Y. Zhou, S.-P. Zhuo, G.-G. Shan and Z.-M. Su, *RSC Adv.*, 2015, **5**, 48881–48884.
380 Y. Wang, Y. Wu, C. Zhou, L. Cao and H. Yang, *Inorg. Chem. Commun.*, 2018, **89**, 5–9.
381 C. Li, J. Huang, H. Zhu, L. Liu, Y. Feng, G. Hu and X. Yu, *Sens. Actuators, B*, 2017, **253**, 275–282.
382 Z. Zhao, J. Hao, X. Song, S. Ren and C. Hao, *RSC Adv.*, 2015, **5**, 49752–49758.
383 J.-J. Huang, J.-H. Yu, F.-Q. Bai and J.-Q. Xu, *Cryst. Growth Des.*, 2018, **18**, 5353–5364.
384 N. D. Rudd, H. Wang, S. J. Teat and J. Li, *Inorg. Chim. Acta*, 2018, **470**, 312–317.
385 J.-X. Wu and B. Yan, *J. Colloid Interface Sci.*, 2017, **504**, 197–205.
386 Y. Yang, L. Chen, F. Jiang, X. Wan, M. Yu, Z. Cao, T. Jing and M. Hong, *J. Mater. Chem. C*, 2017, **5**, 4511–4519.
387 S.-N. Zhao, X.-Z. Song, M. Zhu, X. Meng, L.-L. Wu, J. Feng, S.-Y. Song and H.-J. Zhang, *Chem. – Eur. J.*, 2015, **21**, 9748–9752.
388 S. Dang, T. Wang, F. Yi, Q. Liu, W. Yang and Z. M. Sun, *Chem. – Asian J.*, 2015, **10**, 1703–1709.
389 D.-M. Chen, C.-X. Sun, Y. Peng, N.-N. Zhang, H.-H. Si, C.-S. Liu and M. Du, *Sens. Actuators, B*, 2018, **265**, 104–109.
390 Z. Jin, H. He, H. Zhao, T. Borjigin, F. Sun, D. Zhang and G. Zhu, *Dalton Trans.*, 2013, **42**, 13335–13338.
391 G.-X. Wen, M.-L. Han, X.-Q. Wu, Y.-P. Wu, W.-W. Dong, J. Zhao, D.-S. Li and L.-F. Ma, *Dalton Trans.*, 2016, **45**, 15492–15499.
392 G.-l. Liu, Y.-j. Qin, L. Jing, G.-y. Wei and H. Li, *Chem. Commun.*, 2013, **49**, 1699–1701.
393 S. L. Jackson, A. Rananaware, C. Rix, S. V. Bhosale and K. Latham, *Cryst. Growth Des.*, 2016, **16**, 3067–3071.
394 W. Xie, W. W. He, S. L. Li, K. Z. Shao, Z. M. Su and Y. Q. Lan, *Chem. – Eur. J.*, 2016, **22**, 17298–17304.
395 S. Pramanik, Z. Hu, X. Zhang, C. Zheng, S. Kelly and J. Li, *Chem. – Eur. J.*, 2013, **19**, 15964–15971.
396 Y. Li, S. Zhang and D. Song, *Angew. Chem., Int. Ed.*, 2013, **52**, 710–713.
397 J. Cui, Z. Lu, Y. Li, Z. Guo and H. Zheng, *Chem. Commun.*, 2012, **48**, 7967–7969.
398 X.-H. Jin, J.-K. Sun, L.-X. Cai and J. Zhang, *Chem. Commun.*, 2011, **47**, 2667–2669.
399 J. P. Zheng, S. Ou, M. Zhao and C. D. Wu, *ChemPlusChem*, 2016, **81**, 758–763.
400 Y. Zhang, B. Li, H. Ma, L. Zhang, H. Jiang, H. Song, L. Zhang and Y. Luo, *J. Mater. Chem. C*, 2016, **4**, 7294–7301.
401 M. Zhang, G. Feng, Z. Song, Y.-P. Zhou, H.-Y. Chao, D. Yuan, T. T. Tan, Z. Guo, Z. Hu and B. Z. Tang, *J. Am. Chem. Soc.*, 2014, **136**, 7241–7244.
402 X. Zhao, Y. Li, Z. Chang, L. Chen and X.-H. Bu, *Dalton Trans.*, 2016, **45**, 14888–14892.
403 N. B. Shustova, B. D. McCarthy and M. Dinca, *J. Am. Chem. Soc.*, 2011, **133**, 20126–20129.
404 M. J. Dong, M. Zhao, S. Ou, C. Zou and C. D. Wu, *Angew. Chem., Int. Ed.*, 2014, **53**, 1575–1579.
405 J. x. Ma, X. f. Huang, X. q. Song and W. s. Liu, *Chem. – Eur. J.*, 2013, **19**, 3590–3595.
406 Y. Zhou and B. Yan, *Chem. Commun.*, 2016, **52**, 2265–2268.
407 D. Yan, Y. Tang, H. Lin and D. Wang, *Sci. Rep.*, 2014, **4**, 4337.
408 S. A. A. Razavi, M. Y. Masoomi and A. Morsali, *Inorg. Chem.*, 2017, **56**, 9646–9652.
409 L. Qin, M.-X. Zheng, Z.-J. Guo, H.-G. Zheng and Y. Xu, *Chem. Commun.*, 2015, **51**, 2447–2449.
410 W. Zhang, H. Huang, D. Liu, Q. Yang, Y. Xiao, Q. Ma and C. Zhong, *Microporous Mesoporous Mater.*, 2013, **171**, 118–124.
411 Z.-Z. Lu, R. Zhang, Y.-Z. Li, Z.-J. Guo and H.-G. Zheng, *J. Am. Chem. Soc.*, 2011, **133**, 4172–4174.
412 L. Meyer, F. Schönfeld, A. Zurawski, M. Mai, C. Feldmann and K. Müller-Buschbaum, *Dalton Trans.*, 2015, **44**, 4070–4079.
413 K. C. Stylianou, R. Heck, S. Y. Chong, J. Bacsa, J. T. Jones, Y. Z. Khimyak, D. Bradshaw and M. J. Rosseinsky, *J. Am. Chem. Soc.*, 2010, **132**, 4119–4130.
414 S. A. A. Razavi, M. Y. Masoomi and A. Morsali, *Ultrason. Sonochem.*, 2017, **37**, 502–508.
415 S. A. A. Razavi, M. Y. Masoomi and A. Morsali, *Chem. – Eur. J.*, 2017, **23**, 12559–12564.
416 Y. Yu, J.-P. Ma, C.-W. Zhao, J. Yang, X.-M. Zhang, Q.-K. Liu and Y.-B. Dong, *Inorg. Chem.*, 2015, **54**, 11590–11592.

417 P. Kumar, A. Paul and A. Deep, *Microporous Mesoporous Mater.*, 2014, **195**, 60–66.
418 J.-H. Wang, M. Li and D. Li, *Chem. Sci.*, 2013, **4**, 1793–1801.
419 S. Khatua, S. Goswami, S. Biswas, K. Tomar, H. S. Jena and S. Konar, *Chem. Mater.*, 2015, **27**, 5349–5360.
420 Y. Takashima, V. M. Martínez, S. Furukawa, M. Kondo, S. Shimomura, H. Uehara, M. Nakahama, K. Sugimoto and S. Kitagawa, *Nat. Commun.*, 2011, **2**, 168.
421 J. Zhou, H. Li, H. Zhang, H. Li, W. Shi and P. Cheng, *Adv. Mater.*, 2015, **27**, 7072–7077.
422 F. Drache, V. Bon, I. Senkovska, M. Adam, A. Eychmüller and S. Kaskel, *Eur. J. Inorg. Chem.*, 2016, **2016**, 4483–4489.
423 R.-W. Huang, Y.-S. Wei, X.-Y. Dong, X.-H. Wu, C.-X. Du, S.-Q. Zang and T. C. W. Mak, *Nat. Chem.*, 2017, **9**, 689–697.
424 C. Li, L. Li, S. Yu, X. Jiao and D. Chen, *Adv. Mater. Technol.*, 2016, **1**, 1600127.
425 G. Lu, O. K. Farha, L. E. Kreno, P. M. Schoenecker, K. S. Walton, R. P. Van Duyne and J. T. Hupp, *Adv. Mater.*, 2011, **23**, 4449–4452.
426 J. Hromadka, B. Tokay, R. Correia, S. P. Morgan and S. Korposh, *Sens. Actuators, B*, 2018, **260**, 685–692.
427 J. Tao, X. Wang, T. Sun, H. Cai, Y. Wang, T. Lin, D. Fu, L. L. Y. Ting, Y. Gu and D. Zhao, *Sci. Rep.*, 2017, **7**, 41640.
428 C. Bartual-Murgui, A. Akou, C. Thibault, G. Molnár, C. Vieu, L. Salmon and A. Bousseksou, *J. Mater. Chem. C*, 2015, **3**, 1277–1285.
429 L. Li, X. Jiao, D. Chen, B. V. Lotsch and C. Li, *Chem. Mater.*, 2015, **27**, 7601–7609.
430 G. Lu and J. T. Hupp, *J. Am. Chem. Soc.*, 2010, **132**, 7832–7833.
431 F. M. Hinterholzinger, A. Ranft, J. M. Feckl, B. Rühle, T. Bein and B. V. Lotsch, *J. Mater. Chem.*, 2012, **22**, 10356–10362.
432 A. Mallick, A. M. El-Zohry, O. Shekhah, J. Yin, J. Jia, H. Aggarwal, A.-H. Emwas, O. F. Mohammed and M. Eddaoudi, *J. Am. Chem. Soc.*, 2019, **141**, 7245–7249.
433 W.-Q. Zhang, Q.-Y. Li, J.-Y. Cheng, K. Cheng, X. Yang, Y. Li, X. Zhao and X.-J. Wang, *ACS Appl. Mater. Interfaces*, 2017, **9**, 31352–31356.
434 P. Mani, A. A. Ojha, V. S. Reddy and S. Mandal, *Inorg. Chem.*, 2017, **56**, 6772–6775.
435 X. Shen and B. Yan, *J. Mater. Chem. C*, 2015, **3**, 7038–7044.
436 N.-N. Yang, W. Sun, F.-G. Xi, Q. Sui, L.-J. Chen and E.-Q. Gao, *Chem. Commun.*, 2017, **53**, 1747–1750.
437 P. L. Feng, K. Leong and M. D. Allendorf, *Dalton Trans.*, 2012, **41**, 8869–8877.
438 L.-G. Qiu, Z.-Q. Li, Y. Wu, W. Wang, T. Xu and X. Jiang, *Chem. Commun.*, 2008, 3642–3644, DOI: 10.1039/B804126A.
439 Z.-Q. Li, L.-G. Qiu, W. Wang, T. Xu, Y. Wu and X. Jiang, *Inorg. Chem. Commun.*, 2008, **11**, 1375–1377.
440 C. Zhang, L. Sun, Y. Yan, Y. Liu, Z. Liang, Y. Liu and J. Li, *J. Mater. Chem. C*, 2017, **5**, 2084–2089.
441 X. Zou, G. Zhu, I. J. Hewitt, F. Sun and S. Qiu, *Dalton Trans.*, 2009, 3009–3013, DOI: 10.1039/B822248G.
442 K. Xu, F. Wang, S. Huang, Z. Yu, J. Zhang, J. Yu, H. Gao, Y. Fu, X. Li and Y. Zhao, *RSC Adv.*, 2016, **6**, 91741–91747.
443 F. Wang, C. Dong, C. Wang, Z. Yu, S. Guo, Z. Wang, Y. Zhao and G. Li, *New J. Chem.*, 2015, **39**, 4437–4444.
444 R. Haldar, R. Matsuda, S. Kitagawa, S. J. George and T. K. Maji, *Angew. Chem., Int. Ed.*, 2014, **53**, 11772–11777.
445 F. Wang, C. Dong, Z. Wang, Y. Cui, C. Wang, Y. Zhao and G. Li, *Eur. J. Inorg. Chem.*, 2014, **2014**, 6239–6245.
446 H. Weng and B. Yan, *Sens. Actuators, B*, 2016, **228**, 702–708.
447 J. Chen, F.-Y. Yi, H. Yu, S. Jiao, G. Pang and Z.-M. Sun, *Chem. Commun.*, 2014, **50**, 10506–10509.
448 Z. Guo, X. Song, H. Lei, H. Wang, S. Su, H. Xu, G. Qian, H. Zhang and B. Chen, *Chem. Commun.*, 2015, **51**, 376–379.
449 T. Gong, P. Li, Q. Sui, J. Chen, J. Xu and E.-Q. Gao, *J. Mater. Chem. A*, 2018, **6**, 9236–9244.
450 A. Mallick, B. Garai, M. A. Addicoat, P. S. Petkov, T. Heine and R. Banerjee, *Chem. Sci.*, 2015, **6**, 1420–1425.
451 J.-J. Liu, Y.-B. Shan, C.-R. Fan, M.-J. Lin, C.-C. Huang and W.-X. Dai, *Inorg. Chem.*, 2016, **55**, 3680–3684.
452 Y. Lv, H. Yu, P. Xu, J. Xu and X. Li, *Sens. Actuators, B*, 2018, **256**, 639–647.
453 E.-X. Chen, H.-R. Fu, R. Lin, Y.-X. Tan and J. Zhang, *ACS Appl. Mater. Interfaces*, 2014, **6**, 22871–22875.

